

الجمهورية الجزائرية الديمقراطية الشعبية

République Algérienne Démocratique et Populaire

Ministère de L'Enseignement Supérieur et de la Recherche Scientifique



UNIVERSITÉ FERHAT ABBAS - SETIF1

FACULTÉ DE TECHNOLOGIE

THÈSE

Présentée au Département d'Electrotechnique

Pour l'obtention du diplôme de

DOCTORAT

Domaine : Sciences et Technologie

Filière : Electrotechnique

Option : Commande électrique

Par

BENNIA Ilyas

THÈME

Etude, modélisation et commande d'un micro-réseau multi-sources

Soutenue le 20 /02 /2024 devant le Jury :

SARI Bilal	Professeur	Univ. Ferhat Abbas Sétif 1	Président
HARRAG Abdelghani	Professeur	Univ. Ferhat Abbas Sétif 1	Directeur de thèse
DAILI Yacine	M.C.A.	Univ. Ferhat Abbas Sétif 1	Co-Directeur
CHAOUI Abdelmadjid	Professeur	Univ. Ferhat Abbas Sétif 1	Examineur
MESSALTI Sabir	Professeur	Univ. Mohamed Boudiaf M'sila	Examineur
ZEMMIT Abderrahim	M.C.A.	Univ. Mohamed Boudiaf M'sila	Examineur

Declaration

I hereby declare that the work presented in this thesis has not been submitted for any other degree or professional qualification, and that it is the result of my own independent work.

BENNIA Ilyas

Date

20/02/2024

Publications associated with this research

SCIENTIFIC COMMUNICATIONS

- **Bennia, Ilyas**, Yacine Daili, and Abdelghani Harrag. "Hierarchical control of paralleled voltage source inverters in islanded single-phase microgrids." *Artificial Intelligence and Renewables Towards an Energy Transition 4*. Springer International Publishing, 2021.
- Daili, Yacine, Abdelghani Harrag, and **Ilyas Bennia**. "New droop control technique for reactive power sharing of parallel inverters in islanded microgrid." *Artificial Intelligence and Renewables Towards an Energy Transition 4*. Springer International Publishing, 2021.
- **Bennia, Ilyas**, Yacine Daili, and Abdelghani Harrag "Stationary and Dynamic Reference Frame Comparison Based Microgrid Application." *2nd International Conference on Electronics and Electrical Engineering (IC3E'2020)At Bouira, Algeria*
- **Bennia, Ilyas**, Yacine Daili, and Abdelghani Harrag. "LCL Filter Design for Low Voltage-Source Inverter." *Artificial Intelligence and Heuristics for Smart Energy Efficiency in Smart Cities: Case Study: Tipasa, Algeria*. Springer International Publishing, 2022.
- **Bennia, Ilyas**, Abdelghani Harrag, and Yacine Daili. "Adaptive Resonant Controller Based SOGI-FLL for Three-Phase Voltage Source Inverters." *2022 19th International Multi-Conference on Systems, Signals & Devices (SSD). IEEE, 2022.*

PUBLICATIONS

- **Bennia, Ilyas**, Abdelghani Harrag, and Yacine Dailia. "Small-signal modelling and stability analysis of island mode microgrid paralleled inverters." *Journal of Renewable Energies* 24.1 (2021): 105-120.
- **Bennia, Ilyas**, et al. "Decentralized secondary control for frequency regulation based on fuzzy logic control in islanded microgrid." *Indonesian Journal of Electrical Engineering and Computer Science* 29.1 (2023): 85-100.
- **Bennia, Ilyas.**; Elbouchikhi, E.; Harrag, A.; Daili, Y.; Saim, A.; Bouzid, A.E.M.; Kanouni, B. *Design, Modeling, and Validation of Grid-Forming Inverters for Frequency Synchronization and Restoration. Energies* 2024, 17, 59. <https://doi.org/10.3390/en17010059>

Acknowledgements

First and foremost, all my thankfulness is to Allah who helped and guided me to carry out this work.

I would like to express my deepest gratitude to my supervisors, Pr. Abdelghani HARRAG and Dr. Yacine DALLI, for their unwavering support, guidance, and encouragement throughout my Ph.D. journey. Their expertise and mentorship have been invaluable, and I am forever grateful for their contributions to my academic and personal growth.

I extend my deepest gratitude to Prof. CHAOUI Abdelmadjid, Prof. MESSALTI Sabir, and Dr. ZEMMIT Abderrahim for their invaluable examination of my work. Special thanks to Prof. SARI Bilal for presiding over the jury with wisdom.

I would like to extend my heartfelt thanks to my co-authors, Pr. Josep M. GUERRERO, Pr. Hasan ALRAJHI, Pr. Elhoussin ELBOUCHIKHI, Dr. Allal BOUZID and Dr. Saim ABDELHAKIM, for their invaluable contributions to this research project. Their expertise, collaboration, and dedication have been instrumental in achieving the goals of this study.

Their insights, ideas, and critical feedback have helped shape the research and improve the quality of our findings, and I am grateful for the opportunity to have worked with such talented and committed colleagues.

I would like to extend my special thanks to Pr. Ilhem SLAMA-BELKHODJA the director of the Common Services Unit for Research, MICROGRID Platform and QEHNA research team, for their guidance, mentorship, and support throughout my research. Their leadership and vision have created a stimulating and collaborative environment that has fostered my growth as a researcher.

I would also like to sincerely thank the educational and administrative team of Qehna for their invaluable contributions to this research project. Their collaboration, expertise, and dedication have been instrumental in achieving the goals of this study. I am honored to have had the opportunity to work with such an exceptional group of individuals, and I look forward to future collaborations.

I am also grateful to my family for their patience, prayers, understanding, and for believing in me. They have given me much care, love and support throughout the research.

Table of contents

Declaration	i
Publications associated with this research	ii
Acknowledgements	iii
Table of contents	iv
List of figures	viii
List of tables	xi
Chapter 1: Introduction	1
1.1 Distributed Generation	1
1.2 Microgrid: A new concept	1
1.2.1 Operation Modes of Microgrids	3
1.2.2 Classification of Power Converters in AC Microgrids	4
1.2.3 The DC/AC converters.....	5
1.3 Microgrids control challenges	6
1.4 Thesis objectives	8
1.5 Novel Contributions of the thesis	8
1.6 Thesis structure	9
Chapter 2: Background and literature review	11
2.1 Introduction.....	11
2.2 Droop control concept	12
2.2.1 Case one the output impedance is pure inductive: $Z=jX$	14
2.2.2 Case two the output impedance is pure resistive: $Z=R$	14
2.3 Virtual impedance and droop enhancement.....	17
2.4 Virtual Inertia	20
2.5 Hierarchical Control	22

2.5.1	Centralized Secondary Control	23
2.5.2	Distributed Secondary Control.....	24
2.5.3	Decentralized Secondary Control	26
2.6	Small signal modelling and reactive power-sharing	29
2.7	Conclusion	31

Chapter 3: Modelling, Analysis, and Design of Hierarchical Controlled Parallel Three-Phase

Voltage Source Inverters based MG.....33

3.1	Introduction.....	33
3.2	Description and modelling of the power system	33
3.3	Mathematical models of the VSI.....	34
3.4	Voltage and Current Loops.....	36
3.4.1	Current loop model.....	36
3.4.2	Voltage loop model.....	37
3.5	Inner loops control design	37
3.5.1	PI controller:.....	38
3.5.2	Current loop design:	38
3.5.3	Synthesis of the current loop PI controller	39
3.5.4	Voltage loop design:	41
3.5.5	Synthesis of the voltage loop PI controller	42
3.6	Primary control.....	44
3.6.1	Droop control and virtual impedance loop	44
3.6.2	Coordinated synchronization loop.....	45
3.7	Secondary control for frequency and voltage restoration	47
3.7.1	Frequency Restoration.....	49
3.7.2	Amplitude Restoration.....	50
3.8	Implemented MG Control Analysis	52

3.8.1	Voltage and current waveforms	52
3.8.2	Inverters synchronization to the MG.....	54
3.8.3	Secondary control performances	55
3.8.4	Impact of communication time delays:	56
3.8.5	Synchronization with the main grid.....	57
3.9	Conclusion	58
Chapter 4: Decentralized secondary control for frequency regulation based on fuzzy logic control in islanded microgrid.....		60
4.1	Introduction.....	60
4.2	Method.....	64
4.3	Results and discussion.....	71
4.3.1	Frequency restoration and active power-sharing during load disturbances	72
4.3.2	Synchronization and plug-and-play capability.....	73
4.3.3	Impact of communication latency	73
4.3.4	Comparative study of dynamic response	74
4.3.5	Effect of data drop-out	74
4.3.6	Effect of interferences	75
4.4	Conclusion	79
Chapter 5: Optimized virtual impedance design to improve reactive power sharing and microgrid stability.....		80
5.1	Introduction.....	80
5.2	Microgrid modelling and small-signal stability analysis.....	81
5.2.1	Power measurement-droop control and interface circuit	81
5.2.2	Virtual impedance equations.....	82
5.2.3	Voltage controller loop	84
5.2.4	Current controller loop	84

Study, Modelling and Control of a Multisource Microgrid

Table of contents

5.2.5	LCL filter model	85
5.2.6	Complete inverter model.....	86
5.2.7	Parallel inverters model.....	88
5.2.8	Subsystems models (lines and loads)	88
5.2.9	Entire microgrid model	89
5.3	Eigenvalue analysis and virtual impedance optimization	90
5.3.1	Effect of virtual impedance parameters on system eigenvalue spectrum.....	91
5.3.2	Virtual impedance optimization	91
5.4	Validation of the proposed approach	95
5.4.1	Inverters output power and frequency	96
5.4.2	Converters output current components.....	97
5.4.3	Converters voltage components.....	98
5.4.4	Reactive power step	98
5.5	Conclusions.....	99
	General conclusion.....	102
	References.....	103
	Abstract.....	111

List of figures

Figure 1-1: Microgrid configuration.....	2
Figure 1-2: Operating modes	3
Figure 1-3: Power converter classification a/grid forming b/grid following	5
Figure 1-4: Inverter structure containing six IGBTs with LCL filter	6
Figure 2-1: General scheme of an electrical microgrid.....	12
Figure 2-2: equivalent circuit of an inverter connected to an ac bus.....	13
Figure 2-3: equivalent circuit of two inverters associated in parallel	14
Figure 2-4: P-w and Q-v droop characteristics	15
Figure 2-5: Diagram of droop control for single phase inverters	16
Figure 2-6: Multiloop control droop strategy with the virtual output impedance approach.	17
Figure 2-7: The transition towards an inverter-dominated power system	20
Figure 2-8: Hierarchical control of microgrid.....	22
Figure 2-9: A typical time-scale of frequency-related dynamics in conventional	23
Figure 2-10: Hierarchical Control Structures.	23
Figure 3-1: Three-phase inverter single line diagram interfaced using LCL filter.....	34
Figure 3-2: Inner loops (voltage and current controllers)	37
Figure 3-3: Block Diagram of Current Controller Loops.....	39
Figure 3-4: Block diagram of the closed-loop control for current.....	40
Figure 3-5: Block Diagram of Current Controller Loops.....	42
Figure 3-6: Block diagram of closed-loop control for voltage	43
Figure 3-7: Block diagram of the droop controller and the virtual output impedance in dq synchronous frame.	45
Figure 3-8: Block diagram of the synchronization control loop of a droop controlled MG.	46
Figure 3-9: Block diagram of the entire control system of the MG.....	48
Figure 3-10: Block diagram of the frequency secondary control	49
Figure 3-11: Transient response of the secondary control model for frequency restoration	50
Figure 3-12: Block diagram of the amplitude secondary control	50
Figure 3-13: Transient response of the secondary control model for amplitude restoration	51
Figure 3-14: Output voltage (a) and current (b) waveforms of a VSI	53

Study, Modelling and Control of a Multisource Microgrid

List of figures

Figure 3-15: Iner loops voltage and current components	53
Figure 3-16: Transient response of the output currents (a) VSI1 (b) VSI2, when the VSI 1 is disconnected at t=1s.....	54
Figure 3-17: Synchronization process of inverters (a) frequency of two sides (b) active power, and (c) reactive power contributions of two inverters.....	54
Figure 3-18: Active and reactive power (a) and frequency (b) during load step changes (t=2s and t=4s) and sudden disconnection of inverter 2 (t=6s).....	56
Figure 3-19: Secondary frequency dynamics under different communication delay	57
Figure 3-20: Synchronization process (a) voltage difference (b) Grid and MG voltages.....	58
Figure 4-1: Fundamental structure of a microgrid	60
Figure 4-2: Secondary control topologies; (a) centralized SC, (b) distributed SC, and (c) decentralized SC.....	63
Figure 4-3: Primary and secondary control actions.....	65
Figure 4-4: Proposed decentralized secondary control for microgrids	68
Figure 4-5: Fuzzy logic controller design steps Membership functions (a) the deduction of the rules from a temporal analysis (b) and (c) output surface plot of the fuzzy cotroller	71
Figure 4-6: . Microgrids Configuration of the studied MG	72
Figure 4-7: Performance of proposed controller under load disturbances with black start and plug and play test, (a) active power-sharing, (b) frequency restoration, (c) current, (d) reactive power (e) Black start and PNP - active power-sharing, and (f) Pnp frequency restoration.....	76
Figure 4-8: Performance of proposed controller, (a) frequency restoration under delay time 200ms - Centralized topology, (b) frequency restoration under delay time 200ms - decentralized topology and (c) comparison between fuzzy and PI controllers	77
Figure 4-9: Performance of proposed secondary control considering data drop-out, when compared with PI controller	77
Figure 4-10: Performance of proposed controller under interferences	78
Figure 5-1: Configuration of tested MG.....	81
Figure 5-2: Proposed control scheme of a VSI in island mode	82
Figure 5-3: Reference frame transformation.....	83
Figure 5-4: Fig. 4. The eigenvalue spectrum of the system (a) without virtual impedance (b) effect of increasing the virtual resistance(R_v): $0 < R_v < 10\Omega$, (c) effect of increasing the virtual inductance (L_v): $0 < L_v < 0.1$ H	92

Study, Modelling and Control of a Multisource Microgrid

List of figures

Figure 5-5: Flowchart algorithm for virtual impedance optimization93

Figure 5-6: Eigenvalues trace comparison with and without virtual impedance95

Figure 5-7: Comparison of control method in [7] with the proposed virtual impedance (a) active power; (b) reactive power; (c) frequency /using proposed method, (d) active power; (e) reactive power; (f) frequency/ using method in [7]96

Figure 5-8: Comparison of output currents in control method in [7] with the proposed method (a) inverter1; (b) inverter 2; (c) inverter398

Figure 5-9: Comparison of voltage outputs in control method in [7] with the proposed method (a) inverter1; (b) inverter 2; (c) inverter398

Figure 5-10: Comparison of reactive power sharing using the proposed method and the conventional method in [7]99

List of tables

Table 2-1: Typical line impedance values	17
Table 2-2: Different droop control methods	19
Table 2-3: Summerise of different secondary control technics	28
Table 3-1: microgrid parameters	52
Table 4-1: Summerise of different secondary control technics	67
Table 4-2: Table of rules.....	70
Table 4-3: Simulation Parameters	72
Table 4-4: Table 4. Performance evaluation of proposed scheme through time domain specifications.	78
Table 5-1: Optimized virtual impedances	95
Table 5-2: Microgrid parameters	100
Table 5-3: Comparison of time domain specifications between the conventional method in [7] and the proposed control diagram	101

Chapter 1: Introduction

1.1 Distributed Generation

Industrial development and population growth in recent years are increasing the world's energy needs. Traditional electricity is produced in centralized power plants that are located far from consumers. Central power plants convert primary energy sources like fossil fuel and nuclear to electric power. This power will be transmitted to consumers using long transmission and distribution lines. This way of electricity production has many problems such as environmental impacts and significant power losses.

To eliminate these problems the concept of distributed generators (DG) has been developed last few years. A distributed generator is a small-scale power generation unit that is connected to the electrical grid at a distribution level, as opposed to a large central power plant that is connected at the transmission level. The growth of the DG systems utilization has been accelerated by the use of Renewable Energy Sources (RES) such as solar, wind, hydro, geothermal and biomass since it is sustainable and environmentally friendly than traditional fossil fuels.

In addition to being able to be installed at a distributed level, distributed generation systems based RES can include solar panels, wind turbines, microturbines, fuel cells, and micro-hydro systems, which allows for more decentralized and resilient power systems [1].

1.2 Microgrid: A new concept

For more sustainable and reliable power supply systems, Microgrid (MG) paradigm has gained significant research interest to be the optimal and the ideal solution compared to conventional power generators and grids.

The MG is conceptually defined as a small modular grid, composed by the interconnection of various loads and DG units aggregated with storage devices, like batteries, flywheels and power capacitors on low voltage distribution system. The DG units are interfaced to the MG through power electronic converters equipped with adapted control strategies to ensure the required flexible operation and to ensure the specified power quality and power output. MG have the potential to work either in grid-connected mode where the MG is connected to the main grid to feed excess power into the grid, or in islanded mode, intentionally to provide power for single buildings and small communities or unintentionally in case of grid faults or other external perturbations, which ensure the power supply reliability and sustainability [2]. In contrast to the unidirectional flow of electricity in classic networks,

the MG allows the bidirectional power flow and has a higher degree of controllability and operability. Moreover, MG offers improvement in terms of power quality and a better balance between generation and consumption, also a reduction in grid-side power interruptions and system downtime, and hence improved recovery for power systems [3].

Figure 1-1 depicts a single-line design of a MG based on wind generators, photovoltaic (PV) panels, power storage systems, and distributed loads. The MG is connected to the point of common coupling (PCC) of the utility network using a Bypass. The entire system consists of several distributed generators and distribution loads that require power electronics converters.

With some degree of argument, the following advantages can be attributed to the MG concept:

- Reduced transmission and distribution lines and hence costs
- Reduced transmission and distribution losses
- Increased renewable energy sources integration
- Reduced negative impacts on the environment
- Increased power supply quality and reliability
- Allows for more decentralized and resilient power systems
- continuity of the power supply

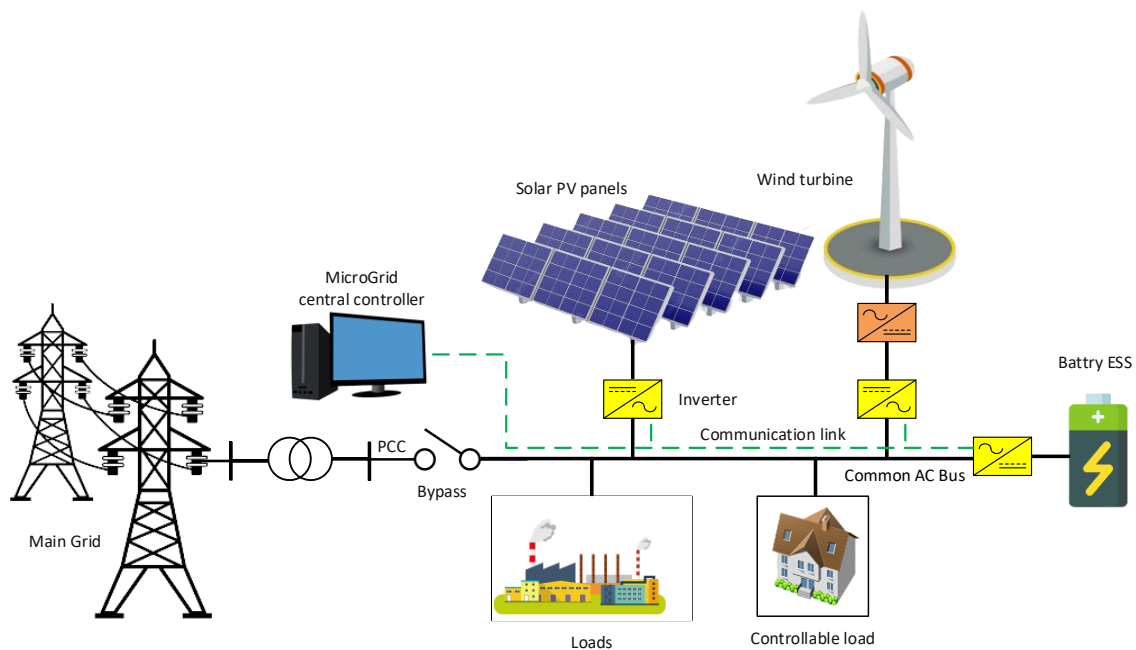


Figure 1-1: Microgrid configuration

1.2.1 Operation Modes of Microgrids

One of the most important features of MGs is the capacity to work in both modes, grid-connected mode and islanding or stand-alone mode. Grid-connected mode when there is an interaction with the main grid, in other manner MG is tied to the power grid. Stand-alone mode as defined by the name due to an autonomous operation the MG become entirely disconnected. In each mode of operation, DG units can be operated either in grid-forming or grid-following control strategies. The transition between grid-connected mode and islanding mode or vice versa is the transient operating mode as can be seen in Figure 1-2 which recapitulates the three modes [4].

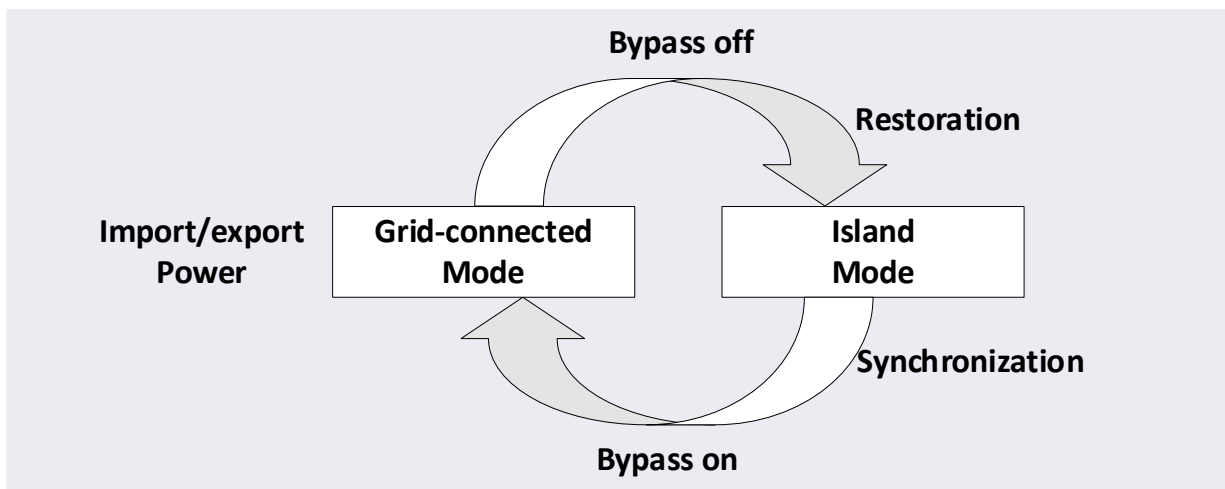


Figure 1-2: Operating modes

1.2.1.1 Grid-Connected Mode

This mode allows the bidirectional power flow between the MG and the main grid by importing the energy when there is a defect in the MG and exporting it in case of excess to support the main grid. In this mode of operation, the voltage amplitude, frequency, and phase are determined by the main grid; these parameters can easily be obtained at the point of common coupling (PCC). The PCC is a connection point between the MG and the main grid. Distributed energy resources usually work under grid-feeding control strategy also they able to work in grid-forming if it is necessary. The synchronization between the main grid and the MG, in this case, is carried out by a phase-locked loop (PLL).

1.2.1.2 Islanded Mode

Islanded mode is similar to a physical island; the MG is isolated from the rest of the utility system, it can be either intentionally for maintenance reasons or unintentionally due to faults, power quality disturbances, and non-scheduled events in the main grid.

To continue supplying the local loads, the MG is in charge of maintaining in a steady-state condition the voltage and frequency within an accepted range. One converter must function as a voltage source at least to guide the network voltage requirements and power quality of the MG, whereas other converters can follow by grid-feeding. In stand-alone mode, distributed generators should maintain the power-sharing between themselves for limiting circulating currents and overload stresses that cause equipment damage. Another challenge in this mode is to detect the islanding conditions, in purpose to protect the MG and ensure reliability, many techniques have been designed in litterateurs. Hence the control of the converter becomes more important in islanded mode.

1.2.1.3 Transient Operating Mode

The transient operation is the transition state between the above-mentioned operating modes in both directions from island operation to grid-connected operation and vice versa; it can have considerable voltage and current fluctuations (as the main cause of lack of inertia), which threaten the stability of the system. The transition mode can be planned or unplanned for many reasons, such as predictive or network disruptions. Control technologies must therefore guarantee a seamless and quick transition when attaching and removing to the PCC.

For the grid restoration, a synchronization procedure of voltage amplitude, frequency and phase is required to ensure a smooth transition, often a PLL is used thereby an islanding detect is needed to guarantee smooth islanding.

1.2.2 Classification of Power Converters in AC Microgrids

The power converters are electronically tied to DG's with the aim of supplying consumers and it can be classified referring to their mode of operation into grid-forming or grid- following also called grid-feeding [5] (see Figure 1-3).

1.2.2.1 Grid-Forming Power Converters

The grid-forming power converters operate equivalently as a voltage source with a reference amplitude V^* and frequency w^* , with a low-output impedance; thus, it requires a considerably precise synchronization system to work in parallel with other grid-forming converters in islanding mode or grid-connected mode. Grid-forming inverters are commonly used in traditional dispatchable generation units such as microturbines and energy storage devices.

1.2.2.2 Grid-Following Power Converters

Grid-following power converters acting equivalently as the current source using references of active and reactive powers, P^* and Q^* , to be supplied, with the presence of high parallel output impedance. They are permanently synchronized with the main grid and in parallel with other grid-following power converters in grid-connected mode operation, while at least one of the power converters should be operating in grid-forming to establish the voltage and frequency references in islanding mode. Grid following converters are mainly used on non-dispatchable RES such as PV and a wind turbine that requires maximum power point tracking (MPPT) controller which sets reference values for P^* and Q^* to exploit the maximum power generated.

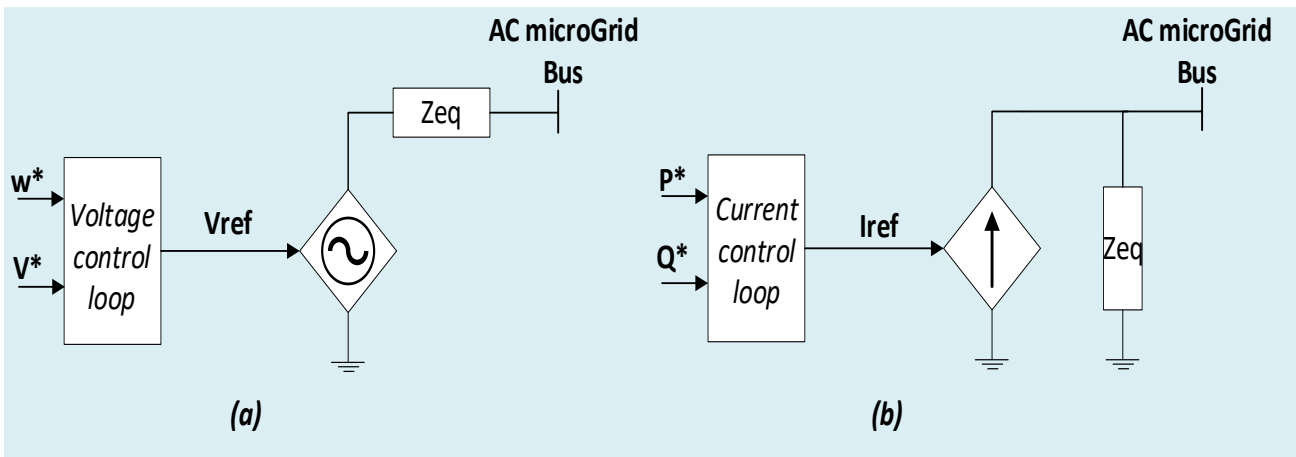


Figure 1-3: Power converter classification a/grid forming b/grid following

1.2.3 The DC/AC converters

The DC/AC converters, generally called inverters are power electronics topologies considered as the key element and the block stone of the MG. Using high switching frequency of solid state devices to generate an AC output while the input is a DC source coming from the renewable energy sources as can be seen in Figure 1-4. The switching devices are controlled using a pulse width modulation technic PWM signals coming from the voltage reference after the modulation. The high switching frequencies of the solid state devices i.e. IGBT (insulated gate bipolar transistor) produce harmonic signals which need to be attenuated using an LCL filter.

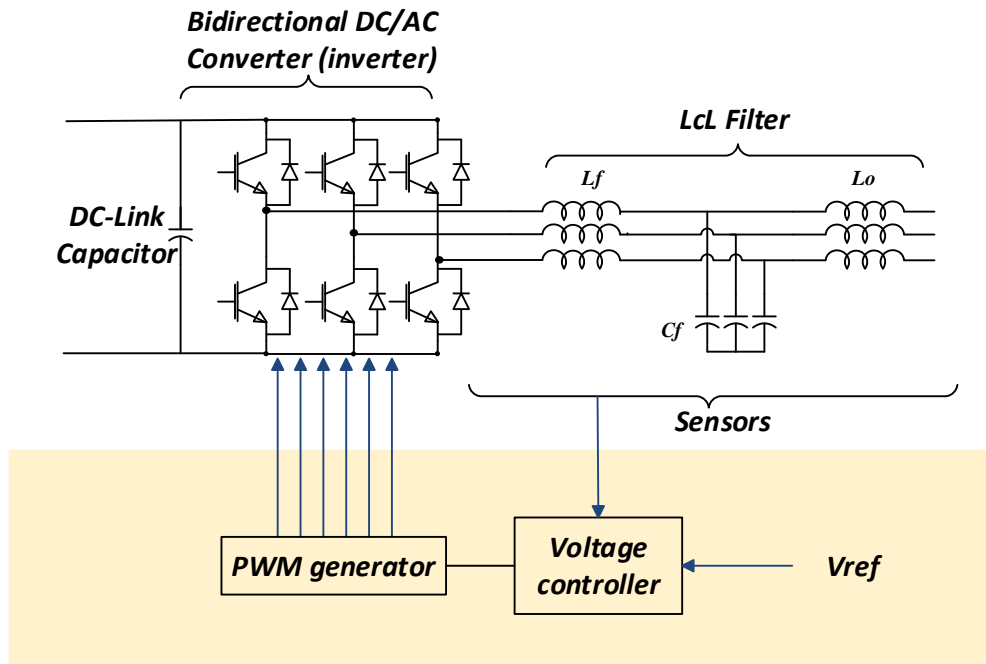


Figure 1-4: Inverter structure containing six IGBTs with LCL filter

1.3 Microgrids control challenges

The current energy situation imposed a necessity for grid transformation, whereas augmentation of the renewable energy sources integration is leading the research community to produce more advanced control techniques to ensure and guarantee the flexibility of MG operation. The development of MGs has faced several challenges in achieving a reliable and secure operation, despite the potential benefits. Many technological deficits need to be addressed as given below:

- Voltage and current control. MG ensure the continuity of power supply and the power quality requirements in island mode operation. Therefore a good design of voltage and current controllers is needed in each local controller of DG units to maintain the voltage and the frequency in the desired limits of the autonomous MG, simultaneously responding to the current demand by the load side [6].
- Stability Issues and load dynamics. MG regroups several energy sources and loads with different inertia, nominal capacities, and dynamics. The presence of synchronous generators (microturbines, hydropower) means large rotational inertia, however, power converters associated with PV have low physical inertia, which results in interactions among sources and hence threatens the MG stability [7]. Similarly in case of supplying complex loads such as dynamic loads, constant loads, inductor motor, nonlinear loads, and electric vehicles could have similar effects [8]. Thus, special control approaches need to be proposed to face the voltage, frequency,

and power-angle stabilities, and also to avoid interactive influences among multi-resources and loads [6].

- Seamless transition between different operation modes. During the transition process between island mode and grid-connected mode in both directions intentionally or unintentionally, large fluctuations and oscillations in voltage and frequency are observed. Minimization of the effects of disturbances during a transition process is necessary for ensuring safe operation and better power quality for local loads [4].
- Power sharing control. MG regroups many DG sources with different power rates and dynamic responses, local controllers should take this into consideration to share the power equally among DG sources and avoid overcharges, to prevent DG unit's damage which can result in system failure. Also, the distances between loads and DG units must be taken into account to increase the system efficiency [9].
- Power quality issues. The most common power quality issues are the harmonics and unbalances, especially in the presence of nonlinear and unbalanced loads. MG controllers can integrate multiple functions to achieve harmonic attenuation, unbalance compensation etc., aiming to enhance the power supply quality [10].
- Synchronization of DG units. In both operation modes, appropriate synchronization technics are necessary. In island mode and for a black start DG units must be synchronized to the MG before connection, in grid-connected mode, the synchronization of the MG with the utility grid must be guaranteed to prevent any system failure and to respect the grid code [11].
- Fault-tolerant control. numerous emergencies can happen during the system operation, such as faults, outages, power quality perturbation or sudden changes in the demand side, and voltage sags; thus, appropriate corrective actions to eliminate the fault and ensure the normal operation of the proposed power-sharing, voltage and frequency restoration control technics during such fault scenarios which enhances the capability and the security of the systems.
- Source intermittency. Renewable energy sources are highly dependent on the weather situation, similarly, the demand side is non-linear and this presents a big challenge for maintaining the balance between the two side's production and consummation. Control technics for MGs are considering the power source as a constant source which is not the real case; thus a variable power source should be considered instead of ideal resources to emulate the real state. Further, the MG is sensitive to power quality issues, so the impact of weather on the weather-dependent

sources and their sudden power output variation should be considered during load-support controller design. Likewise, demand-side varying power.

1.4 Thesis objectives

The main concern of this thesis is fundamental investigations of modelling and control of parallel voltage source inverters (VSI's) based island MGs. The thesis presents a hierarchical control scheme for VSI's system comprising two layer of control. Also, the thesis presents a decentralized secondary control for restoring MG frequency deviations. Additionally, the thesis presents a mathematical model of a MG and investigates the effects of the MG parameters on its stability. Furthermore, the reactive power sharing is improved based on an optimized virtual impedance.

The objectives of the thesis are listed as follows:

- To review existing literature on MG control technics in order to provide a comprehensive overview of current knowledge and understanding.
- To produce a model of a MG controlled using hierarchical control topology to study and analyses the system responses and controllers' performance.
- To develop a new decentralized secondary control technique that can be used to restore the system frequency.
- To create a mathematical model of an islanded MG and to study the influence of the MG parameters on the system stability.
- To enhance the reactive power sharing and the MG stability using optimization based on a MG mathematical model.

1.5 Novel Contributions of the thesis

The contributions of the thesis are summarized as follows:

- Presents a systematic method for modelling, control design, and stability analysis of AC MG's based hierarchical control including primary and secondary control with validated results using MATLAB-Simulink software.
- Design of a novel fuzzy-based decentralized secondary control for frequency restoration and active power-sharing in an islanded MG. This controller uses the local frequency error to generate an extra term for compensating the deviation and maintaining accurate active power-sharing

- Studying and investigation of a mathematical model for an islanded MG. based on the component connection method technic, the mathematical model started from the individual state-space models of the inverters, network and loads, that are associated to form the complete model. The influence of each inverter parameter and the other components were investigated.
- Design of a novel controller that enhances the reactive power sharing between parallel-connected inverters. This controller reduces the dependency on communication and the risk of system instability if this communication link was lost.
- Development of a small signal mathematical model for autonomous MG including virtual impedances, consisting of three parallel inverters that is used to study the influence of the virtual impedance on the system stability. The study has shown that for certain limits of the virtual impedance values the system stability can be lost.
- Design of optimal virtual impedances for an island MG using an optimization algorithm. The range of the MG system stability was identified based on the developed MG small signal mathematical model and genetic algorithm
- Improvement of the islanded MG stability and reactive power sharing based on the optimal design of virtual impedances. The optimization algorithm maintains the reactive power-sharing error at its minimum value through a specific objective function.

1.6 Thesis structure

- Chapter 2 presents the background and the literature review of the AC MGs control technics, especially hierarchical control topology with its three layer of control primary, secondary and tertiary control. Another concern about stability studies is presented.
- Chapter 3 introduces a hierarchical control scheme for the paralleled VSI system comprising two levels. The primary control includes the droop method and the virtual impedance loops, in order to share active and reactive power. The secondary control restores the frequency and voltage amplitude deviations produced by the primary control. Also, a synchronization algorithm is presented in order to connect the MG to the grid.
- Chapter 4 presents a fuzzy-based decentralized secondary control for frequency restoration and active power-sharing in an islanded MG, Also the validity of the proposed controller is verified based on several tests.

- Chapter 5 addresses a systematic way of developing a small-signal state-space model of the inverter-based microgrids. Each sub-module is modelled in state-space form and all are combined together on a common reference frame. The complete model is linearized around an operating point and the resulting system matrix is used to derive the eigenvalues. The eigenvalues (termed 'modes') indicate the frequency and damping of oscillatory components in the transient response. After that, a novel small-signal model for autonomous MG including virtual impedances is proposed. Additionally, optimal virtual impedances are designed based on a new optimization algorithm using a genetic algorithm. The eigenvalue analysis identifies the stability ranges and the optimization algorithm maintains the reactive power-sharing error at its minimum value through the objective function. The proposed approach is tested using MATLAB-Simulink software.

Chapter 2: Background and literature review of microgrid control

2.1 Introduction

The reality that microgrids incorporate numerous DG units connected and interfaced electronically using inverters in grid-connected or island mode, increases the complexity and leads to additional control challenges, especially during transition mode where the stability of the microgrid system needs to be ensured, moreover the voltage and frequency regulation with the accurate power sharing between the DG units under different conditions in island mode, as well as the active and reactive power flow between the microgrid and the main grid, as a result, a reliable control topology combining all of these characteristics has been an active area of research [12].

Figure 2-1 presents a single-line topology of a microgrid that consists of a Photovoltaic (PV) system, wind turbine and a battery energy storage system, these sources are interfaced to the point of common coupling using inverters and cables. Each unit controls its inverter using local controllers to ensure stability and power sharing between units. The microgrid is connected to the main grid using a static transfer switch (STS) which is controlled and supervised by a microgrid central controller (MGCC) that is responsible for the transfer between the two modes of operation, in addition, it sends all DG configurations and set-points of voltage, frequency and power through a low-bandwidth communication link. Based on the studies in [13] and [14] where they concluded that the DC dynamics can be neglected during the design of the power controllers, it is worth mentioning here that the DC sources in all DGs are assumed to have a stable and regulated output, ready to be used by the DC/AC converters. The control of the DC sources will not be discussed in this thesis.

In this chapter the existing control technics in the literature are reviewed and discussed briefly focusing on the main issues faced during the microgrid control development, along with current findings from relevant research, In terms of voltage controllers, load sharing, modelling, and stability concerns, the thesis focuses on control techniques, notably in island mode.

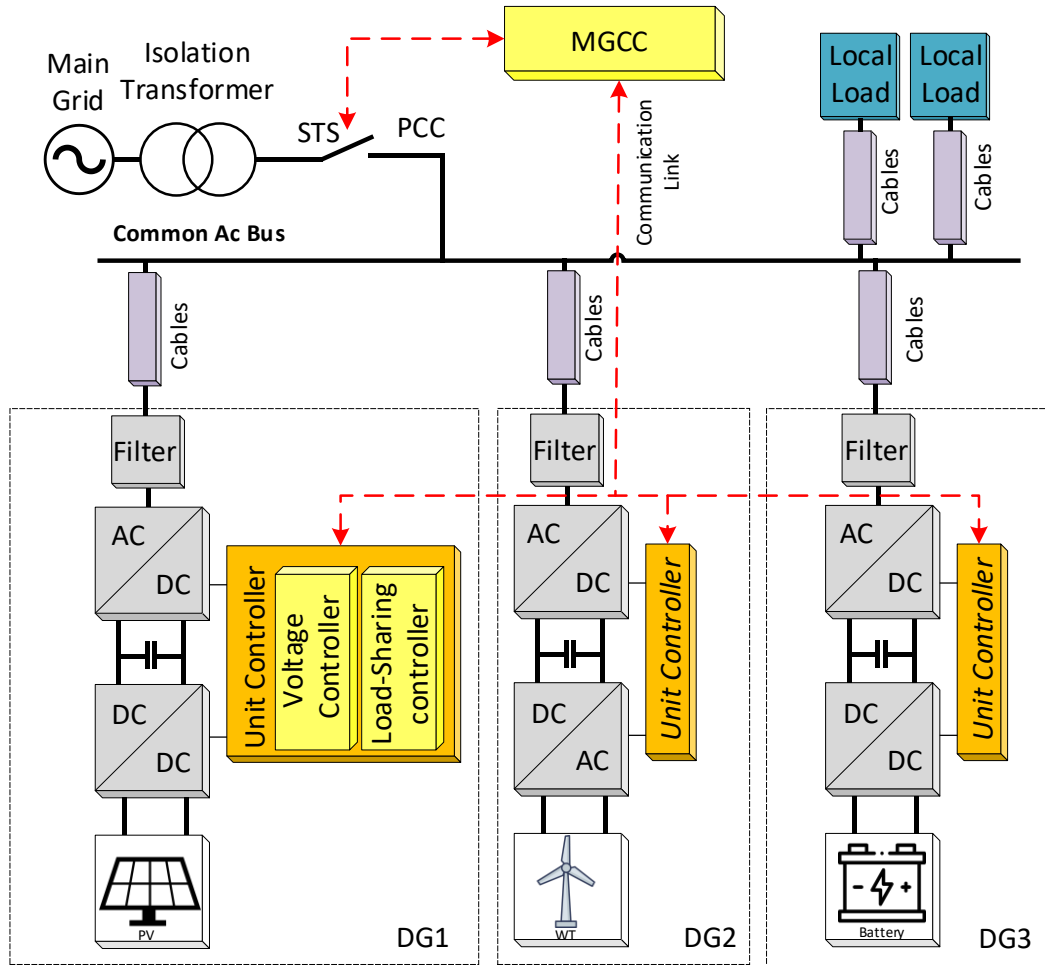


Figure 2-1: General scheme of an electrical microgrid

2.2 Droop control concept

Droop control is widely considered to be the most important wireless strategy has the ability to adjust the voltage and frequency while sharing the active and reactive power demands among parallel generation units without any need for external communication among inverters. This idea is derived from the classic power system theory and mimics the synchronous generator behaviour, in which generator frequency decreases when the grid utility power demand is increased [15]. In grid-connected mode, the control of power generated to the grid is easy to implement using droop control or other controllers. But, the benefit of droop control arrives in island mode, where the power-sharing is required according to the droop curves with free communication [16]. Thus the traditional droop control can be presented as given below:

$$\begin{aligned} \omega &= \omega^* - mP \\ V &= V^* - nQ \end{aligned} \tag{2.1}$$

Where m, n are the droop parameters, and ω^*, V^* are the frequency and voltage references, P and Q are the measured active and reactive powers output.

To better understand the source of these equations Figure 2-2 [17] depicts the equivalent circuit of an inverter connected to an AC bus which can be considered as a grid or a point of common compliance

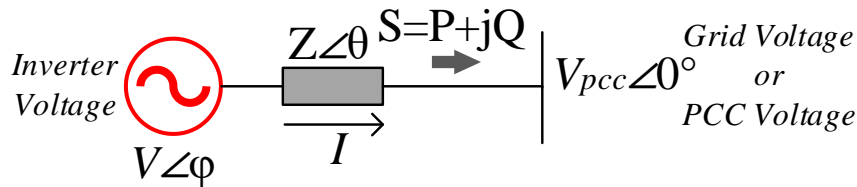


Figure 2-2: equivalent circuit of an inverter connected to an ac bus

The apparent power injected into the bus can be illustrated as:

$$S = P + jQ \tag{2.2}$$

Where P and Q are the active and reactive powers respectively flowing from the inverter to an AC bus through the impedance Z and they can be expressed as follows:

$$P = \left(\frac{VV_{pcc}}{Z} \cos\phi - \frac{V_{pcc}^2}{Z} \right) \cos\theta + \frac{VV_{pcc}}{Z} \sin\phi \sin\theta$$

$$Q = \left(\frac{VV_{pcc}}{Z} \cos\phi - \frac{V_{pcc}^2}{Z} \right) \sin\theta - \frac{VV_{pcc}}{Z} \sin\phi \cos\theta \tag{2.3}$$

Where Z and θ are the amplitude and the phase of the output impedance, respectively; V_{pcc} is the common bus voltage; and ϕ is the phase angle between the inverter output and the microgrid voltages.

Notice that the droop control is highly dependent on the output impedance of inverters, which is depending on the control loops, and the impedance of the power lines (mainly resistive in low voltage applications).

Figure 2-3 shows two inverters associated in parallel and providing energy to a common load. Each inverter is interfaced through an output impedance to the load bus.

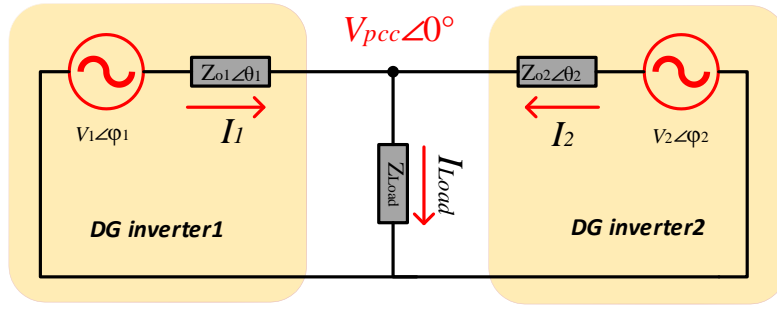


Figure 2-3: equivalent circuit of two inverters associated in parallel

The exported P and Q powers from inverters to the load are related to the output impedance. The output impedance can be predominantly inductive or resistive and this results in the way that the inverter controls the exported power.

2.2.1 Case one the output impedance is pure inductive: $Z=jX$

By assuming that the output impedance of the inverter is mainly inductive ($\theta=90^\circ$) due to the large filter-inductor value. And by substituting θ in the power flow equations (2.3) the new active and reactive power equations became:

$$P = \frac{VV_{pcc}}{X} \sin\phi \quad (2.4)$$

$$Q = \frac{VV_{pcc}}{X} \cos\phi - \frac{V_{pcc}^2}{X}$$

Where X is the inverter output reactance, by assuming that phase difference ϕ between V and V_{pcc} is small enough to consider $\sin \phi \approx \phi$ and $\cos \phi \approx 1$, thus,

$$P = \frac{VV_{pcc}}{X} \phi \quad (2.5)$$

$$Q = \frac{V_{pcc}}{X} (V - V_{pcc})$$

And hence the active power P is controlled by the power angle ϕ while the reactive power is controlled by the voltage magnitude difference $V - V_{pcc}$, consequently a P-w and Q-V droop is obtained as mentioned in equations (2.1)

2.2.2 Case two the output impedance is pure resistive: $Z=R$

By considering a resistive output impedance ($\theta=0^\circ$) and based on the assumption that the phase difference ϕ is small enough the power flow equations in (2.3) became:

$$P = \frac{V_{pcc}(V - V_{pcc})}{R} \tag{2.6}$$

$$Q = -\frac{VV_{pcc}}{R}\phi$$

Where R is the inverter output impedance, it is clear that the roles are exchanged where the active power is can be controlled by the voltage magnitude difference and the reactive power can be controlled by the phase difference which gives a resistive droop control as expressed in the following equations :

$$\omega = \omega^* + mQ \tag{2.7}$$

$$V = V^* - nP$$

Therefore a P-w, Q-V droop control must be used in case of inductive output impedance, and a P-V, Q-w droop in case of a resistive output impedance. As a result, the design of an output impedance is recommended to improve decoupling between active and reactive power and to avoid the line impedance impact over power-sharing.

In the remains of this thesis, the inverters output impedance is considered to be inductive; therefore, P-W and Q-V curves are adopted as shown in Figure 5. In this way, the inverter can introduce the desired active and reactive power to the main grid, controlling the output voltage and responding to linear load changes.

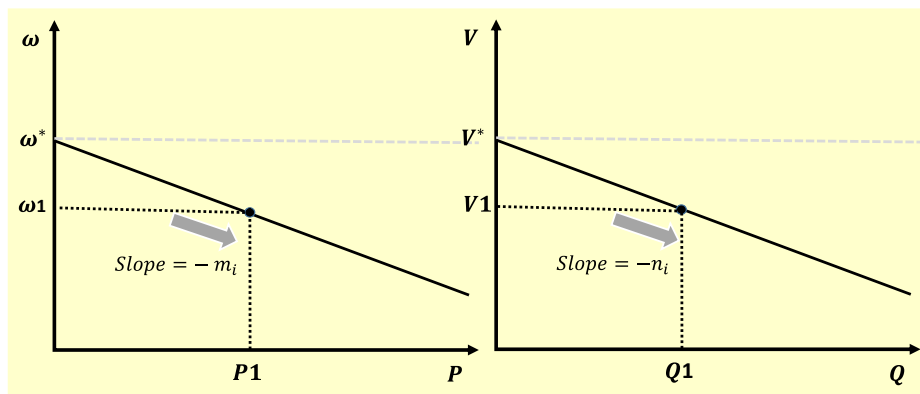


Figure 2-4: P-w and Q-v droop characteristics

For the two modes of operation (grid-connected, island modes), the droop control equations are as follows, Island mode:

$$\omega = \omega^* - mP \tag{2.8}$$

$$V = V^* - nQ$$

Where m, n are the droop parameters, and ω^*, V^* are the frequency and voltage references, P and Q are the measured active and reactive powers output.

In grid-connected mode:

$$\begin{aligned} \omega &= \omega^* - m(P - P^*) \\ V &= V^* - n(Q - Q^*) \end{aligned} \tag{2.9}$$

Where P^*, Q^* are the references of the expected exported active and reactive power, sequentially, and these profiles are sent by the MGCC.

Active P and reactive Q powers can be measured and averaged using low-pass filters (LPF) with reduced bandwidth [18].

Notice that the droop coefficients m and n can be calculated using the following equations:

$$\begin{aligned} m &= \frac{\Delta\omega}{\Delta P} \\ n &= \frac{\Delta V}{\Delta Q} \end{aligned} \tag{2.10}$$

Where $\Delta\omega$ is the maximum frequency deviation allowed (typically $\mp 2\%$), and ΔV is the maximum voltage amplitude deviation (typically $\mp 5\%$), and $\Delta P, \Delta Q$ are the nominal active and reactive power respectively.

Figure 2-5 shows the typical droop control diagram for a single-phase VSI.

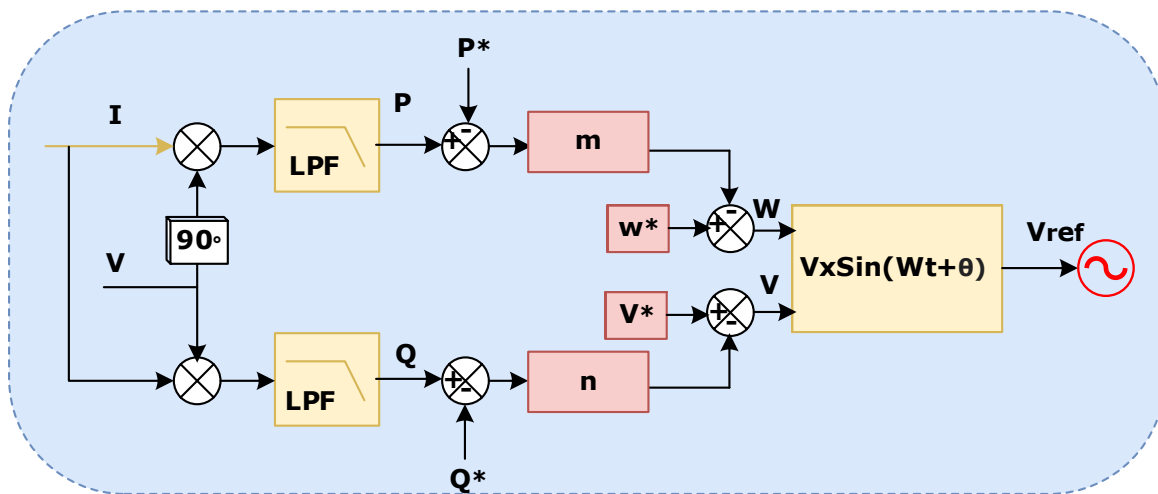


Figure 2-5: Diagram of droop control for single phase inverters

Table 2-1: Typical line impedance values

Line Type	R (Ω /Km)	X (Ω /Km)	R/X
Low voltage line	0.642	0.083	7.7
Medium voltage line	0.161	0.19	0.85
High voltage line	0.06	0.191	0.31

2.3 Virtual impedance and droop enhancement

In order to defeat the problem of power coupling and current sharing created by high R/X ratio in low voltage distribution systems as depicted in table2-1 [15], virtual impedance loops were suggested in the literature to increase the current sharing among the inverters by standard the output impedance of the inverters without needing supplementary physical inductors/resistors which increase size and cost. Thus, it alleviates the effect of the network and line impedances on the droop control [19]; the diagram of control associated with the droop control is illustrated in Figure 2-6.

Several approaches have been reported in this way, an adaptive virtual output impedance is proposed in [20] to improve reactive power-sharing, as well as the line impedance unbalances, including a soft starter operation to avoid the initial current peak, which results in a seamless hot-swap operation this approach allows the modification of the transient response by acting on the main control parameters.

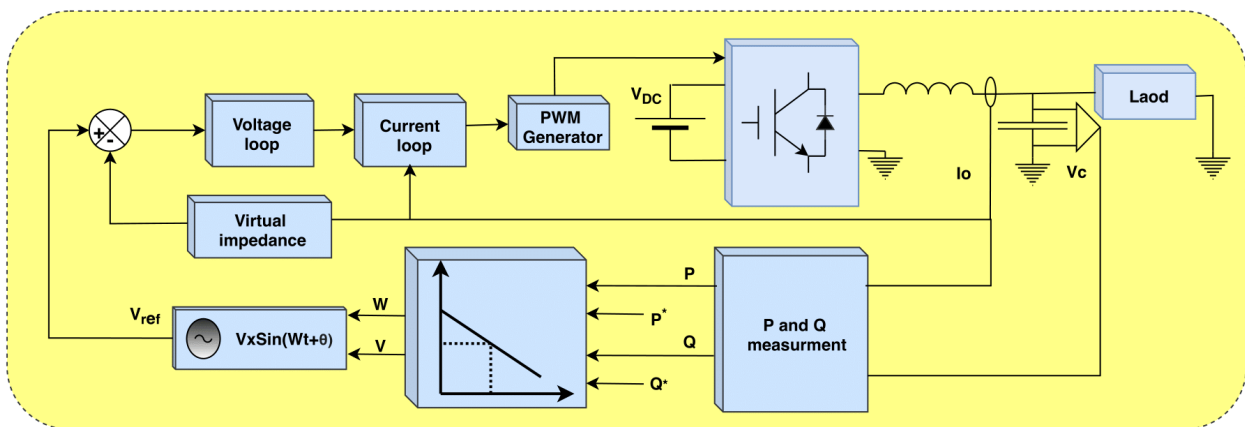


Figure 2-6: Multiloop control droop strategy with the virtual output impedance approach.

Similarly in [21], an adaptive droop control with virtual impedance is proposed in order to decouple real and reactive power functions; this approach helps to improve the load power-sharing efficiency among distributed generations (DGs) without needing knowledge of the line impedances. The

proposed approach is more adaptive to complex impedance situations, although the limitation is characterized by the reduction of the dynamic response with non-linear loads. Further, an enhanced virtual impedance is proposed in [22] to improve the reactive and harmonic power-sharing by using virtual impedance at the fundamental and selected harmonic frequencies. As a result, the accuracy of power-sharing and PCC voltage quality is improved. Likewise, a decentralized adaptive droop control with virtual impedances is proposed in [23]. The proposed control can operate either in islanded or grid-connected mode to enhance the power loop dynamics. Moreover, in [24] a comparison is shown between the impact of the resistive, inductive, inductive-resistive, and resistive-capacitive virtual impedance loops on the development of a single-phase MG. The virtual impedance loops have an inherent trade-off between current sharing and voltage harmonic distortion at the PCC when harmonic loads are connected to the MG. Resistive-capacitive virtual impedance loop achieves the most suitable trade-off among current sharing accuracy and voltage harmonic distortion which occurs at the PCC. The resistive-capacitive virtual impedance loop reaches the minimum voltage THD at the PCC of 2.11 % with the minimum current sharing variance of 10 % from the ideal current output, thereby indicating its effectiveness when compared to other virtual impedance techniques; further, a new droop control technic has been proposed in [25] in order to enhance the reactive power-sharing by injecting a small perturbation in the active power loop. A summary of droop control technics is illustrated in Table 2-2, showing the features and the disadvantages of each technic.

As mentioned previously, the line impedance difference between various inverters has a big impact on droop control and power-sharing accuracy. Therefore many enhancement has been reported in the literature: an adaptive droop-control method is presented in [26] which can decouple active and reactive power flow. This control method can serve in grid-connected and islanded modes, with an improved transient response unaffected by the grid-impedance magnitude and phase. In [27], an improved droop control method is proposed based on voltage compensation by measuring the real reactive power error between the local inverter. The main advantages of this approach are the high power-sharing accuracy, and it does not require any complicated algorithms or the value of the line impedance the robustness against communication failures even when the communication is interrupted. In addition, a QV' droop control method with V' restoration mechanism is proposed in [28] to improve reactive power sharing regardless of line impedance effect by adding a dynamic relationship between the converters reactive power output and its voltage amplitude output, which defeat the effect of line impedances on the reactive power flow. The main defects noted in this

method are the lack of reactive power-sharing accuracy with the increment of complexity and stability. In [29], a modified Q/V droop control is proposed for accurate reactive power-sharing based on the above-mentioned Q/V' droop control with the additional term. The deviation of the reactive power set point is eliminated by the proposed V' restoration technique and the reactive power sharing error can be further decreased by nearly 1%. In different cases, the line impedance has no influence on power-sharing. However, as the conventional Q V' droop control, the initial conditions may have a big influence in this case, notice that the system may be destabilized easily. Further, a generalized droop control (GDC) is presented in [30] to outline the active and reactive power effects on the voltage and frequency. The GDC provides simultaneous voltage and frequency control but it's extremely dependent on the line parameters, which makes the implementation of this technique more complex when the MG scales are adequately large (number of parameters, calculation time), to overcome this problem, an adaptive neuro-fuzzy inference system (ANFIS) based GDC is used to eliminate the influence of line parameters and MG structure. The main weak points of the proposed ANFIS are the poor voltage regulation and power-sharing accuracy; notice that the ANFIS is not tested for a nonlinear and unbalanced load. Another improved droop control strategy based on a changeable reference is proposed in [31] for compensating the frequency and improving active power sharing accuracy. This approach has high effectiveness and robustness. Unfortunately, it is applicable only for low MGs where the line resistance is predominant.

Table 2-2: Different droop control methods

Control	Concept	Advantage	Disadvantage
Classical Droop	<ul style="list-style-type: none"> ● P/W with Q/V slops 	<ul style="list-style-type: none"> ● No communication ● High reliability ● Not complex 	<ul style="list-style-type: none"> ● Voltage and frequency deviation ● P&Q coupling power control ● Slow dynamics response ● Circulating currents ● Line Impedance mismatch effect
Virtual Impedance Loop+Droop	<ul style="list-style-type: none"> ● Virtual impedance loop associated with conventional droop method 	<ul style="list-style-type: none"> ● Decoupling P and Q power control ● Less harmonics circulating currents ● Eliminate line Impedance mismatch effect ● Economic 	<ul style="list-style-type: none"> ● Poor reactive power-sharing ● Threat system stability

Adaptive Droop Control	<ul style="list-style-type: none"> ● Integral loop and adaptive droop control ● Derivative term with adaptive droop control 	<ul style="list-style-type: none"> ● Good dynamic response ● High power-sharing accuracy ● Smoothing power oscillation ● Less circulating current 	<ul style="list-style-type: none"> ● Circulating currents ● Complicated ● Threat system stability
Robust Droop	<ul style="list-style-type: none"> ● Robust droop control 	<ul style="list-style-type: none"> ● Good frequency and voltage regulation performances ● High reliability ● voltage drop restoration 	<ul style="list-style-type: none"> ● High total harmonic distortion of current components ● Poor reactive power-sharing accuracy

2.4 Virtual Inertia

inverter-interfaced DGs have very poor inertia, regrouping them as grid-following units in MGs can introduce frequency instability; in contrast, the conventional power system is mainly fed by synchronous generators (SGs), which usually have a kinetic energy tank in the rotating mass, inertia can temporarily provide additional energy supply with quick response, thus maintaining transient frequency during transient power disturbances [32]. The transition toward inverter-dominated power systems, as depicted in Figure 2-7, brings more challenges for control technics.

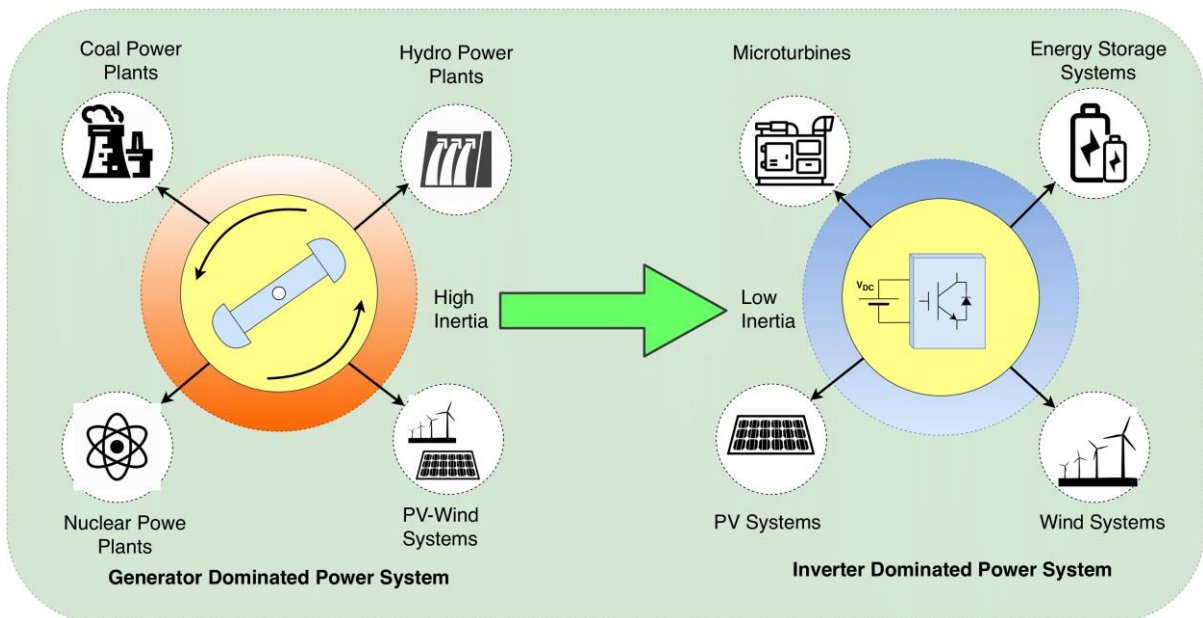


Figure 2-7: The transition towards an inverter-dominated power system

Traditional voltage-source-based grid-supporting control strategies only copy the steady-state output characteristics of a synchronous generator (SG) (e.g., droop control) where they are unable

to provide sufficient inertia aid to face large disturbance as the connection of an important load or a ground fault. The frequency of the MG may deviate too quickly to be preserved inside the tolerance by frequency restoration control. To address this problem, a modified droop control method is proposed in [33], where the droop gain is modified based on the df/dt observed by the inverter during the transition. This approach can diminish the short-term storage requirements of a MG where frequencies are a major constraint. Another approach called virtual synchronous generator (VSG) control is studied and compared with droop control in [34] for both stand-alone mode and grid-connected mode. The only difference between the two approaches is that VSG has virtual inertia with the emulation of the swing equation, while droop control has no inertia. However, droop control can be viewed as a particular case of VSG control if inertia, parameter, and damping factor are set to zero. The main results of this comparison are VSG has larger inertia than droop control and, therefore, better frequency stability. The active output power of droop control is less oscillatory than that of VSG, but this problem can be fixed by tuning the damping factor and/or the output reactance. Likewise, a small-signal model of VSG is estimated by a droop control with a well-designed first-order lead-lag unit in P droop. This modified droop control, which can be named inertial droop control, suggests that VSG control and proposed inertial droop control inherit the advantages of droop control, and besides, provides inertia support for the system. Further, an extended virtual synchronous generator is developed in [35] to increase inertia and damping it consists of merging the concept of the virtual rotor, virtual primary, and virtual secondary control as a virtual controller to stabilize and adjust the system frequency. An H robust control method is proposed in [35] for optimal tuning of the virtual parameters. This correlating is a functional and suitable approach to the optimal and robust designing of the VSG parameters. The virtual controller presents a superior performance in the presence of high-uncertainty circumstances and extreme disturbances. In [36], based on adaptive virtual inertia, a virtual synchronous generator control is proposed to enhance the transient frequency regulation of the AC MG, when the system frequency deviates happens, the adaptive inertia control presents large inertia to slow the transient process and thus attenuate the frequency deviation. On the other hand, when the system frequency begins to restore, small inertia is adjusted to accelerate system dynamics with a fast transient process. Thus, this flexible inertia adaptive property combines the merits of large inertia and small inertia, which contributes to the enhancement and support the dynamic frequency response.

2.5 Hierarchical Control

The major causes of developing a hierarchical control are to provide smartness and flexibility to MGs [37] by distributing the control responsibilities over levels as represented in Figure 2-8, which help to decouple the control parameters as well as establishing a management system for frequency and voltage compensation [38].

For power flow direction and power-sharing, a global hierarchical multilayer control for DC and AC MGs is presented the first time in [37] by considering three levels illustrated follow:

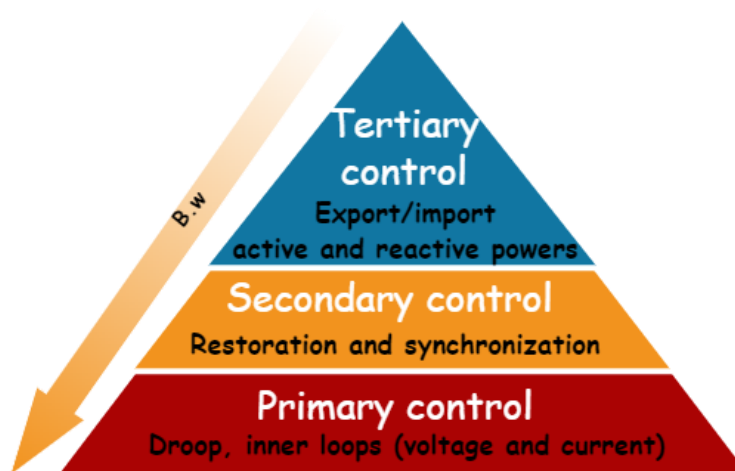


Figure 2-8: Hierarchical control of microgrid.

- The primary control is based on the droop method, which allows the parallel connection of different power sources, hence sharing loads wirelessly [39]. Besides the voltage and current regulation in terms of a defined reference, including a virtual output impedance loop for increasing the droop features especially active power sharing accuracy.
- The secondary control is responsible for eliminating the deviations produced by the primary control for both frequency and voltage it can include a synchronization control loop to ensure a seamless transition between operation modes (grid-connected or islanded). Also, islanding detection can be included in this level [37] [40].
- The tertiary control is the highest and slowest control layer in the hierarchical control, referring to the time scale in Figure 2-9. It takes the power flow management task by importing and exporting the active and reactive power from/to the external electrical distribution system [41].

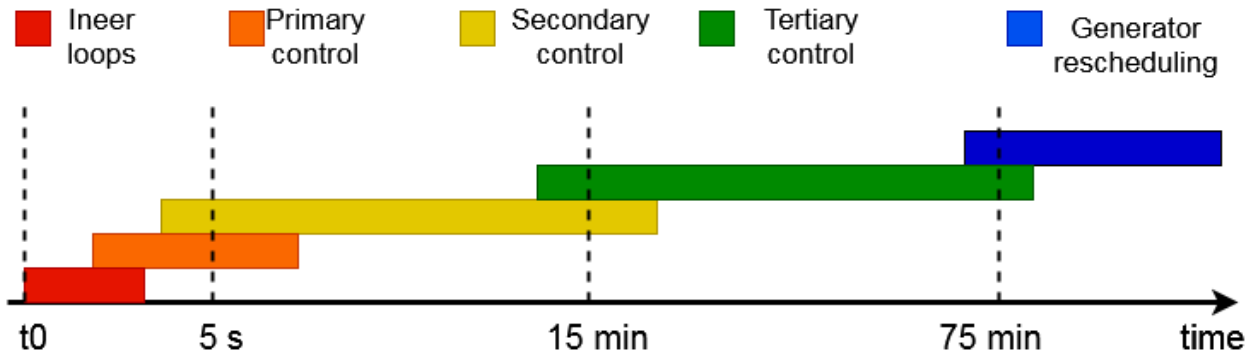


Figure 2-9: A typical time-scale of frequency-related dynamics in conventional

Notice that the bandwidth must be reduced with an increase in the control level to guarantee that the command and reference signals from the highest level to the lower levels will have a low effect on the stability and robustness performance [37].

Hierarchical control structures can be divided into three structures as reviewed in [42] [43] and exposed in Figure 2-10 based on how the supervisory control system (secondary control), is designed in a centralized or distributed structure, or a hybrid structure composed by combining both structures mentioned previously.

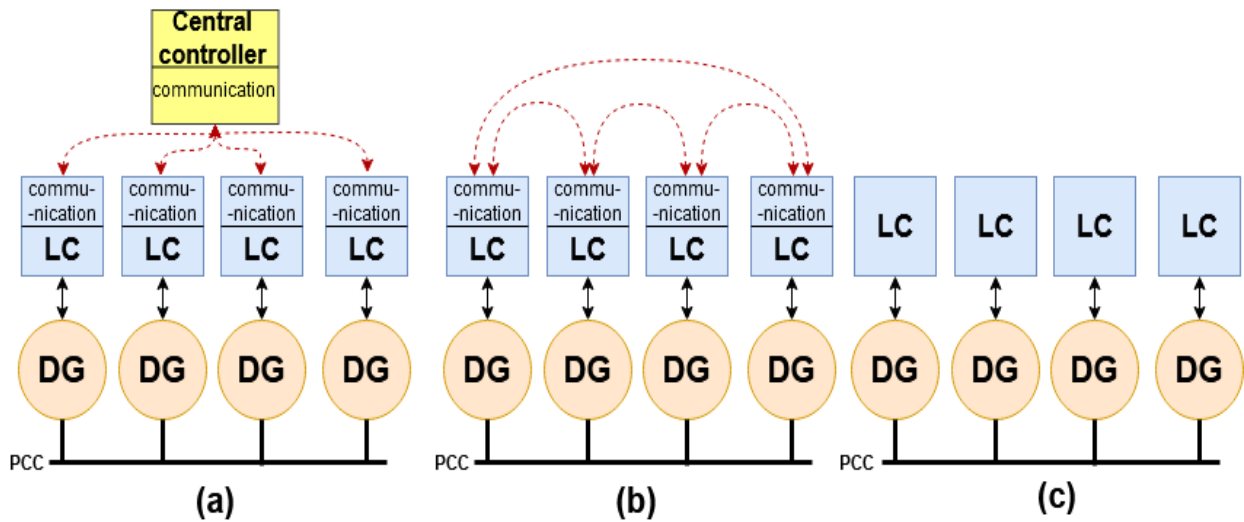


Figure 2-10: Hierarchical Control Structures.

2.5.1 Centralized Secondary Control

In the centralized approach for secondary control, the MG is managed and optimized by a central supervisor controller called the MG central controller (MGCC) [44]. This latter collects all the measurements and provides set points for local controllers. Hence this bidirectional communication between MGCC and local controllers ensure a reliable and efficient operation of the MG by regulating

the voltage and frequency, and also managing the active and reactive power, which allows an optimal operation and monitoring of the system [45]. However, the need for communication and remote measurement threat the system stability through time delays and data drops, which degrade the power quality as well as communication failure can interrupt the electricity supplying. Recently a PI-CSC has been developed in [46], where the CSC is implemented utilizing LabVIEW; similarly, a CSC is designed and implemented in [38] with the stability analysis. A CSC approach is presented in [47] for unbalanced voltage and harmonics reduction in the PCC, aiming to limit the computation resources, a cooperative CSC is presented in [48] based on an event-triggered approach which means fewer controller updates are required. A CSC with a super-high bandwidth is proposed in [49]. Moreover, a CSC based on the second-order generalized integrator-based frequency-locked loop (SOGI-FLL) is implemented and tested under different operating conditions in [50]. Artificial intelligence has been introduced in CSC as described in [51]. In this study, an online ANN tuning approach is applied to the system to update the secondary controller's gains; it has the advantages of good performances under load changes and disturbance out of the operating point and the independence of human interaction. Another approach is developed in [52], based on a fuzzy-PI to coordinator between the demand response and secondary frequency control for limiting the frequency overshoots/undershoots owing to communication delays, as shown in [53]. Further, the communication delays effect is addressed in many papers: in [54], the authors suggested a retuning and modifying of controller parameters. Similarly, to deal with this issue, a model predictive controller (MPC) and a smith predictor-based controller are proposed in [55], where the MPC approach has the disadvantage of the slowly dynamic response compared to the smith predictor technic.

2.5.2 Distributed Secondary Control

Numerous distributed secondary control approaches for MGs have been shown in the literature; the distributed approach proposes communication between MG units for enhanced reliability, security, optimality, independence, and intelligence [43]. Where these units can take decisions cooperatively by interacting with each other to reach the best-evaluated solution based on local measurements and the sharing of information without any central control [56]; distributed control techniques are grouped into averaging distributed consensus and event-triggered methods. multi-agent system [43].

2.5.2.1 Average-based DISC

This approach consists of calculating the average values of voltage and frequency amplitude, starting with the local measurements of these parameters for all DGs units and then sharing them using

communication to generate the control signal to transfer to the primary layer eliminating the steady-state errors [57] [58], ref [59] presented an average based DISC and performed it experimentally. An enhanced DISC is introduced in [60] using localized information and nearest-neighbour communication to achieve secondary control actions with fast dynamics and retain of the active power-sharing.

2.5.2.2 Consensus-based DISC

In the literature, consensus usually refers to algorithms pointing to the agreement between all DGUs, the robustness of this technique is established in several researchers' works even in the presence of communication delays. With the target of compensating the voltage and frequency in the MG, consensus-based techniques are widely used in the last years. A PI-consensus-based DISC is presented in [61] it has the advantages of simplicity and higher control accuracy under disturbances and communication delays. Another optimal DISC is designed in [62] taking into account the network design, convergence performance, network-relevant time delays, and communication costs a multi-objective optimization criterion is suggested, and the robustness of this technique is proved by simulation results. Moreover, a DISC-based model predictive control is proposed in [63] where the secondary voltage control is converted to a tracker consensus problem of distributed MPC, similarly, ref [64] proposed a distributed consensus optimization of inertia for fast-frequency, besides, a DISC based-consensus protocol is proposed in [56] it has the ability to work in both grid-connected modes.

2.5.2.3 Event-triggered DISC

Recently a vast amount of literature discussed the event-triggered control technic to reduce the computation burden; this approach has been increasingly used at the SC layer of MG, due to the reduced information exchange between DGUs during maintaining stability [65] within continuous data exchange among DGUs, the desired data can be shared when a condition is achieved, or an event is triggered. Hence, a sampled-data control method is executed, and data is exchanged by a predefined mechanism on ETC [66]. An event-triggered distributed model predictive control (DMPC) is introduced in [67] based on two event-triggering conditions; this approach reached reduced computation and communication burdens with maintaining the good performances of the dynamic system, ref [68] developed a hybrid-triggered mechanism-based DISC where the reduction of computational and communication burden is proved. Moreover, a distributed optimal frequency regulation is studied in [69] using an event-triggered mechanism for the regulation algorithm building .further, based on the Lyapunov stability analysis approach, an event-triggered consensus algorithm

is investigated in [70], which can support the plug-and-play function within the established communication topology.

According to [71] centralized topologies generally have a higher performance and are more suitable for large MGs than distributed ones. Likewise, this latter has a more reliable control system, a simple control algorithm, and less expensive control hardware.

2.5.3 Decentralized Secondary Control

Communication links in secondary control reduce the reliability of the MG system; in case of a single failure, it will affect the stability. Hence new technics which do not need any communication have emerged. To enhance the resilience of MGs and drop out of the communication network, the decentralized technics have been divided into three groups according to [43].

2.5.3.1 Local Variable, MPC, and time-dependent protocol-Based DESC

latterly, several papers have proposed DESC technics fully using different methods in islanded MGs [60], a secondary switched control with no communications is presented in [72]. Based on a time-dependent protocol to switch between two control configurations; however, the time-dependency increases the complexity of the solution and threatens the system's stability and resiliency. Similarly, a local frequency restoration is designed in [73] which is based on load or generation change detection. After that, a control action following a time-driven protocol is scheduled, another decentralized frequency restoration technic is developed in [74] by improving the frequency rate with a constant and adopting only local information. Further, a decentralized model predictive SC is presented in [75] utilizing a controlled auto-regressive moving average (CARMA) model, which is enhanced the dynamic response and the power quality. Moreover, a decentralized optimal frequency is designed in [76] with the advantages of being simple and optimal and easy to implement without the need for switch control or event-driven protocol and no time-dependent; authors in [77] present a decentralized adaptive frequency restoration by adding a new term of power derivative to droop this technic can compensate the frequency deviation. However, the settling time of this is too slow; a decentralized, scalable, robust voltage control is proposed in [78]. It has the advantages of maintaining the system stability and presents good performance against disturbances and load changes also the adaptability with the plug-and-play functionality.

2.5.3.2 Estimation-Based DESC and DIESC

Recently numerous papers have proposed a DESC for AC islanded MGs based on state estimation due to their communication-free feature, the distribution system state estimation (DSSE) has been

introduced in [79] for enhancing the robustness, and system observability, in ref [80] a DESC was proposed based on load power demand estimation which is used to change automatically the bias of the droop characteristics to regulate the voltage and frequency deviation, another method was designed in [81] based on adaptive state estimator to obtain the dynamic response of the whole system which provides for all units their own information. Similarly, based on the large-signal model to obtain the other unit dynamics, a non-linear state estimator is developed in [82]. Moreover, a state observer based on KALMAN filter theory to estimate reactive power and system voltages are presented in [83], where the calculation burden of the estimator is reduced due to the reduced model, despite the communication-free feature, the estimation based technics still depend on the MG topology to inform the dynamics of others DGs to the local units which make it not adaptable in case of topology changes. Likewise, one of the most interesting approaches has been proposed by [84] using a consensus protocol and based on the unique feature of frequency as a global variable in stand-alone MGs; this latter is used to estimate others DGs units active power which provides an accurate active power-sharing, the advantages of this approach compared to the aforementioned techniques is the reduced computational burden and it's less complicated.

Distributed estimation secondary control DIESC has been addressed in [85]. This approach consists of maintaining the equilibrium between generation and demand-side by estimating the difference of active power using a finite time consensus protocol which allows the frequency restoration, another estimator distributed technic based on predictive voltage control is presented in [86]. Regardless of the advantages of DIESC they still need communication which affects the whole system in case of interruption.

2.5.3.3 Washout Filter-Based DESC

Installed locally with droop control, the washout filter is considered as an equivalent SC; this approach is communication-free, and it has the advantage of making the voltage and frequency robust against load changes [87]. Moreover, a generalized washout filter control scheme is proposed in [88] compared to the last one; this approach has the advantage of improved transient response under load and feeder perturbation and reduced overshoot in the output voltages in case of dynamic disturbances. Similarly, a second-order washout filter-based power-sharing for UPS systems is designed in [89] to enhance the dynamic response under load by adding a lead filter.

The aforementioned technics are recapitulated and classified in Table 2-3, presenting their concept, advantages, and disadvantages.

Table 2-3: Summerise of different secondary control technics

Control	Concept	Advantage	Disadvantage
Centralized Secondary Control	<ul style="list-style-type: none"> ● Central Controller 	<ul style="list-style-type: none"> ● Active and reactive power management ● Harmonic cancellation ● Real-time monitoring of the system ● Unbalanced current reduction 	<ul style="list-style-type: none"> ● any failure in Communication infrastructure or CSC affects the overall MG system ● Communication delays and data drop
Distributed Secondary Control	<ul style="list-style-type: none"> ● Average-based DISC ● Consensus-based DISC ● Event-triggered DISC 	<ul style="list-style-type: none"> ● Robust to single-point-failures ● Easy to implement (An embedded controller is enough) ● flexibility and redundancy ● less expensive control hardware ● Higher control accuracy under disturbances and communication delays ● Simple control algorithm ● Easy to implement ● Plug-and-play operation ● Robust to single-point-failures ● Reducing the recomputation and communication ● support the plug-and-play function ● Easy to implement ● Robust to single-point-failures 	<ul style="list-style-type: none"> ● Communication complexity ● Clock drifts ● Voltage stability and reactive power-sharing ● Communication infrastructure ● Reducing the recomputation and communication ● Voltage stability and reactive power-sharing ● Communication infrastructure ● Clock drifts ● Voltage stability and reactive power-sharing ● Zeno Phenomenon ● Communication infrastructure

Decentralized Secondary Control	<ul style="list-style-type: none"> ● Washout Filter-Based DESC 	<ul style="list-style-type: none"> ● Fully decentralized ● Low complexity ● Easy to implement 	<ul style="list-style-type: none"> ● Steady-state error ● slow dynamic response
	<ul style="list-style-type: none"> ● Local Variable-Based DESC 	<ul style="list-style-type: none"> ● Fast active power responses ● Communication-free 	<ul style="list-style-type: none"> ● Increase complexity ● Time-dependent ● slow dynamic response
	<ul style="list-style-type: none"> ● Estimation-Based DESC 	<ul style="list-style-type: none"> ● Communication-free ● Precise active and Reactive power-sharing independently 	<ul style="list-style-type: none"> ● Depend on the modeling of the system ● High computational burden

2.6 Small signal modelling and reactive power-sharing

Droop control is widely considered to be the most important wireless strategy because it has the ability to adjust the voltage and frequency at the same time, sharing the power demands among parallel generation units without any need for external communication among inverters [16]. However, non-accurate power sharing is observed in complex MGs (complex impedance) [90], especially reactive power due to the lack of the decoupling ability of droop control. Hence, the efficiency and stability of the MG are easily affected by the uncontrollable coupling of the distributed generation units. Moreover, large power circulating-currents between parallel inverters were reported in [91]. This issue is considered a common drawback of the existing droop control methods.

In the literature, many ways have been suggested to reduce power-sharing errors. One of the simplest is the virtual impedance loop, which is used to change the system's impedance and make power-sharing independent of the real impedance. To enhance the system stability and restrict the power couplings, a virtual impedance design and an implementation method were first proposed in [19]. The improved virtual impedance control approach was used in [20] for better power-sharing performance. It can achieve accurate regulation of DG unit equivalent impedance at both fundamental and selected harmonic frequencies. Furthermore, the feasibility of virtual impedances was discussed in [92] through the implementation of different virtual impedances and analyzing their issues. Virtual admittance was introduced in [93] as a way to share harmonic currents and reduce

transmission losses. It has the advantage of being applicable to any inverter topology and/or mode of operation, including VSI-VCM and VSI-CCM. Further, an optimized virtual impedance controller was employed in [94] to prevent reactive power-sharing errors. The main idea was to estimate the network's reactive power-sharing errors based on local load measurements. The systematic method to determine the feasible interval and optimal value of the virtual impedance was developed in [95]. The authors developed a systematic method for determining the feasible interval and optimal value of the virtual impedance while taking into account power decoupling, reactive power sharing, system damping, and node voltage status. The adaptive virtual impedance was proposed in [23]. This approach uses real and reactive power mismatches to serve as an input for the integral controllers and then elaborates the virtual inductive and resistive components. An improved droop control strategy via integrating coupling compensation and virtual impedance loops is proposed in [96]. The coupling compensation includes angular frequency deviation compensation and voltage deviation compensation, which reduces the influence of uncontrollable coupling. A MG model including virtual impedances and phase-locked loop (PLL) is introduced in [97]. The virtual impedances were optimized using PSO, this approach maximizes the MG stability index and minimizes the reactive power mismatches. In [98], a dq-frame asymmetrical virtual impedance was discussed to prevent the GFM inverters from losing synchronization in grid-connected mode under high disturbances.

However, due to the lack of inertia in such systems, the unpredictability and variation of the output power of renewable energies (RES) caused by intermittency and load consumption changes, small perturbations, such as transient power impact, voltage and frequency deviations, overshoots, and transient oscillations, can easily threaten dynamic stability [99]. Small-signal stability analysis can be used to evaluate MG stability around the equilibrium operating point; several parameters, such as power controllers, voltage and current controller coefficients, and LCL filter parameters, are important in MG stability [100], [7], [101]. A small signal state-space model of the entire MG from droop controller to network and loads was derived in [102] and the stability ranges of key parameters were defined, which have a high effect on the damping frequency of oscillatory components in the transient response. The modified droop control was proposed in [103] to enhance the dynamic response and stability margin. As a result of this study, the lack of stability of inverters prevents the use of higher droop parameters. In addition, the effect of reconfiguration and network type (mesh/radial) on the small-signal stability margin is analyzed in [104] for an autonomous MG. It is noted that the reconfiguration and network type have a significant impact on the small-signal stability

margin. An evaluation of MG stability under different active power sharing conditions was performed in [105] using small signal stability, and optimal droop gains were used to improve the stability. Although the internal model-based current and voltage controllers were compared to conventional PI controllers by using a state-space model and performing eigenvalue analysis on an islanded inverter [106]. Further, the parametric uncertainties were studied in [107] using a small signal stability strategy. Using lead compensators cascaded in series for real power-frequency droop control in [108] resulted in an improvement in the MG small-signal stability. Likewise, the generalized theoretical framework for small-signal stability analysis was proposed in [109], where the generator and load frequency-domain characteristics, primary and secondary control loops, as well as communication latency, were synthesized. The effect of the time constant and the droop constant on small signal stability for autonomous MGs was investigated in [110], and it is observed that high values of these parameters could lead to unstable operation regions. In contrast, the MG is robust to variations of cable length, power factor, and scenarios of generation. Comprehensive small-signal stability analysis for SG-based MGs was developed in [111] in order to assess the effect of loading conditions on the small-signal stability of droop-controlled and PQ-controlled SGs, and it is observed that droop-controlled SGs present less stability or even instability in light loading conditions. In contrast, the presence of PQ-controlled SGs in the presence of droop-controlled SGs can result in better stability of SG-based MG at light loading conditions. The eigenvalues analysis and parameter optimization for islanded MG using small-signal stability were proposed in [112], and it was discovered that wide range parameter optimization can significantly improve stability. A novel technique to assess the small signal stability based on state space and graph theory was proposed in [113], which allows the reduction of the computational burden of high-dimensional system. Furthermore, it is capable of coping with the uncertain parameters and system structure. Based on an optimized nonlinear droop relation, a complete small-signal state-space model of the MG system was developed in [114] considering the dynamics of the overall system and is updated periodically. The PSO algorithm was adopted for the optimization.

2.7 Conclusion

The state of the art of MG's modelling and control has been reported in this chapter, starting with the definition of the MG concept, and after that, the most used control technic for parallel inverters. Droop control is well explained with its advantages and drawbacks. The droop control enhancement and the virtual impedance approaches are reviewed. The virtual inertia concept for more grid-

forming MG is illustrated and reviewed. The hierarchical control with its three layer of control is discussed with more focus on the secondary control with its three topologies of control. Finally, the small signal modelling and the reactive power-sharing technics to reduce the power mismatch caused by the different line structures is reviewed.

Chapter 3: Modelling, Analysis, and Design of Hierarchical Controlled Parallel Three-Phase Voltage Source Inverters based MG

3.1 Introduction

This chapter focuses on modelling, analysis, and design of hierarchical controlled parallel three-phase voltage source inverters in islanded MG. A mathematical model for the three-phase VSIs based on a synchronous reference frame is developed. The voltage and current controllers consist of two feedback loops an outer feedback loop of the capacitance-voltage and an inner feedback loop of the output inductance current. The outer voltage loop is employed to enhance the controller response speed and to minimize the steady-state error. The inner current loop is used to provide active damping for the resonance created by the LCL filter. The hierarchical control scheme is adopted for the MG control including two layers of control to achieve a high level of reliability, stability, and power quality. The primary control involves the use of the droop method and virtual impedance loops to share active and reactive power, while the secondary control restores frequency and amplitude deviations caused by the primary control. Additionally, a synchronization algorithm is proposed to connect the MG to the grid. The performance and robustness of the MG hierarchical control architecture are demonstrated through simulation results.

3.2 Description and modelling of the power system

In a power-electronic interfaced MG, DG units are equipped with voltage source inverters (VSI) which can operate in stand-alone and grid-connected modes of operation. VSIs are the block stone of MG, VSI's used as an interface between distributed generators and loads, their main role is to convert the dc power into ac power and supply the entire MG. The VSIs are controlled by the pulse width modulation (PWM) signals which generate harmonic components that decrease the power quality. Thus filters are required to mitigate harmonics and avoid disturbance caused by this latter to not affect the other loads which lead to enhancing the power quality of the whole system. The current harmonic limitations are defined in [115], and to reach the recommended limitations, the LCL filter is considered to be the most adapted topology for its cost due to the reduced size of the passive elements and its high capability to attenuate the high-frequency harmonics, for better quality MG current [116]. The LCL topology is adopted in this work as can be seen in Figure 3-1 the inverter is associated with the LCL filter to form the VSI. A mathematical model of the VSI will be developed in

the next section to help for designing the cascade loops of the zero layer which contains the voltage and the current compensators.

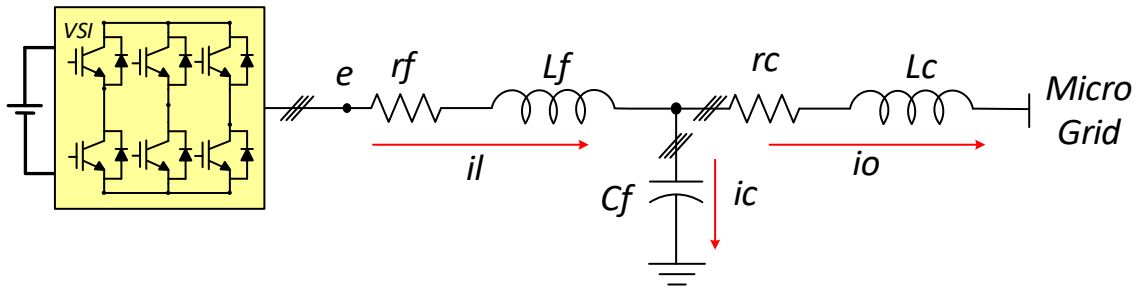


Figure 3-1: Three-phase inverter single line diagram interfaced using LCL filter

3.3 Mathematical models of the VSI

By applying Kirchhoff's current law on the circuit in Figure 3-1, the relation between the currents flowing through the LCL filter can be described by:

$$i_{f,abc} = i_o + i_c \quad (3.1)$$

And by applying Kirchhoff's voltage law, the voltages can be described by the following equations:

$$e_{abc} = r_f i_{l,abc} + L_f \frac{di_{l,abc}}{dt} + v_{o,abc} \quad (3.2)$$

$$\frac{dv_{o,abc}}{dt} = (1 / C_f) i_{c,abc} \quad (3.3)$$

$$v_{o,abc} = r_c i_{o,abc} + L_c \frac{di_{o,abc}}{dt} + V_{PCC,abc} \quad (3.4)$$

With

e_{abc} : Inverter output voltage

L_f : Output inductance inverter side

r_f : The equivalent series resistance

$i_{l,abc}$: The current flowing through the L_f inductance inverter side

$v_{o,abc}$: Capacity voltage

C_f : Filter capacity

$i_{c,abc}$: Current flowing through the capacity

L_c : Output inductance grid side/coupling inductance

r_c : The equivalent series resistance

$i_{o,abc}$: The current flowing through the L_c inductance grid side

$V_{PCC,abc}$: The voltage at the point of common coupling PCC

The inverter output voltages e_{abc} are obtained through the switching devices (IGBTs) using the PWM technic. The switching frequencies generate harmonics that are attenuated using the LCL filter which acts as a low-pass filter.

A dq transformation is used to transform the system from the natural ABC frame to the dq synchronous reference using Park transformation.

After transformation and rearrangement using the Park transformation, the relationship between currents in the dq frame is given by:

$$\begin{cases} i_{ld} = i_{od} + i_{cd} \\ i_{lq} = i_{oq} + i_{cq} \end{cases} \quad (3.5)$$

And the transformed voltage equations are given by:

$$\begin{cases} e_d = L_f s i_{ld} + r_f i_{ld} + v_{od} - \omega L_f i_{lq} \\ e_q = L_f s i_{lq} + r_f i_{lq} + v_{oq} + \omega L_f i_{ld} \end{cases} \quad (3.6)$$

$$\begin{cases} i_{cd} = C_f s v_{od} - \omega C_f v_{oq} \\ i_{cq} = C_f s v_{oq} + \omega C_f v_{od} \end{cases} \quad (3.7)$$

$$\begin{cases} v_{od} = r_c i_{od} + L_c s i_{od} + v_{PCCd} - \omega L_c i_{oq} \\ v_{oq} = r_c i_{oq} + L_c s i_{oq} + v_{PCCq} + \omega L_c i_{od} \end{cases} \quad (3.8)$$

Where ω is the MG frequency and s is the Laplace operator.

By substituting (3.7) in (3.5), and after the rearrangement, we obtain:

$$\begin{cases} \dot{i}_{ld} = C_f s v_{od} - \omega C_f v_{oq} + i_{od} \\ \dot{i}_{lq} = C_f s v_{oq} + \omega C_f v_{od} + i_{oq} \end{cases} \quad (3.9)$$

3.4 Voltage and Current Loops

For the voltage and current controllers, a cascade loop has been used; the current loop must have the fastest response and hence the highest bandwidth. The voltage loop must be slower than the current loop and it must be quick enough to guarantee that the system operates properly, a PI controller has been employed for both regulators. This choice has been made due to the straightforward design of the PI controller gains and the simplicity of modelling it in dq reference frames for developing a small-signal model for MG in the next chapter.

3.4.1 Current loop model

The current loop state space model can be modelled as follows:

$$\begin{cases} \dot{X}_I = A_I X_I + B_I U_I \\ Y_I = C_I X_I + D_I U_I \end{cases} \quad (3.10)$$

Based on the equation (3.10) and (3.6) the state space representation of the current loop is described as follows:

$$s \begin{bmatrix} i_{ld} \\ i_{lq} \\ i_{l0} \end{bmatrix} = \begin{bmatrix} -\frac{r_f}{L_f} & -\omega & 0 \\ \omega & -\frac{r_f}{L_f} & 0 \\ 0 & 0 & -\frac{r_f}{L_f} \end{bmatrix} \begin{bmatrix} i_{ld} \\ i_{lq} \\ i_{l0} \end{bmatrix} + \frac{1}{L_f} \begin{bmatrix} e_d - v_{od} \\ e_q - v_{oq} \\ e_0 - v_{o0} \end{bmatrix} \quad (3.11)$$

The system (3.11) is assumed to be balanced, which means that the homopolar sequence is nul and the rest of the current loop model is written as follows:

$$S \begin{bmatrix} i_{ld} \\ i_{lq} \end{bmatrix} = \begin{bmatrix} -\frac{r_f}{L_f} & -\omega \\ \omega & -\frac{r_f}{L_f} \end{bmatrix} \begin{bmatrix} i_{ld} \\ i_{lq} \end{bmatrix} + \frac{1}{L_f} \begin{bmatrix} e_d - v_{od} \\ e_q - v_{oq} \end{bmatrix} \quad (3.12)$$

The terms $\omega L_f i_{lq}$ and $\omega L_f i_{ld}$ in equation (3.6) represent a coupling between the two equations e_d and e_q . In other words, a variation of the current i_{ld} will create a variation of the current i_{lq} and vice-versa.

3.4.2 Voltage loop model

The voltage loop state space model can be modelled as follows:

$$\begin{cases} \dot{X}_V = A_V X_V + B_V U_V \\ Y_V = C_V X_V + D_V U_V \end{cases} \quad (3.13)$$

Based on equations (3.13) and (3.9) the state space representation of the voltage loop is as follows:

$$s \begin{bmatrix} v_{od} \\ v_{oq} \end{bmatrix} = \begin{bmatrix} 0 & -\omega \\ \omega & 0 \end{bmatrix} \begin{bmatrix} v_{o,d} \\ v_{o,q} \end{bmatrix} + \frac{1}{c_f} \begin{bmatrix} i_{ld} - i_{od} \\ i_{lq} - i_{oq} \end{bmatrix} \quad (3.14)$$

3.5 Inner loops control design

The objective of any control system is to shape the response of the system according to a given reference and to maintain the stability of the system in the closed loop, with the desired performance, while minimizing the effect of disturbances, measurement noise, and avoiding the saturation of controllers, despite the uncertainties of modelling, variations of parameters or change of the operating point. The control diagram in Figure 3-2 consists of an external voltage loop which provides the current reference and an internal current loop that provides the signals for the PWM block. This type of control is called multi-loop voltage control or cascade control. It is usually chosen for current and voltage control of VSI's MG's due to its superior disturbance rejection performance and current limiting capability [117].

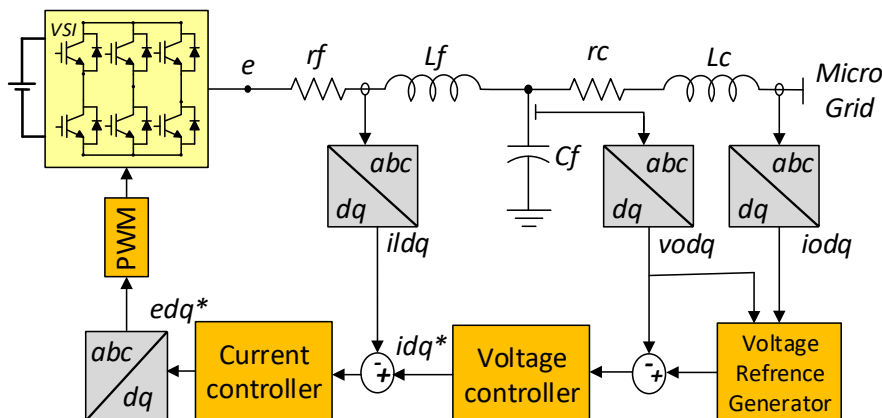


Figure 3-2: Inner loops (voltage and current controllers)

When using the grid forming configuration, the voltage and frequency references are offered by the local controller such as droop control.

3.5.1 PI controller:

The classic PI (proportional, integral) controller is the most used technique for several decades in various applications, in particular for inverters current-controlled because of its simplicity and straightforward implementation. However, it is considered an unsatisfactory solution for alternative current regulation due to large steady-state tracking errors. This error can be reduced by increasing the PI gain and bandwidth, unfortunately, it also pushes systems towards their stability limits. The PI controller can be adaptively combined with artificial intelligence technics such as fuzzy logic, neural networks, etc. to increase its robustness and adaptation [118].

3.5.2 Current loop design:

The current control loop is responsible for the characteristics of the injected current. It is highly desirable that the inverter current be free of low-order harmonics. High-frequency harmonics can be eliminated with the LCL filter. Current control for the inner loop is developed using standard feedback control. The current control can be expressed by the following system of equations:

$$\begin{cases} e_d^* = (k_{pc} + k_{ic} / s)(i_{ld}^* - i_{ld}) - \omega L_f i_{lq} + v_{od} \\ e_q^* = (k_{pc} + k_{ic} / s)(i_{lq}^* - i_{lq}) + \omega L_f i_{ld} + v_{oq} \end{cases} \quad (3.15)$$

Where: e_d^* and e_q^* are the d and q axis components of the voltage modulation signals, respectively; i_{ld} and i_{lq} are the values of the inductance current for the d and q axis components, respectively; k_{pc} and k_{ic} are the proportional and Integral PI regulator parameters for current control. L_f represents the inductance of the filter inverter side.

Figure 3-3 shows the detailed diagram of the current control loop. It should be noted that all the current control loops, all signals in the loop feedforward and the feedback loop are direct quantities [119]. The control of the current loop is achieved by the following steps:

- 1- The current references i_{ld}^* and i_{lq}^* of the dq axes are compared to their measured current values i_{ld} et i_{lq} according to the following equations $e_{id} = i_{ld}^* - i_{ld}$ and $e_{iq} = i_{lq}^* - i_{lq}$, respectively.

- 2- The error between the two values of the current i_{id} and i_{id} of the two axes d and q passes through the controller of the internal control loop which is represented by the $Ki(s)$ to generate U_{id} and U_{iq}
- 3- The PWM input signals ed^* and eq^* components are produced by $ed^* = U_{id} + V_{id} + V_{od}$ et $eq^* = U_{iq} + V_{iq} + V_{oq}$ where V_{id} and V_{iq} are two signals that allow the decoupling of the control loop between the direct i_{id} and quadrature i_{iq} currents; similarly V_{od} and V_{oq} are two supplementary signals added to suppress their impact on the current loop.

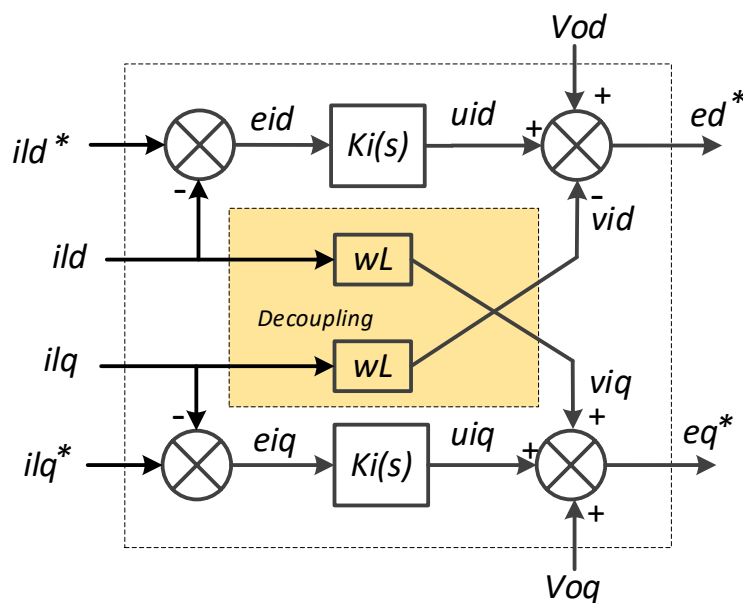


Figure 3-3: Block Diagram of Current Controller Loops

3.5.3 Synthesis of the current loop PI controller

The transfer function of the d component of the current loop is identified by:

$$\frac{i_{id}(s)}{e_{id}(s)} = \frac{1/L_f}{s + r_f/L_f} \quad (3.16)$$

With $ed^* = ed$

For the inner loop current regulator, the following properties are desirable[120]

- 1- fast transient response with minimal overshoot
- 2- precise current control

- 3- zero static error in steady state
- 4- less sensitivity to parametric uncertainties of the system

In order to decouple the dynamics of the loops, the internal loop (current loop) must be designed to have faster dynamics compared to the outer loop (voltage loop). Also because the dynamic current is much faster.

From Figure 3-3 it can be considered that the two current control loops of the two axes d and q are similar; thus the corresponding controllers can also be identical. Since the switching frequency is significantly higher than the line frequency, sample delays can be neglected in controller synthesis [121].

In Figure 3-4, $K_i(s)$ is the PI controller, i_{ld}^* is the current control signal and i_{ld} is the measured current.

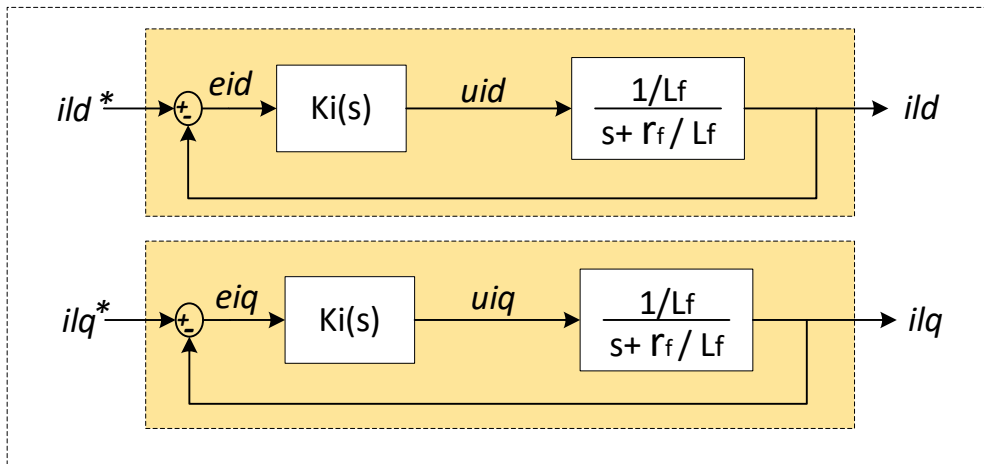


Figure 3-4: Block diagram of the closed-loop control for current

The transfer function of the current PI regulator is:

$$K_i(s) = k_{pc} + \frac{k_{ic}}{s} \tag{3.17}$$

From the block diagram in Figure 3-4, the closed loop transfer function for the current loop is as follows:

$$\frac{i_{ld}}{i_{ld}^*} = \frac{k_{pc}}{L_f} \frac{s + k_{ic} / k_{pc}}{s^2 + \frac{r_f + k_{pc}}{L_f} s + \frac{k_{ic}}{L_f}} \tag{3.18}$$

By assimilating the equation (above) with the quadratic characteristic equation the damping factor and the natural oscillation frequency can be obtained as follows:

$$\xi_i = \frac{(r_f + k_{pc}) / L_f}{2\sqrt{k_{ic} / L_f}} \quad (3.19)$$

$$\omega_{ni}^2 = k_{ic} / L_f \quad (3.20)$$

Hence, the parameters of the current regulator can be designed as follows:

$$\begin{cases} k_{pc} = 2\xi_i\omega_{ni}L_f - r_f \\ k_{ic} = L_f\omega_{ni}^2 \end{cases} \quad (3.21)$$

According to the theory of optimal techniques $\xi_i = 0,707$ and ω_{ni} are based on the time domain specification. Usually, the natural frequency is selected as $\omega_n = \omega_s / 50$, with ω_s is the switching frequency.

3.5.4 Voltage loop design:

Voltage regulation is required to inject good-quality energy. The external voltage control loop is developed using the standard feedback/feedforward control and commonly it uses a PI controller.

The voltage control can be expressed as:

$$\begin{cases} i_{ld}^* = (k_{pv} + k_{iv} / s)(v_{od}^* - v_{od}) - \omega C_f v_{oq} + F i_{od} \\ i_{lq}^* = (k_{pv} + k_{iv} / s)(v_{oq}^* - v_{oq}) + \omega C_f v_{od} + F i_{oq} \end{cases} \quad (3.22)$$

Where i_{ld}^* and i_{lq}^* are the d and q axis inductance current references, respectively; v_{od}^* and v_{oq}^* are the voltage references; ω is the MG frequency; k_{pv} and k_{iv} are the proportional and integral parameters of the PI regulator. For voltage control; C_f represents the capacitance of the filter and F is the feedforward current gain. Figure 3-5 shows the block diagram of the voltage control loop. The voltage control loop is achieved by the following steps:

- 1- the dq voltage components v_{od}^* and v_{oq}^* are compared to their measured values v_{od} and v_{oq} as follows $evd = v_{od}^* - v_{od}$ et $evq = v_{oq}^* - v_{oq}$ respectively

- 2- the voltage errors evd and evq pass through the external loop controller which is represented by $Kv(s)$, the outputs of the controller are uvd and uvq

- 3- The dq current set points ild^* and ilq^* are obtained using $ild^* = Uvd + iVd + iod$ et $ilq^* = uvq + ivq + ioq$ where; iVd et iVq are feedforward signals that allow the decoupling between the two voltages v_{od} and v_{oq} . i_{od} and i_{oq} are feedforward signals which permit the attenuation of the dynamic effect of the load on vod and voq meanwhile accelerate the dynamic response.

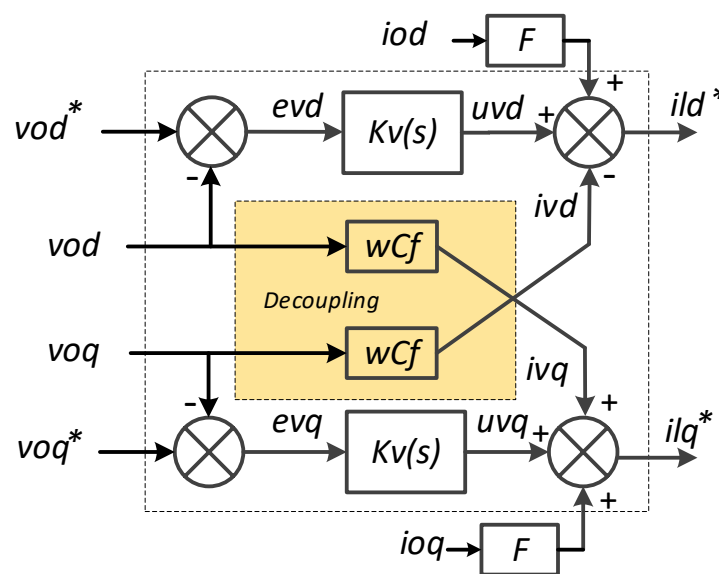


Figure 3-5: Block Diagram of voltage Controller Loops

3.5.5 Synthesis of the voltage loop PI controller

The transfer function of the voltage loop in the d-axis is:

$$\frac{v_{od}(s)}{i_{ld}(s) - i_{od}(s)} = \frac{1}{C_f s} \quad (3.23)$$

For voltage control, the following properties are desirable:

- 1- fast transient response with minimal overshoot
- 2- precise voltage control
- 3- zero static error in steady-state
- 4- less sensitivity to parametric uncertainties of the system

According to Figure 3-5, we can consider the same remarks as the current loop of the corresponding controllers can be identical [122]

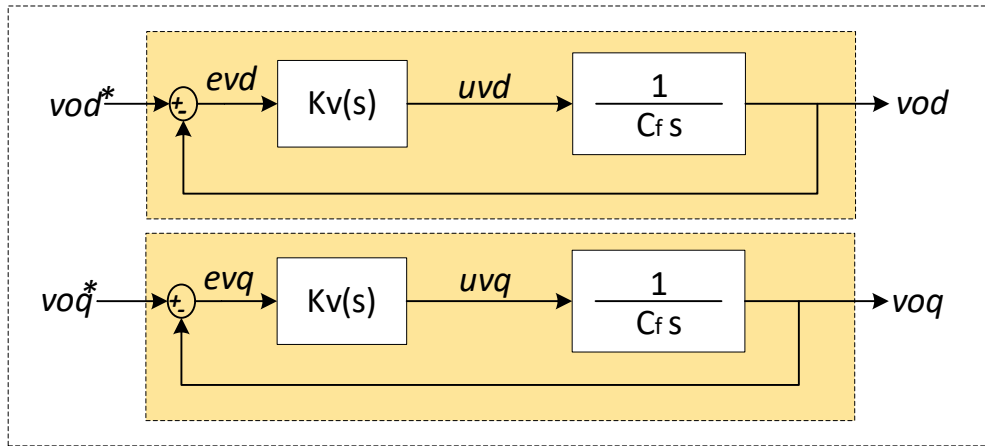


Figure 3-6: Block diagram of closed-loop control for voltage

The transfer function of the voltage PI regulator is

$$K_v(s) = k_{pv} + \frac{k_{iv}}{s} \quad (3.24)$$

From the block diagram in Figure 3-6, the closed-loop transfer function of the voltage loop is as follows:

$$\frac{u_d}{u_d^*} = \frac{1}{C_f} \frac{k_{iv} + k_{pv}s}{s^2 + \frac{k_{pv}}{C_f}s + \frac{k_{iv}}{C_f}} \quad (3.25)$$

Similar to the process of designing the current loop controller, the damping factor ξ_v and the natural oscillation frequency ω_{nv} of the voltage loop can be obtained as follows:

$$\xi_v = \frac{k_{pv} / C_f}{2\sqrt{k_{iv} / C_f}} \quad (3.26)$$

$$\omega_{nv}^2 = k_{iv} / C_f \quad (3.27)$$

Hence the voltage regulator parameters can be designed as follows:

$$\begin{cases} k_{iv} = C_f \omega_{nv}^2 \\ k_{pv} = 2\xi_v C_f \omega_{nv} \end{cases} \quad (3.28)$$

ξ_v is chosen equal to 0,707 and ω_{nv} is chosen as $\omega_s/500$.

3.6 Primary control

3.6.1 Droop control and virtual impedance loop

In order to share the power equally between the paralleled inverters and to ensure the power flow, the reference of the voltage control loop v_{ref} is provided by the primary control that comprises the droop controller and the virtual impedance loop. The amplitude and the phase of the voltage reference are generated by the droop control according to the measured active and reactive powers. The droop functions can be expressed as follow [7]:

$$\begin{aligned}\omega &= \omega_o^* - m_p P \\ v_{od} &= V_o^* - n_q Q \\ v_{oq} &= 0\end{aligned}\tag{3.29}$$

Where ω_o^* , V_o^* are the nominal frequency and voltage references, m_p , and n_q are the droop coefficients for the frequency and the voltage, respectively. Notice that the d-axis is aligned with the phase A voltage in a three-phase system, thus the q-component is equal to zero.

The droop coefficients m_p and n_q can be selected based on the following equations:

$$\begin{aligned}m_p &= \Delta\omega / \Delta P \\ n_q &= \Delta V / \Delta Q\end{aligned}\tag{3.30}$$

Being $\Delta\omega$ and ΔV are the maximum frequency and voltage amplitude deviations, respectively, ΔP and ΔQ are the rated active and reactive powers, respectively.

The averaged power can be calculated through a low-pass filter to attenuate the high-frequency noises as illustrated as follows:

$$\begin{aligned}P &= \frac{\omega_c}{s + \omega_c} \frac{3}{2} (v_{od} i_{od} + v_{oq} i_{oq}) \\ Q &= \frac{\omega_c}{s + \omega_c} \frac{3}{2} (v_{od} i_{oq} - v_{oq} i_{od})\end{aligned}\tag{3.31}$$

A virtual impedance loop has been added in the primary control to improve the current sharing between the VSIs by fixing and normalizing the output impedance of the VSI which will determine the P/Q power angle/amplitude relationship (inductive droop) thus avoiding

using additional physical inductors/resistors. Figure 3-7 shows the additional block of the virtual impedance loop, the output impedance of the VSI must be inductive sufficiently. Thus the additional block of the virtual impedance loop can be expressed as shown follows [38]:

$$\begin{cases} v_{vir d} = R_v \cdot i_{od} - \omega L_v \cdot i_{oq} \\ v_{vir q} = R_v \cdot i_{oq} + \omega L_v \cdot i_{od} \end{cases} \quad (3.32)$$

Where R_v and L_v the virtual resistance and inductance value, $v_{vir dq}$ and i_{odq} are the virtual voltage compensation and output current in dq – frame respectively.

The closed-loop modelling and the stability analysis of the virtual impedance loop have been studied in previous works [10], [19] and will be not addressed in this chapter.

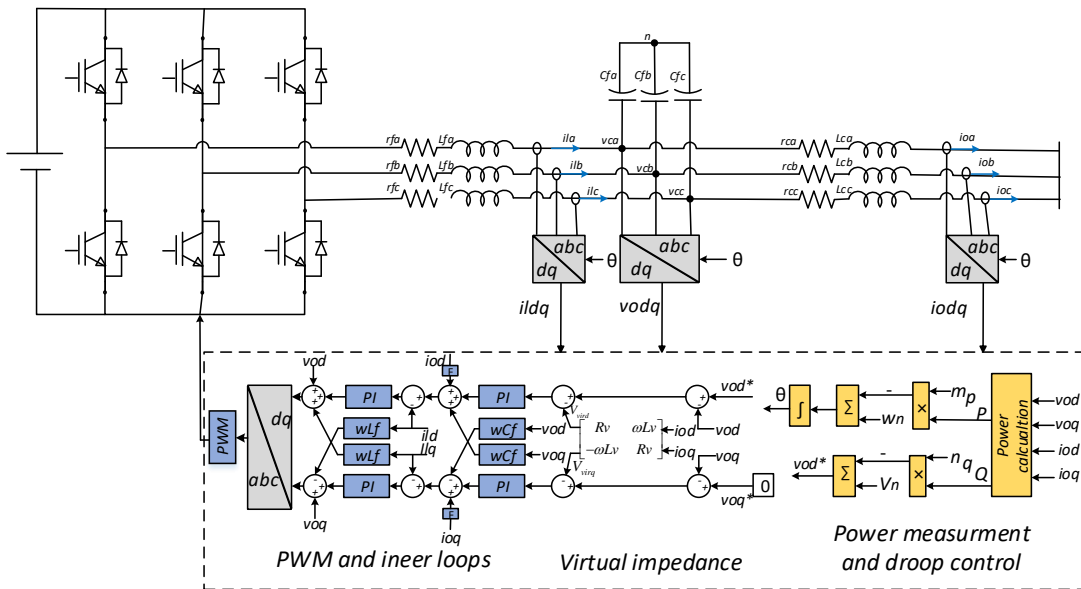


Figure 3-7: Block diagram of the droop controller and the virtual output impedance in dq synchronous frame.

3.6.2 Coordinated synchronization loop

Before connecting the VSIs to the MG or the connection of the MG to the utility grid for grid-connected operation a synchronization process is needed, the synchronization process provides a seamless connection which mitigates the current fluctuations and maintains the system stability. The synchronization is achieved through the synchronization control loop in a synchronous dq reference frame as presented in Figure 3-8.

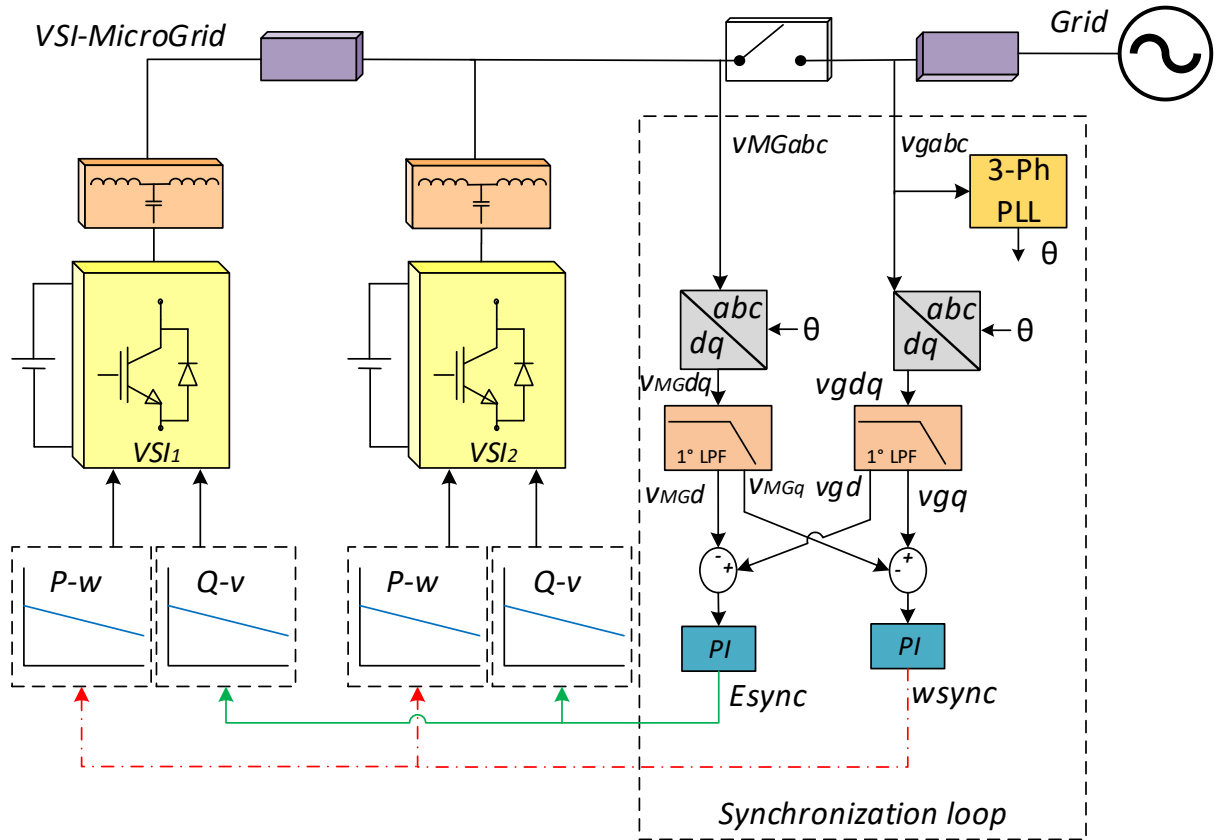


Figure 3-8: Block diagram of the synchronization control loop of a droop-controlled MG.

In case of scheduling a grid-connected mode operation, the synchronization is released by using the direct and the quadrature voltage components of the grid and the MG, V_{dqg} and v_{dqg} .

Similarly, for connecting an incoming VSI to the MG, the direct and the quadrature voltage components of the MG and the incoming VSI are used. The synchronization is achieved when the voltage components are equal $V_{dMG}=V_{dg}$ and $V_{qMG}=V_{qg}$, for this a synchronization structure is needed.

The synchronization structure includes a three-phase PLL, a low pass filter and a PI controller for both axis direct and quadrature.

$$E_{sync} = (v_{dg} - v_{dMG}) \frac{\omega_c}{s + \omega_c} \frac{k_{ps}s + k_{is}}{s} \quad (3.33)$$

$$\omega_{sync} = (v_{qg} - v_{qMG}) \frac{\omega_c}{s + \omega_c} \frac{k_{ps}s + k_{is}}{s} \quad (3.34)$$

Where k_{ps} and k_{is} are the PI parameters, which are the same for both axes and ω_c is the filter cut-off frequency. E_{sync} and ω_{sync} are the synchronization controller output signals to be added for the droop controller functions P-w and Q-v respectively, at each VSI to synchronize itself. Notice that the three-phase PLL is used to extract the phase angle of the utility grid that is used after to transform both grid and MG voltages from the abc reference frame to the dq reference frame.

3.7 Secondary control for frequency and voltage restoration

The secondary control is introduced to compensate the steady-state error caused by the droop control deviations after load connection to meet the grid standard. Secondary control, also called Load-Frequency Control (LFC) in Europe or Automatic Gain Controller (AGC) in USA, should maintain the frequency deviation within the allowable range, e.g.+- 0.1 Hz in North of Europe or +- 0.3 Hz in the Union for the Co-ordination of Transmission of Electricity, Continental Europe. The secondary control compensators for frequency and voltage can be expressed as follows [40]:

$$\begin{aligned}\omega_{rest} &= k_{pF} (\omega_{MG}^* - \omega_{MG}) + k_{iF} \int (\omega_{MG}^* - \omega_{MG}) dt \\ E_{rest} &= k_{pE} (E_{MG}^* - E_{MG}) + k_{iE} \int (E_{MG}^* - E_{MG}) dt\end{aligned}\tag{3.35}$$

Where k_{pF} , k_{iF} , k_{pE} and k_{iE} are the control gains of the secondary control regulators, notice that ω_{rest} and E_{rest} must be saturated to not exceed the maximum and minimal limits of the voltage and frequency drops.

The entire control system including inner loops, virtual impedance, droop control and secondary control is depicted in Figure 3-9.

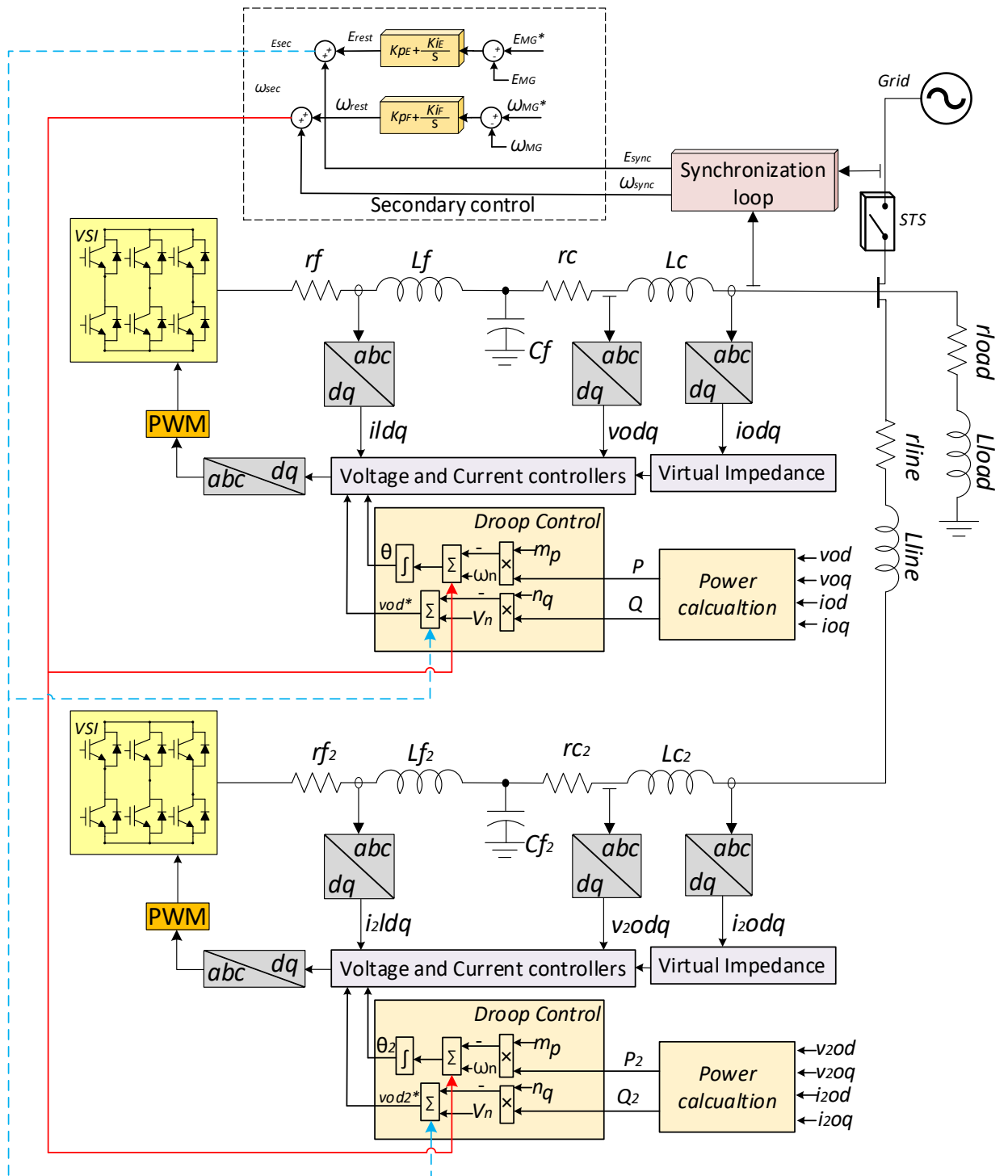


Figure 3-9: Block diagram of the entire control system of the MG

3.7.1 Frequency Restoration

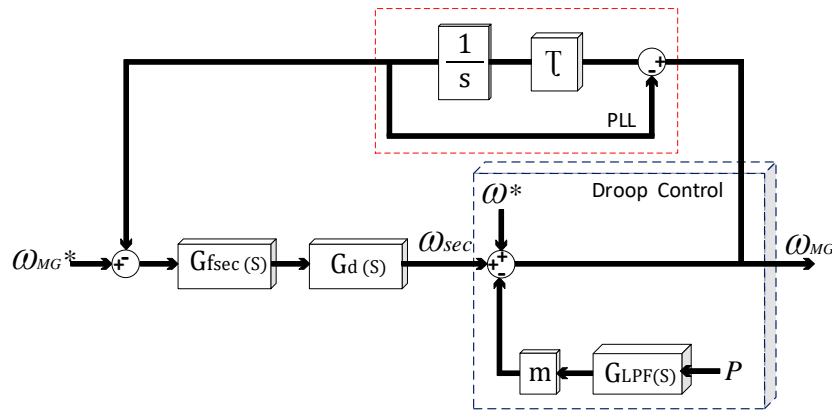


Figure 3-10: Block diagram of the frequency secondary control

To design the frequency secondary controller gains and to ensure the system stability, the model depicted in Figure 3-10 is used, it consists of three main blocs; the droop control bloc to determine the MG frequency, a reduced first-order PLL model to measure the MG frequency and the secondary control compensator $G_{fsec}(s)$ associated with a delay transfer function $G_d(s)$ to mimic the communication lines delay. From the developed model in Figure 3-10 the equation can be obtained:

$$\omega_{MG} = \frac{G_{fsec}(s)G_d(s)}{1 + G_{fsec}(s)G_d(s)G_{PLL}(s)} \omega_{MG}^* - \frac{mG_{LPF}(s)}{1 + G_{fsec}(s)G_d(s)G_{PLL}(s)} P \quad (3.36)$$

Where the transfer function of each bloc is as follows:

$$G_{fsec}(s) = \frac{k_{pF}s + k_{iF}}{s},$$

$$G_{PLL}(s) = \tau / (s + \tau),$$

$$G_d(s) = \frac{1}{s + 1.5\omega_s},$$

$$G_{LPF}(s) = \frac{\omega_c}{s + \omega_c},$$

Consequently, the closed loop transfer function P-to-WMG can be obtained as follows:

$$\omega_{MG} = - \frac{m\omega_c s (s^2 + sa + b)}{s^4 + s^3c + s^2d + se + f} P \quad (3.37)$$

With the following parameters:

$$\begin{aligned}
 a &= \tau + 1.5T_s \\
 b &= 1.5T_s \tau \\
 c &= 1.5T_s + \omega_c + \tau \\
 d &= \omega_c (1.5T_s + \tau) + \tau (1.5T_s + k_{pF}) \\
 e &= \tau (\omega_c (k_{pF} + 1.5T_s) + k_{iF}) \\
 f &= \tau k_{iF} \omega_c
 \end{aligned}$$

Figure 3-11 depicts the step response of the model in (3.37) for a P step change. This model allows us to adjust properly the control parameters of the secondary control and to study the limitations of the communications delay.

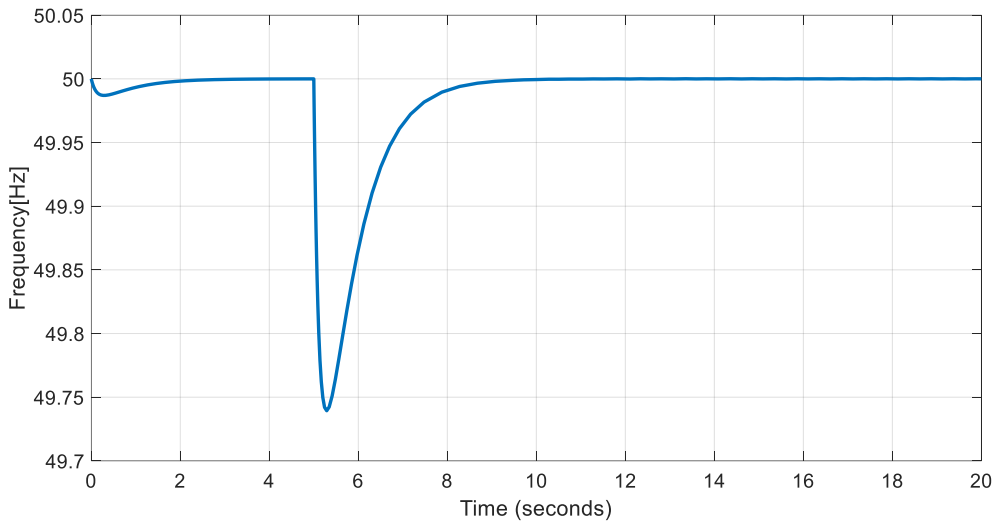


Figure 3-11: Transient response of the secondary control model for frequency restoration

3.7.2 Amplitude Restoration

A similar method has been followed to adjust the voltage secondary controller parameters [38], the obtained block diagram, in this case, is depicted in Figure 3-12

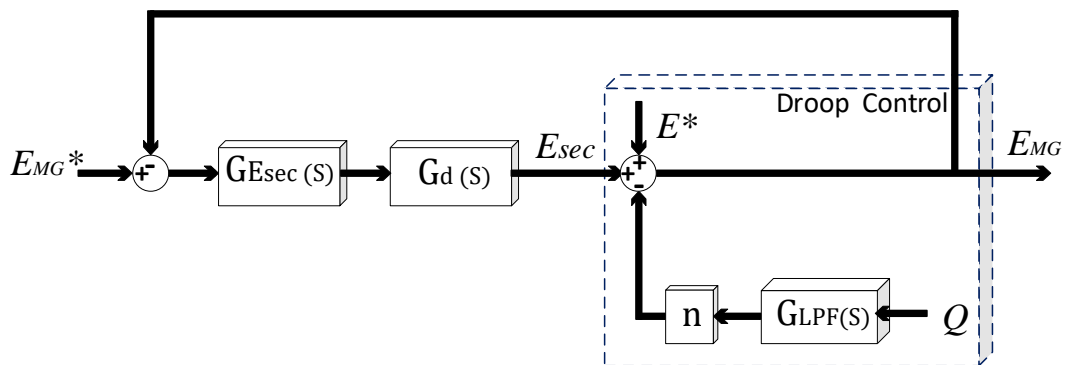


Figure 3-12: Block diagram of the amplitude secondary control

By the same procedure the closed loop voltage dynamic model is:

$$E_{MG}^* = \frac{G_{Esec}(s)G_d(s)}{1 + G_{Esec}(s)G_d(s)} E_{sec} - \frac{nG_{LPF}(s)}{1 + G_{Esec}(s)G_d(s)} Q \quad (3.38)$$

Being $G_{Esec}(s)$ is the voltage compensator

$$G_{Esec}(s) = \frac{k_{pE}s + k_{iE}}{s} \quad (3.39)$$

Thus the closed loop transfer function of the voltage secondary controller from Q-to-EMG can be expressed as follows:

$$E_{MG} = -\frac{n\omega_c s(s+1.5)}{s^3 + as^2 + bs + k_{iE}\omega_c} Q \quad (3.40)$$

Where

$$\begin{aligned} a &= k_{pE} + \omega_c + 1.5 \\ b &= \omega_c(k_{pE} + 1.5) + k_{iE} \\ c &= k_{iE}\omega_c \end{aligned}$$

By using this model, the dynamics of the system for a step change in Q can be obtained as shown in Figure 3-13.

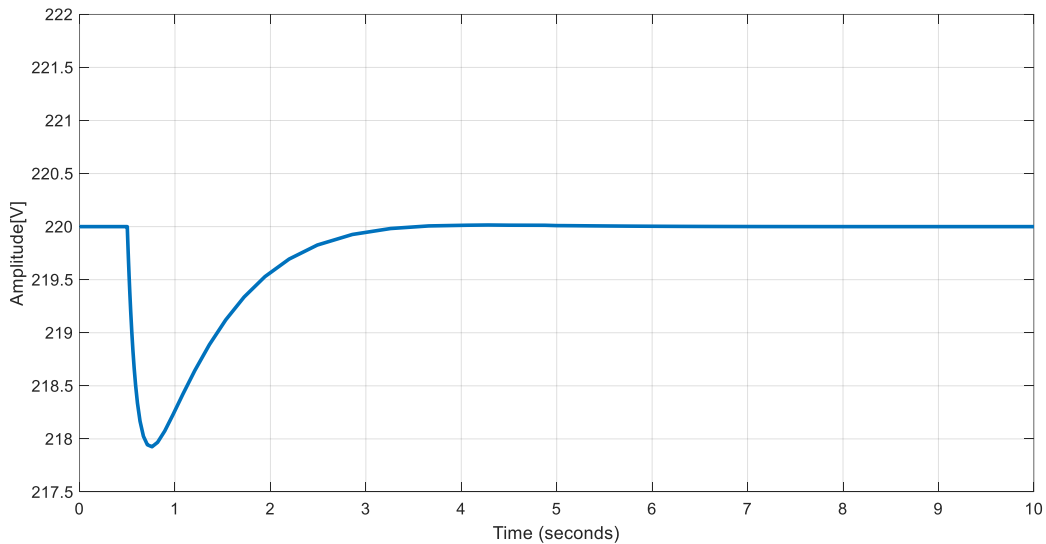


Figure 3-13: Transient response of the secondary control model for amplitude restoration

3.8 Implemented MG Control Analysis

In order to implement and test the feasibility of the theoretical analysis developed above, a MG model was built in Matlab-Simulink as illustrated in Figure 3-9. The used parameters are listed in Table 3-1. The MG model consists of two VSIs interfaced using LCL filter and connected to each other through a line, and they are supplied a local load.

Table 3-1: microgrid parameters

Inverter parameters (10 kVA rating)			
Parameter	Value	Parameter	Value
f_s	8 kHz	C_f	50 F
L_f	1.35 mH	r_f	0.1 Ω
L_c	0.35 mH	r_c	0.03 Ω
Line and Load parameters			
r_{line}	0.1 Ω	r_{load}	25 Ω
L_{line}	0.35 mH	L_{load}	1e-5 mH
Primary control parameters			
m_p	9.4e-5 (= 0.3% droop)	n_q	1.3e-3(= 2% droop)
W_n	314.16 rad/sec	V_n	311 V
W_c	31.41 rad/sec		
R_v	0.0370	L_v	0.0200
Voltage and current Controller parameters			
Voltage controller		Current controller	
K_{pv}	0.037	K_{iv}	393
K_{pc}	10.5	K_{ic}	16e3
F	0.75		
Secondary control			
K_{pE}	0.2	K_{iE}	0.05
K_{pF}	0.01	K_{iF}	5
τ	50ms		

3.8.1 Voltage and current waveforms

Figure 3-14 shows the voltage and the output current waveforms of the VSI supplying a local load, and Figure 3-15 depicts the dynamic response of the voltage and the current loops in the dq frame for both axes.

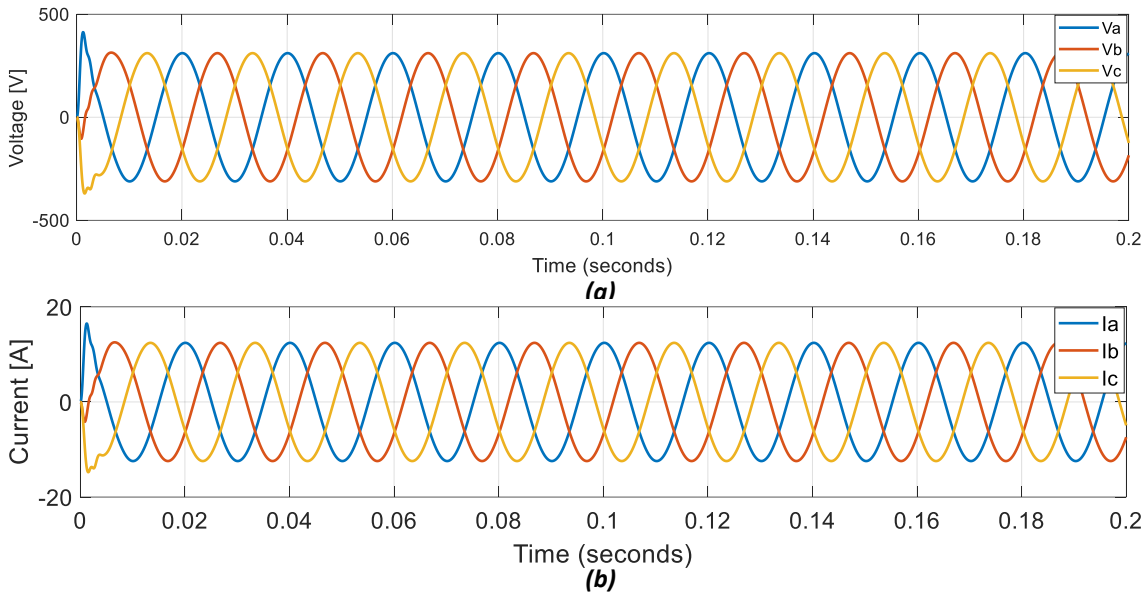


Figure 3-14: Output voltage (a) and current (b) waveforms of a VSI

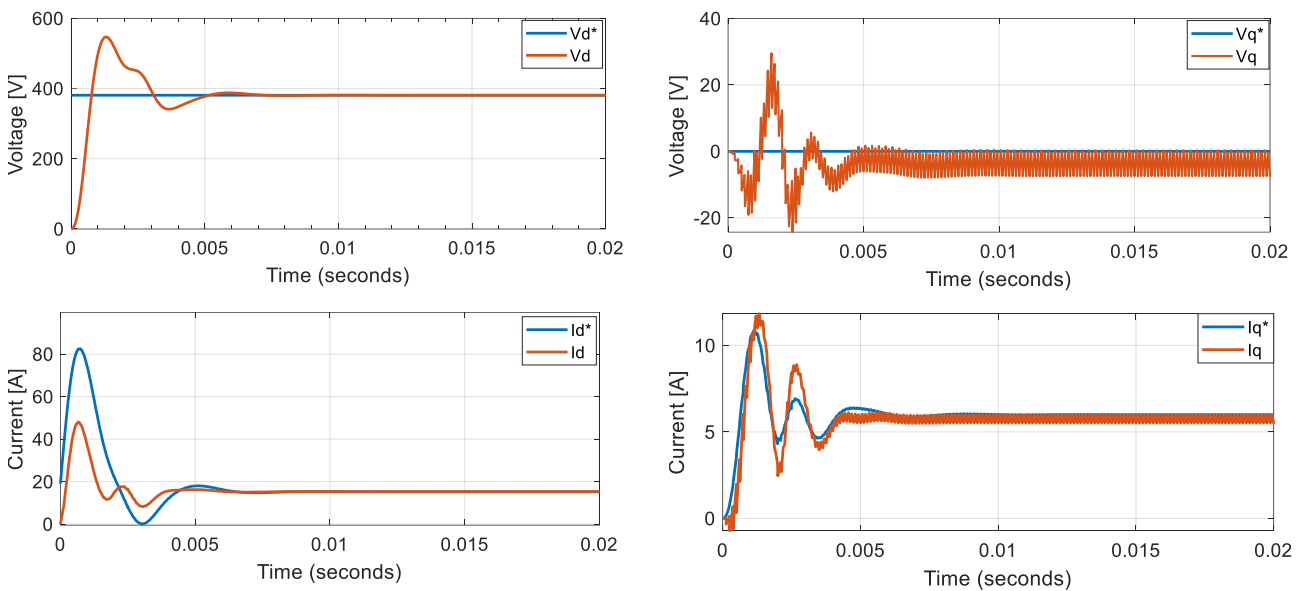


Figure 3-15: Inner loops voltage and current components

Figure 3-16 shows the output currents of the two paralleled VSIs controlled using droop control in stand-alone mode, at the beginning both inverters share the load equally, after that at $t=1s$ the second inverter is disconnected and the other one carried out the feeding of the load which ensure the continuity of supplying energy in case of one of the inverters is tripped. This test shows the strength of the droop control in sharing power among inverters without any need of communication which increases the system reliability.

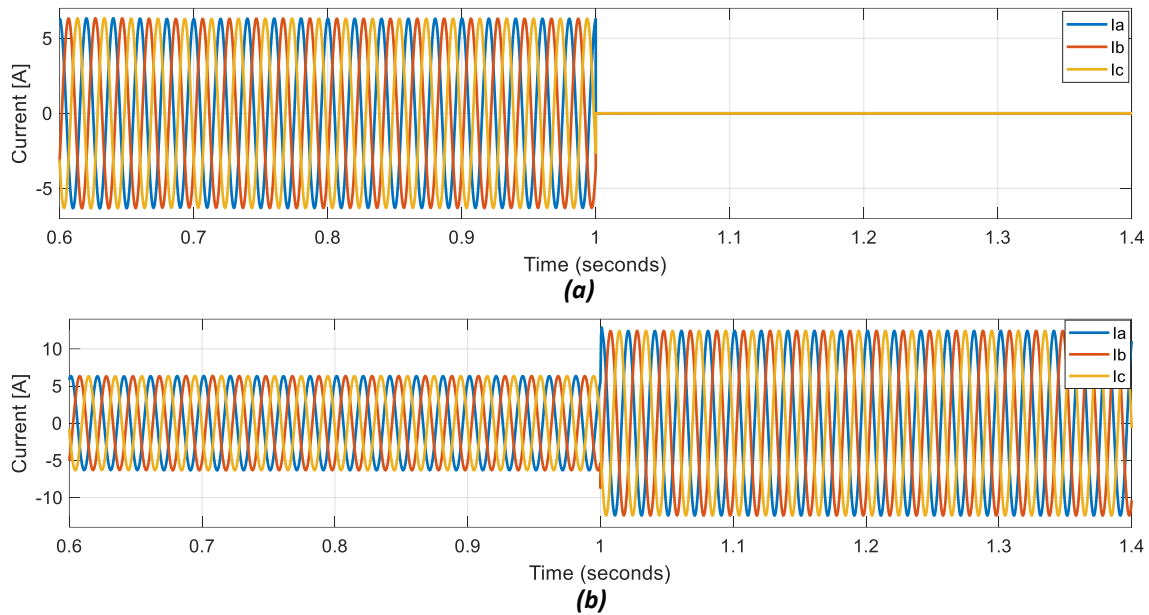


Figure 3-16: Transient response of the output currents (a) VSI1 (b) VSI2, when the VSI 1 is disconnected at $t=1$ s.

3.8.2 Inverters synchronization to the MG

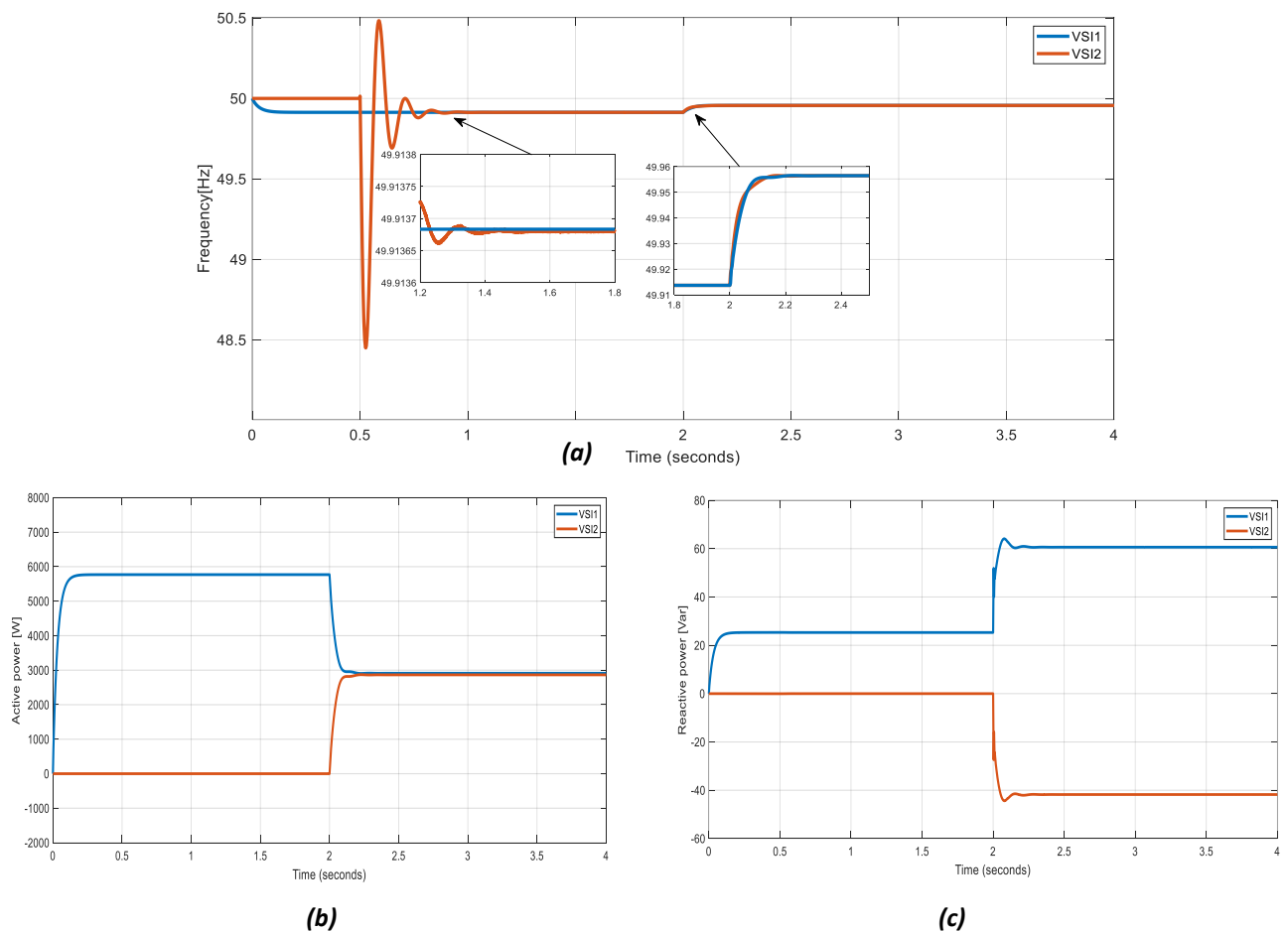


Figure 3-17: Synchronization process of inverters (a) frequency of two sides (b) active power, and (c) reactive power contributions of two inverters

In case of one of the inverters is tripped it needs to be reconnected to the MG another time. Before the connection of the incoming inverter, it needs to be synchronized to the MG as demonstrated in Figure 3-17, the same synchronization process will be used to synchronize the incoming inverter to the MG. Figure 3-17a shows the frequency of both the MG and the incoming inverter, at $t=0.5$ s the synchronization process is enabled and which resulted in frequency fluctuations of the incoming inverter. At $t=2$ s the synchronization is achieved and the incoming inverter is connected which is immediately started sharing active power with the other inverter as can be seen in Figure3-17b.

3.8.3 Secondary control performances

This test demonstrates how secondary control restores the voltage and frequency of the MG. The voltage rms value and frequency of the MG are successfully recovered, and the static deviations caused by the droop control were removed. As can be seen in Figure 3-18a the secondary control is activated at $t=0.5$ s and the system starts recovering the frequency to its nominal value, after that the system subjected load changes at $t= 2$ s and $t=4$ s, the secondary control acted for both sudden changes and eliminates the deviation similarly when the inverter two is disconnected at $t=6$ s the secondary control is acted quickly and the frequency is kept at its set point after 2s.

The same dynamic response is remarked on the voltage rms curve since the transfer function presented in this section are very close for this the result is not depicted here.

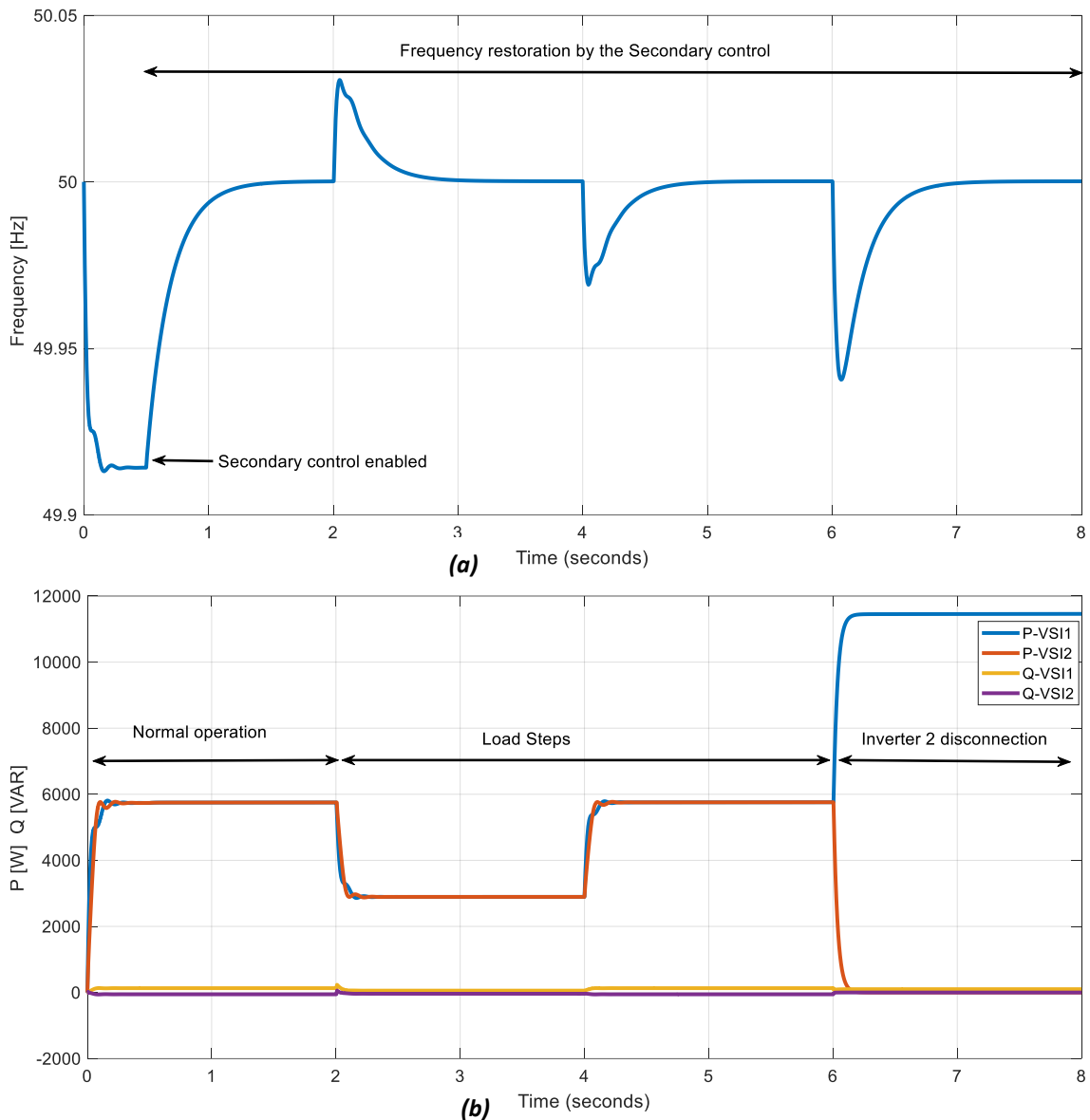


Figure 3-18: Active and reactive power (a) and frequency (b) during load step changes ($t=2s$ and $t=4s$) and sudden disconnection of inverter 2 ($t=6s$).

3.8.4 Impact of communication time delays:

Communication infrastructures play a critical role in MG operation by providing and exchanging the data between the MGCC and the DG units local controllers. In secondary control, the voltage and frequency correction signals are sent using the MGCC through a low-bandwidth communication infrastructure to restore the deviations caused by the primary control. For this, the communication delay effect on the secondary control has been investigated for different time delay amounts. Figure 3-19 shows the voltage and frequency during the restoration process, it is clear that the communication delays cause oscillations in both voltage and frequency, and the increase of the time delay results in high oscillations up to 300 ms where the system stability becomes threatened.

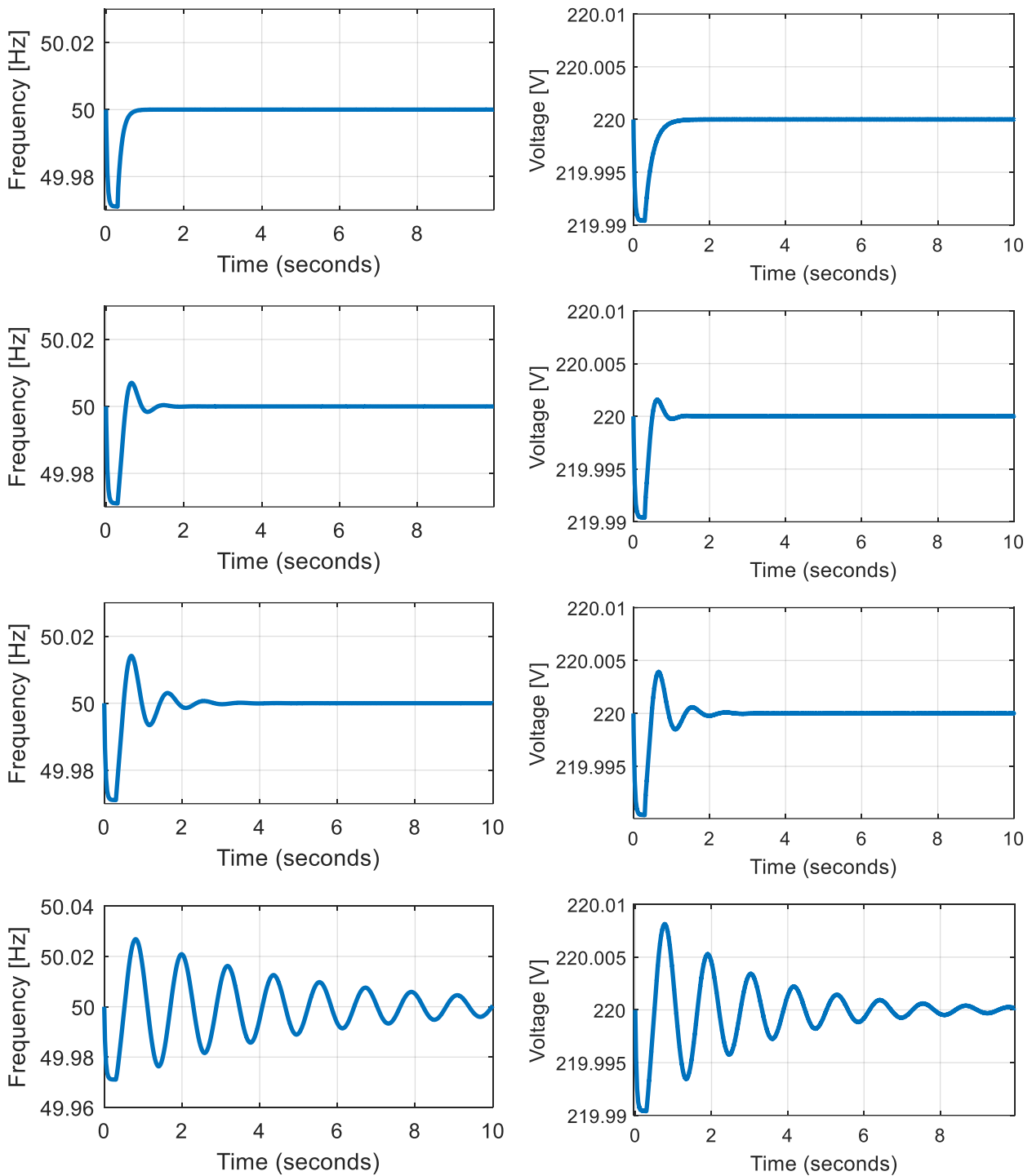


Figure 3-19: Secondary frequency dynamics under different communication delay

3.8.5 Synchronization with the main grid

Synchronization is necessary for the transition mood from island mode to grid-connected mode to avoid high current fluctuations and equipment damage. The synchronization process between DG unit and the main grid is illustrated in Figures 3-20a and 3-20b as can be seen at the start of the synchronization the voltage waveforms are not synchronized yet and the voltage difference between

the MG and the grid is high, during the synchronization process the voltage waveforms are started becoming closer to each other Figure3-20b and the voltage difference is start decreasing as can be seen in Figure 3-20a, at the end of the process the voltage waveforms are matched and the voltage error value is decreased to zero which ensures a seamless transition mode, notices that the synchronization process has no impact on the system stability since the bandwidth is much more reduced.

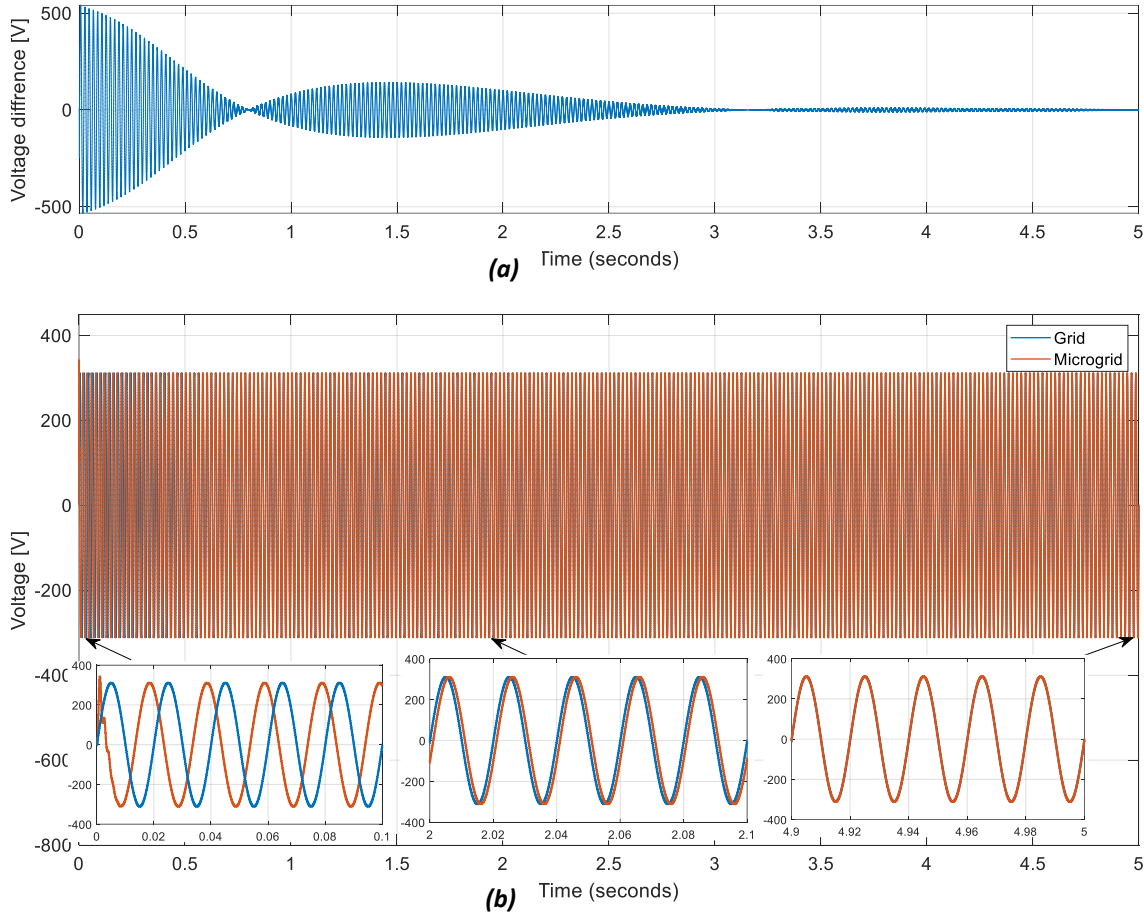


Figure 3-20: Synchronization process (a) voltage difference (b) Grid and MG voltages

3.9 Conclusion

This chapter proposes a systematic method for designing a hierarchical controlled three-phase MG. Based on a dq synchronous reference frame, the control structure was designed until the secondary control including two layers of control. The inner loops or the zero layer of the VSI consist of the voltage and the current controller based on PI controller. The primary control comprises the droop control and the virtual impedance approaches, which are responsible of sharing the active power equally among inverters. Synchronization loops were illustrated for seamless connection in case of performing a grid-connected mode or connecting an incoming inverter to the MG. The secondary

control based on a centralized topology using communication links, is established in order to eliminate the voltage and frequency deviations caused by the primary control.

Each control layer has been modelled, and the closed-loop system dynamic response of the secondary control has been analysed to simplify the compensator parameters selection. Simulation results have illustrated the highly reliable performances of the MG system.

Chapter 4: Decentralized secondary control for frequency regulation based on fuzzy logic control in islanded microgrid

4.1 Introduction

Hierarchical control topology is the most adopted approach for MG control and it attracted more and more attention due to its capability to meet MG’s control challenges [37]. Hierarchical control is divided into three layers, first one is primary control which is based on droop control [16], virtual impedance, voltage and frequency control loops, this layer is fully decentralized and no communication infrastructures are needed, their main task is to maintain voltage and frequency regulation, and to share active and reactive powers between voltage source inverters equally [121]. In contrast, the tertiary layer requires communication to manage the power flow among the MG and the external electrical distribution system, the secondary control layer (SC) permits compensating the voltage and frequency deviations caused by the inherent characteristic of droop control in the primary control layer [43], the SC is classified into three categories according to the implementation topology as illustrated in Figure 4-2, the first one which is the most recognized is the centralized topology as can be seen in Figure 4-2(a), the centralized SC use a microgrid central controller (MGCC)

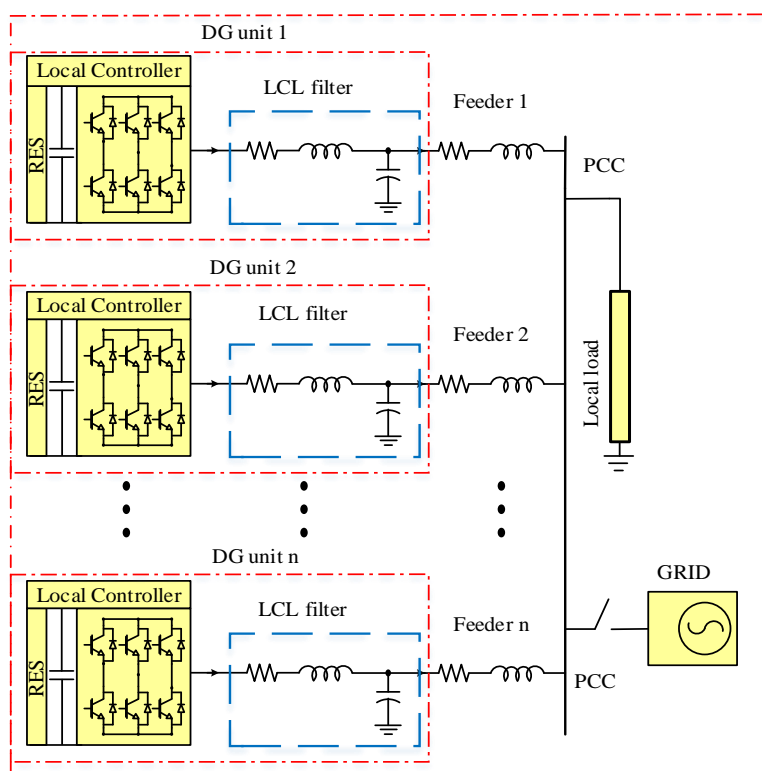


Figure 4-1: Fundamental structure of a microgrid

[123] to send and receive information using a communication infrastructure [124], the second one is the distributed control approach Figure 4-2(b), where the DG units work cooperatively by communicating with each other to attain an agreement situation among all DG units [125], the last one is the communication free decentralized technique as depicted in Figure 4-2(c), which is implemented locally like primary control.

The centralized and distributed secondary control topologies are highly dependent on communication infrastructures which increase the complexity and the cost. Moreover, the needing for a communication system reduces the reliability and the resiliency of the MG due to uncertainties such as communication delays [126] and data-drop out, also communication systems expose the system to cyber-attack threats [127], as a result, many literatures proposed fully decentralized technics, an equivalent secondary control based on a washout filter is proposed in [87] it has the advantage of low complexity, however, it suffers from steady state-error and slow dynamic response which need to be improved in future works. Based on state-estimation new approaches have been addressed in [82] their major superiority is in the accurate active and reactive power-sharing independently; however, these approaches related to the system model which serve as an alternative of communication infrastructures by estimating the state of the remains DG units in the MG system , thus a high computational burden is required and hence leading to increase the complexity and cost which reduce the efficiency of the system, further a decentralized secondary control approach (SC) utilizes the active power estimation is developed in [84] unlike the above-mentioned state-estimation techniques, which require a complete knowledge of the MG topology to estimate the variables, this approach uses the unique property of the frequency in islanded MGs as a global variable in steady state to estimate the active-power, the only drawback is the slow dynamic restoration up to 2s, in [72] a switched secondary frequency compensation is proposed based on switching between two configurations as the secondary control is established using a low-pass filter which exhibits design trade-off between transient response and accuracy, this approach breaks this design trade-off and provides fast transient response with small error in steady-state while using a time-dependent control which increases the complexity, especially the parameters design which decreases the system stability, although a decentralized optimal secondary controller is developed in [128] based on a quadratic cost function in the form of a linear quadratic regulator (LQR) solution with a straightforward and simple design procedure, a frequency self-restoration based on droop

control is presented in [129], it has a fast dynamic response, but it suffers from overshoots with the presence of ripples in the steady-state response.

As can be observed from the previous paragraph, the existing decentralized techniques suffer from many drawbacks such as steady-state error, slow dynamic response, time and system dependent, complexity and high computational burden. In addition, no study investigated the effect of interferences such as emergency control, plug, and play of DG units with a high-priority task. Therefore, this paper proposes a decentralized secondary control for frequency regulation and active power-sharing based on fuzzy logic control in islanded MG, the fuzzy logic can be used as an intelligent approach to deal with the imperfections of the conventional controllers aiming to cover the complex systems with their uncertainties and inaccuracies, the proposed secondary control is fully decentralized, except in the emergency conditions where the system is controlled using a MGCC and tertiary control. Based on a fuzzy logic controller and on the unique feature of frequency in islanded MGs as a global variable in steady state, the objective was to elaborate a robust control for the frequency while at the same time respecting the dynamic constraint and treatment-time to achieve a fast dynamic restoration without overshoot and ripples in a steady-state regime, an enhanced dynamic behaviour of a PI regulator was used for the design of the fuzzy controller, simulation results show the high performances and capabilities of the proposed technique. The main contributions and novelties of this paper can be listed as shown in:

- This model takes advantage of the unique feature of the frequency in islanded MGs as a global variable to develop a decentralized topology.
- Developing a fuzzy controller to eliminate frequency deviation of microgrids meanwhile ensuring the precise active power sharing between inverters, the proposed controller offers a quick dynamic frequency recovery and it is much faster than conventional controllers with accurate active power tracking and its design with implementation are straightforward.
- In contrast of distributed approach, the proposed method is communication-free.
- Event detection, time dependent-protocols, and state estimation are not required.
- The settling time is improved by 50% compared to the conventional PI controller.

Study, Modelling and Control of a Multisource Microgrid

Chapter 4: Decentralized secondary control for frequency regulation based on fuzzy logic control in islanded microgrid

- Similarly in the presence of 30 % and 70 % of packet losses the settling time is improved by 81% and 90 % respectively which confirms the high performance.
- No overshoots and oscillations in frequency are presented in case of the presence of communication delays and no ripples in the steady-state response.
- It shows high flexibility and robustness during plug-and-play operation.
- Interferences such as emergency control and economic dispatch have no impact on the proposed controller.

The rest of this chapter is structured as shown in: Section 2 the secondary control function in a multilayer control structure with the proposed method are described, moreover, the existing secondary control technics were listed and compared in terms of their advantages and disadvantages. Section 3 exhibits the simulation results based on multiple scenarios including the comparison, the results were discussed in the same section. Finally, the conclusion in section 4.

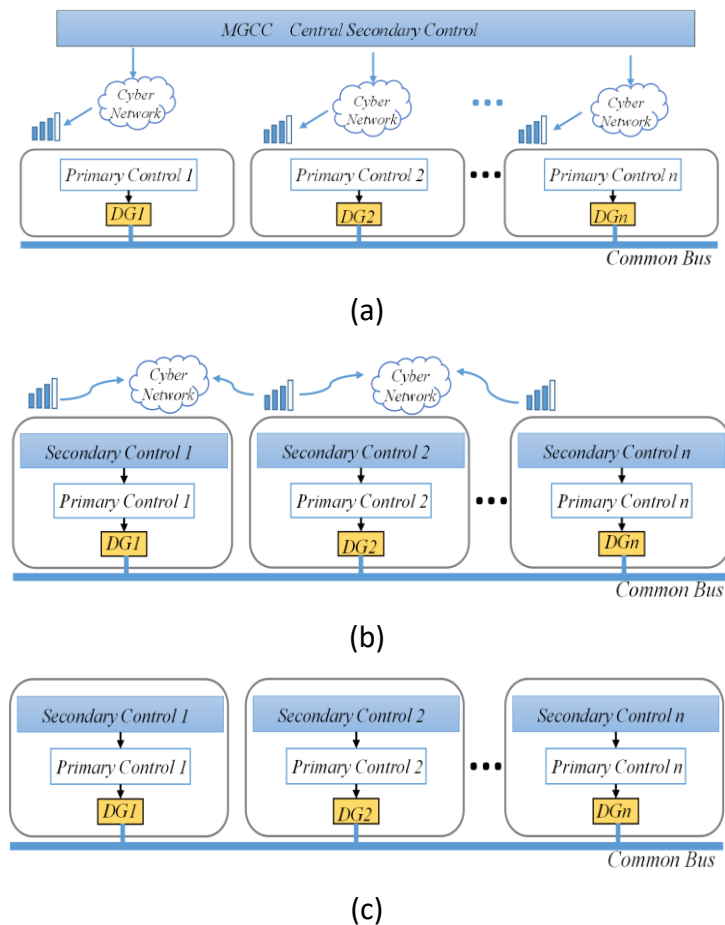


Figure 4-2: Secondary control topologies; (a) centralized SC, (b) distributed SC, and (c) decentralized SC

4.2 Method

The first layer of the hierarchical control is represented by the droop control which adjusts the frequency and voltage according to the measured active and reactive power based on the droop coefficient m_i and n_i calculated according to the small-signal analysis presented in [130], it can be expressed as:

$$\omega_i = \omega^* - m_i P_i \quad (4.1)$$

$$V_i = V^* - n_i Q_i \quad (4.2)$$

Being, ω_i and ω^* refer to the angular frequency and its reference respectively, P_i is the active power output, V_i and V^* refer to the voltage amplitude output and its reference, Q_i the reactive output. As shown in (4.1), ω_i and V_i are used to synthesize the three-phase reference voltage to be provided for the inner current and voltage control loops. It is clear from the above-mentioned equation that a change in both active and reactive powers leads to frequency and voltage change respectively, especially when adding loads this leads to the frequency and voltage droops, which result in steady-state errors that need to be compensated.

The secondary control eliminates these deviations by providing an extra term to the primary layer and it can be expressed mathematically by:

$$\lim_{t \rightarrow t_f} \omega_i(t) = \omega^* \quad (4.3)$$

$$\lim_{t \rightarrow t_f} V_i(t) \approx V^* \quad (4.4)$$

Practically, it is impossible to achieve perfect voltage regulation and reactive power sharing using only the droop method in (4.2) since the voltage is a local output variable of the MG. In this sense, this paper focused only on the MG frequency compensation and supposed that the Q-V droop control loop adjusts the V_i for the DG units. Thus, to attain an accurate active power-sharing and impose the reference frequency without steady-state errors, the SC level provides an extra term to (4.1) as shown in:

$$\omega_i = \omega^* - m_p \cdot P_i + \delta\omega_i \quad (4.5)$$

The additional control term $\delta\omega_i$ provided by the SC to the primary layer and ω_i is the corrected frequency of i th DG unit which leads to maintaining the frequency at its nominal value as can be seen in Figure 4-3. Noticing that another extra term is required for the synchronization and to ensure a seamless transition between operation modes, either for synchronizing the DG units between each other in case of plug-and-play operation or to synchronize the MG with the classical grid in case of grid-connected mode generally the synchronization loop considered as part of SC; moreover, an islanding detection approach also can be included in this level.

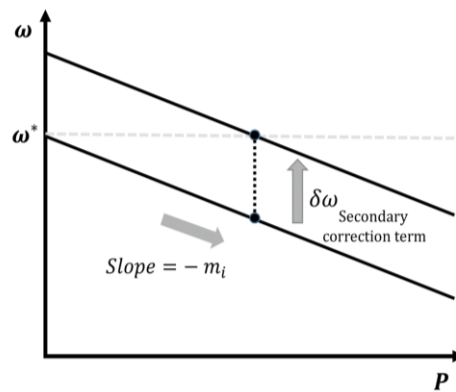


Figure 4-3: Primary and secondary control actions

Table 4-1 summarizes the advantages and disadvantages of different secondary control technics including the proposed one. As mentioned before for the centralized topology the need for communication and remote measurement threat the system stability through time delays and data drops, which degrade the power quality as well as communication failure can interrupt the electricity supply. Similarly, the distributed approach proposes communication between microgrids units for enhanced reliability, but, in case of a single failure of communication, it will affect the entire stability. Hence new communication less technics have emerged, to enhance the resilience of MGs and drop out of the communication network.

The proposed secondary control is fully decentralized, except in emergency conditions where the system is driven using the upper layer which is the tertiary control. Based on a fuzzy logic controller the objective was to design a robust control for the frequency meanwhile respect the dynamic constraint and treatment time, the structure of the controller is depicted in Figure 4-4. The use of fuzzy logic controllers in the last decade has been widely increased for power systems and power electronics applications [131], [132] the conventional secondary controller based on PI regulators

suffers from many drawbacks due to their design which is tuned on a predefined operating point, any change in the operating conditions outside the operating point leads to the loss of system stability due to the incapability of the PI controller for providing suitable performances, moreover, it has a slow dynamic response which can affect the sensitive loads such as data centers. Fuzzy logic can be used as an intelligent approach to deal with the imperfections of the conventional controller aiming to cover the complex systems with their uncertainties and inaccuracies. A fuzzy-PI structure is used to perform the fuzzy controller based on a PI behaviour profile, the gains are adapted in function of the frequency error and the derivative of the error.

The input error e_ω and their derivative de_ω values are normalized as shown in:

$$e_\omega = K_{e_\omega} (\omega^*(k) - \omega_i(k)) \quad (4.6)$$

$$de_\omega = K_{de_\omega} (e_\omega(k) - e_\omega(k-1)) / T_z \quad (4.7)$$

Where T_z is the sampling time and K_{e_ω} , K_{de_ω} are the normalization gains or the scaling factors. The output generates the variation of the corrective term which is after the integration and normalization gives the external signal ω_i . The scaling factors are very important in the design of the controller to adjust the sensibility of the fuzzy controller and the stability of the system, it allows the normalization of the inputs and the outputs in the required gap of the universe of discourse, these parameters are obtained after trial and error method. Fuzzification is the process of transforming a crisp input value into a fuzzy value that is achieved by the use of the information in the knowledge base. Although various types of curves can be used. Triangular, gaussian, and trapezoidal membership functions which are the most popular in the fuzzification process. The implementation of these types of membership functions can be easily achieved using embedded controllers.

Table 4-1: Summarise of different secondary control technics

Control	Concept	Advantages	Disadvantages
Centralized Secondary Control	- Central Controller [133], [134]	<ul style="list-style-type: none"> - Active and reactive power management - Harmonic cancellation - Real-time monitoring of the system - Unbalanced current reduction 	<ul style="list-style-type: none"> - any failure in Communication infrastructure or CSC affects the overall MG system - Communication delays and data drop
Distributed Secondary Control	<ul style="list-style-type: none"> - Average-based DISC [125] - Consensus-based DISC [135], [136] - Event-triggered DISC [134], [137] 	<ul style="list-style-type: none"> - Robust to single-point-failures - Easy to implement (An embedded controller is enough) - flexibility and redundancy - less expensive control hardware - Higher control accuracy under disturbances and communication delays - Simple control algorithm, easy to implement - Plug-and-play operation - Robust to single-point-failures - Reducing the recomputation and communication - support the plug-and-play function - Easy to implement - Robust to single-point-failures 	<ul style="list-style-type: none"> - Communication complexity - Clock drifts - Voltage stability and reactive power-sharing - Communication infrastructure - Reducing the recomputation and communication - Voltage stability and reactive power-sharing - Communication infrastructure - Clock drifts - Voltage stability and reactive power-sharing - Zeno phenomenon - Communication infrastructure
Decentralized Secondary Control	<ul style="list-style-type: none"> - Washout Filter-Based DESC [138] - Local Variable-Based DESC [139], [128] - Estimation-Based DESC [140], [141] - Proposed DESC based fuzzy logic controller 	<ul style="list-style-type: none"> - Fully decentralized and easy to implement - Low complexity - Fast active power responses - Communication-free - Communication-free - Precise active and Reactive power-sharing independently - Communication-free - Quick dynamic frequency recovery - No overshoots and oscillations in frequency - Accurate active power-sharing - Easy to design and implement 	<ul style="list-style-type: none"> - Steady-state error - Slow dynamic response - Increase complexity - Time-dependent - Slow dynamic response - Depend on the modeling of the system - High computational burden - Fuzzy controller scaling factors are selected based on trial and error method.

- No steady-state error
- No impact of interferences
- Less computational burden

The membership functions are defined mathematically with many parameters. To enhance the performances of the fuzzy logic controller these parameters can be adapted to obtain the desired outputs. The distribution and the number of the membership functions in the universe discourse are very crucial, and the calculation time of the algorithm should be considered especially for the practical implementation a good design mean less computational burden and hence less cost. The design steps are illustrated in Figure 4-5. Triangular and trapezoidal membership functions have been selected for the input and output variables distributed in five symmetric and equidistant subsets are selected as can be seen in Figure 4-5(a). The universe of discourse gap is determined between [-1.5 1.5], this choice makes the fuzzification easier because it decreases the computation time in the real-time implementation.

The different groups are defined using the following linguistic variables:

- NL: Negative Large
- NS: Negative Small
- ZE: Zero
- PS: Positive Small
- PL: Positive Large

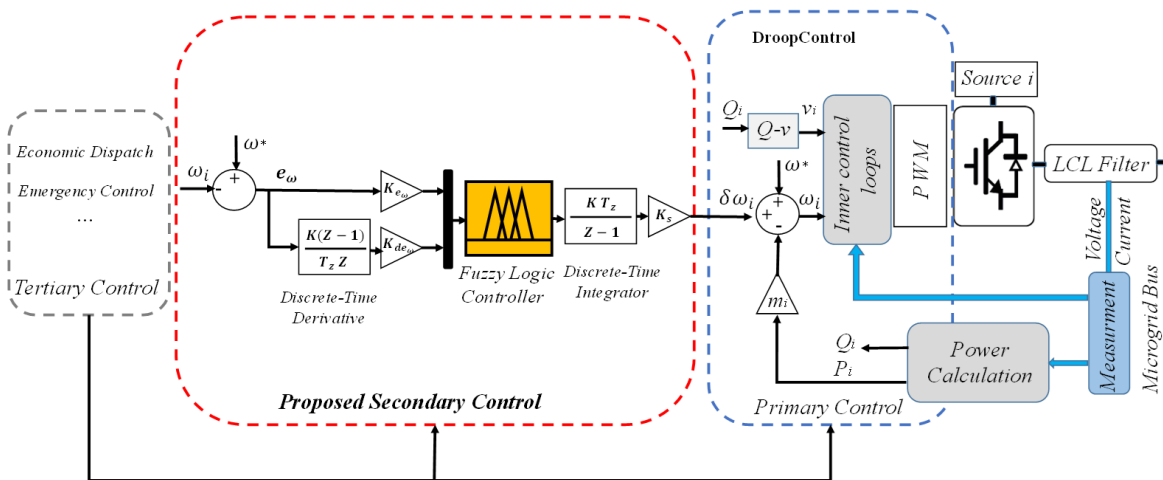


Figure 4-4: Proposed decentralized secondary control for microgrids

The rules base plays an important role in the behaviour of the fuzzy controller, hence a good design of the table of rules leads to better performances, generally the construction of the interference table is based on qualitative analysis of the process. From the previous study [133] of the closed-loop system behaviour using a PI controller and based on the expertise, fuzzy rules are established to tie the inputs and output. The general form of the step response and the derivative of the error are shown in Figure 4-5(b). Depending on the amplitude of e_ω and the sign of de_ω , the response is divided into four intervals (from (1a) to (4a)) such that:

$$\left\{ \begin{array}{l} a_1 : e_\omega > 0 \text{ et } de_\omega < 0 \\ a_2 : e_\omega < 0 \text{ et } de_\omega < 0 \\ a_3 : e_\omega < 0 \text{ et } de_\omega > 0 \\ a_4 : e_\omega > 0 \text{ et } de_\omega > 0 \end{array} \right. \quad (4.8)$$

For instance, at the start of the compensation (point 1) the response is strongly inferior to the reference, and hence the error is PL and their derivative value is ZE, thus the output control signal should be PL. When the error is near zero (point 2) and their derivative value is NL the output signal changes to ZE to avoid a big overshoot value, after the overshoot (point 3), the error is NL and their derivative also, thus the output signal should be strongly reversed to NL, in case of the overshoot still exist and the error is NS with the response is near to the reference (point 4), thus the error derivative value changes their sign to PS, in this case, the output signal should be ZE to minimize the undershoot.

Since there are five fuzzy sets, this implies twenty-five possible combinations of these inputs, and therefore twenty-five rules.

The rules are like this:

1- If (e_ω is NL) and (de_ω is NL) then ($\Delta\delta\omega_i$ is NL)

25- If (e_ω is PL) and (de_ω is PL) then ($\Delta\delta\omega_i$ is PL).

Hence the inference matrix deduced according to the reasoning of "McVicar-Whelan" is as shown in Table 4-2, The Mamdani method is used for the interference method.

Defuzzification is the process of converting the fuzzy output sets produced by the inference mechanism. To generate the most certain low-level controller action. Many methods exist in

literature to perform the defuzzification, the most popular is the center of gravity method which is used in this case due to its reputation in the control field to obtain the variation of the external term, where the $\Delta\delta\omega_i$ is determined from the geometric center of the variable fuzzy output, their discrete equation is as shown in:

$$\Delta\delta\omega = \frac{\sum_{i=1}^n \delta\omega(x_i) \mu_{\delta\omega}(x_i)}{\sum_{i=1}^n \mu_{\delta\omega}(x_i)} \tag{4.9}$$

Notice that as mentioned before the fuzzy controller gain values play a crucial role in obtaining the suitable dynamic response, previous tests of the controlled system are helpful in the selection of the initial values of the fuzzy logic controller gains. If there is a lack of information about the controlled system, the suitable parameters can be calculated by trial and error method or using optimization algorithms such as particle swarm optimization as presented in [142]. The PSO approach is an excellent optimization methodology and a promising method for solving the optimization problem of the fuzzy logic controller and defining the suitable parameters, further, a quasi-oppositional harmony search (QOHS) algorithm is adopted in [143] which is a new variant of derivative-free metaheuristic algorithm that mimics natural and systematic phenomena. Figure 4-5(c) depicts the output surface for the fuzzy controller, it gives the first output variable according to the first two input variables.

Table 4-2: Table of rules

e_ω	NL	NS	ZE	PS	PL
de_ω					
NL	NL	NL	NL	NS	ZE
NS	NL	NL	NS	ZE	PS
ZE	NL	NS	ZE	PS	PL
PS	NS	ZE	PS	PL	PL
PL	ZE	PS	PL	PL	PL

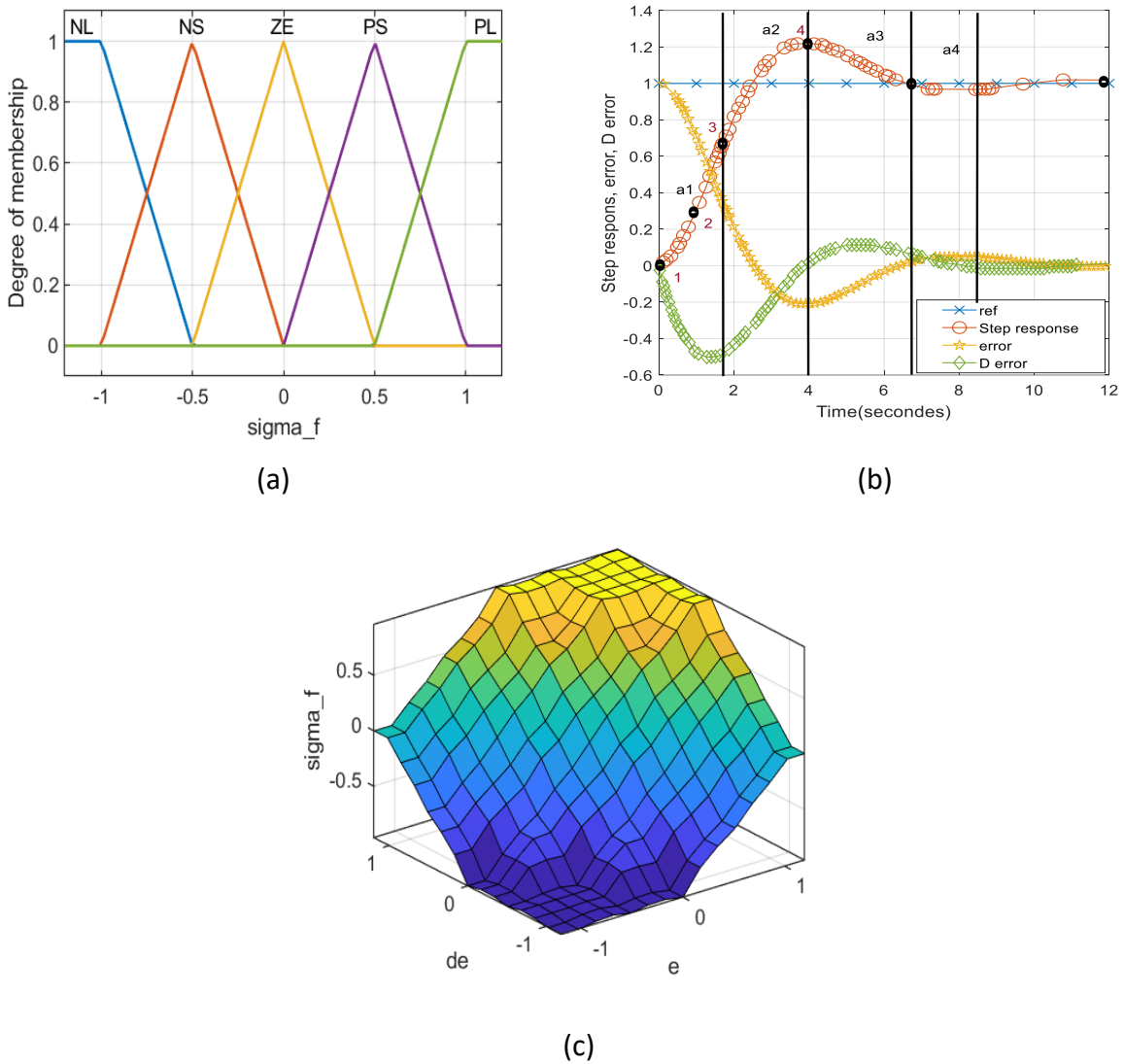


Figure 4-5: Fuzzy logic controller design steps Membership functions (a) the deduction of the rules from a temporal analysis (b) and (c) output surface plot of the fuzzy cotroller

4.3 Results and discussion

To evaluate the effectiveness and the performance of the proposed technic, a MG simulation model is set up on MATLAB software as shown in Figure 4-6. It consists of two DG inverters with the same rating powers forming an islanded MG and LCL filters are used, a low pass filter is integrated into the output of the power measurement units in the primary level to suppress harmonics. The electrical and control parameters are listed in Table 4-3, all parameters have been adjusted based on the developed model, the proposed controller is studied and analyzed in the following parts.

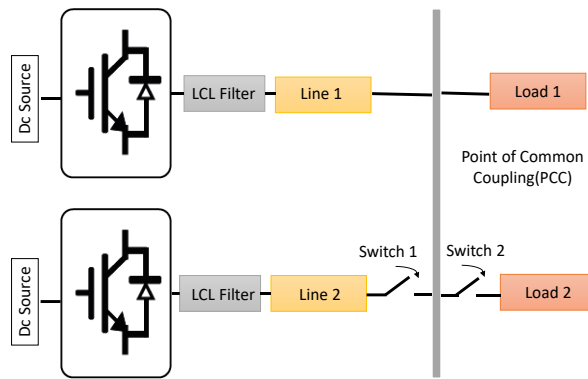


Figure 4-6: Microgrids Configuration of the studied MG

Table 4-3: Simulation Parameters

Parameter	Symbol	Value
Powerstage		
Nominal Voltage	V	311 V
Nominal Frequency	f	50 Hz
Input / Output Inductance of LCL filter	L/L_o	800 /250 uH
Filter Capacitance	C	60 uF
Line 1	$R1/L1$	0.5/1 mΩ/uH
Line 2	$R2/L2$	2/3 mΩ/uH
Load 1	–	500 W
Load 2	–	500 W
DC Voltage	V_{dc}	400 V
Primary&Voltage/Current P Control for DG1/DG2		
Voltage proportional gain/integral term	0.2/100	
Current proportional gain /integral term	5/400	
Proportional frequency droop	m	0.0003 W/rd
Proportional amplitude droop	n	0.001 Var/V
Decentralized Secondary control		
Scale factor proportional term for error	Ke_{ω}	1
Scale factor proportional term for error derivative	$Ke_{d\omega}$	0.1
Integral term	K_S	1000

4.3.1 Frequency restoration and active power-sharing during load disturbances

This test is performed to evaluate the frequency compensation and the accuracy of sharing active power, the obtained curves are exhibited in Figure 4-7. It consists of comparing the conventional P- ω droop control method with the proposed decentralized secondary control. First at t=0s until t=3 s the MG system is running under the conventional droop control and the two load are connected as can be seen in Figure 4-7(a) and 4-7(b) from t=0 s to t=3s the droop mechanism is adjusting the frequency magnitude according to the measured active power and a considerable frequency deviation from its nominal value is presented, while the active power-sharing is well maintained by

the droop mechanism until $t=3$ s the communication free proposed control is activated thus the deviation is compensated while maintaining an accurate active power-sharing (see Figure 4-7(a)). A load change is applied to the MG system to confirm the high performance of the proposed control, as shown in Figure 4-7(a) at $t=6$ s load 2 is turned off the active power is decreased and the frequency is perturbed by presenting an overshoot for a certain time, however, this perturbation is removed due to the fast response of the proposed controller and the frequency is restored to their nominal value within an acceptable range. The current is decreased smoothly without presenting disturbances Figure 4-7(c), the load 2 is turned on another time at $t=9$ s similarly, the proposed SC compensate the error quickly and fixed the frequency to their reference value, the current is increased to supply the loads Figure 4-7(d). The reactive power-sharing is not equal as shown in Figure 4-7(d) due to the inherent limitation of the droop control method [25].

4.3.2 Synchronization and plug-and-play capability

The black start and synchronization process of the two DGs units is performed in this test. The connection and disconnection of the second DG unit to the MG system is realized as can be observed in Figure 4-7(e) from the interval $t \in [0,1$ s] the black start occurred where the two sources are synchronized to each other and they immediately start feeding the load meanwhile sharing the active power equally. At $t=1$ s the second DG unit is intentionally disconnected, and the rated power of the first DG unit is increased immediately to ensure supply continuity. At $t=2$ s DG unit two is reconnected and the active power signals are matched after 0.5s which confirms the capability of maintaining the active power sharing during these circumstances. The frequency drop in Figure 4-7(f) during the black start and load disturbance refers to the droop mechanism, similarly for the frequency overshoot at the load disconnection, the action of the proposed DSC compensates this deviation quickly and restores it to its rated value with a better dynamic response. Noticing that every reconnection to the MG system necessitates a synchronization procedure often using a PLL to match the frequency and the phase angle with the MG to minimize circulating currents among DG units besides eliminating fluctuations and disturbances.

4.3.3 Impact of communication latency

Communication infrastructures for data exchange are a crucial part of MGs, especially in the secondary control layer. To show the communication less feature of the developed controller this latter is compared with a centralized SC as presented in Figure 4-8. The centralized SC suffers from

major drawbacks represented by time delay and data drop-out. Firstly a communication time delay is simulated using the same electrical parameters for both MG models to achieve an accurate comparison using centralized and decentralized SC under an amount of communication latency equal to 200 ms. As observed in Figure 4-8(a) the frequency response of the centralized topology presents damped oscillation with a big settling time equal to 1.7s, the increment of the time delay leads to the loss the system stability, however, the decentralized SC f Figure 4-8(b) isn't impacted by the communication because it implemented locally, with a reduced settling time estimated by 0.2 s.

4.3.4 Comparative study of dynamic response

To verify and confirm the superiority of this method, the fuzzy logic controller is compared with the conventional PI controller used in [40]. The comparison investigates the dynamic response of the system and the compensation time, as can be seen in Figure 4-8(c). The compensation for the fuzzy logic controller starts after 0.06s from the drop of frequency, however in the case of the PI regulator the compensation starts after 0.15s; moreover, the fuzzy controller reaches the nominal value in 0.5s on the other hand 1.3s for the PI controller which confirms the flexibility and the rapidity of the proposed control, the same way in case of adding or removing loads the dynamic response of proposed controller is quick than the PI controller with a neglected overshoot. The above-mentioned tests show the flexibility of the proposed technic under different disturbances constraints and their behaviours against this test are very satisfactory.

4.3.5 Effect of data drop-out

Data drop-out or packet loss is one of the major drawbacks of communication systems. It can directly affect and degrade the performance of the system outputs. The performance of the proposed SC in the presence of packet losses has been tested and compared to the PI controller in real-time simulation considering the different amounts of data drop-out, 30%, and 70%. As shown in Figure 4-9 it can be observed that both controllers have acceptable performance in eliminating the frequency deviation for 30% data drop-out when data drop-out is up to 70%, the proposed SC can recover the system in 0.5 s; however, the PI controller is unable to recover the frequency quickly, it takes about 3 s to restore the system into their nominal frequency, comparing to the PI controller the proposed SC has a fast and flexible dynamic response which guarantee the stability of the system.

4.3.6 Effect of interferences

In real systems, there may exist interferences. In the case of a MG system interferences can be represented in emergency control, plug and play of DG units with a high priority task. In this test the simulation involves an interfering node sending disturbing traffic and disturbing high-priority tasks executing in the controller node, it can be seen in Figure 4-10 that the interferences with high-priority tasks have no impact on the proposed SC and the recovering time and the dynamic response are not affected which confirm the high performance of the proposed controller.

The purpose of this paper was to elaborate a decentralized secondary control that is achieved using a fuzzy controller and based on the unique property of the frequency in islanded MGs as a global variable. The performed tests and scenarios show the main features of the developed SC, represented in a reduced settling time compared to the conventional PI controller about 50% improvement, high flexibility against the plug-and-play operation with a smooth transition at every connection and disconnection of DG units no current fluctuations were observed, the packet losses almost has no impact on the SC and the system, in contrast of the conventional control which tends to have a slow dynamic response, interferences such as emergency control were simulated using the real-time toolbox to analyze the performance of the controller in real condition and results have shown high robustness against interferences. The performance of the proposed controller are evaluated through time domain specifications in Table 4-4.

Study, Modelling and Control of a Multisource Microgrid

Chapter 4: Decentralized secondary control for frequency regulation based on fuzzy logic control in islanded microgrid

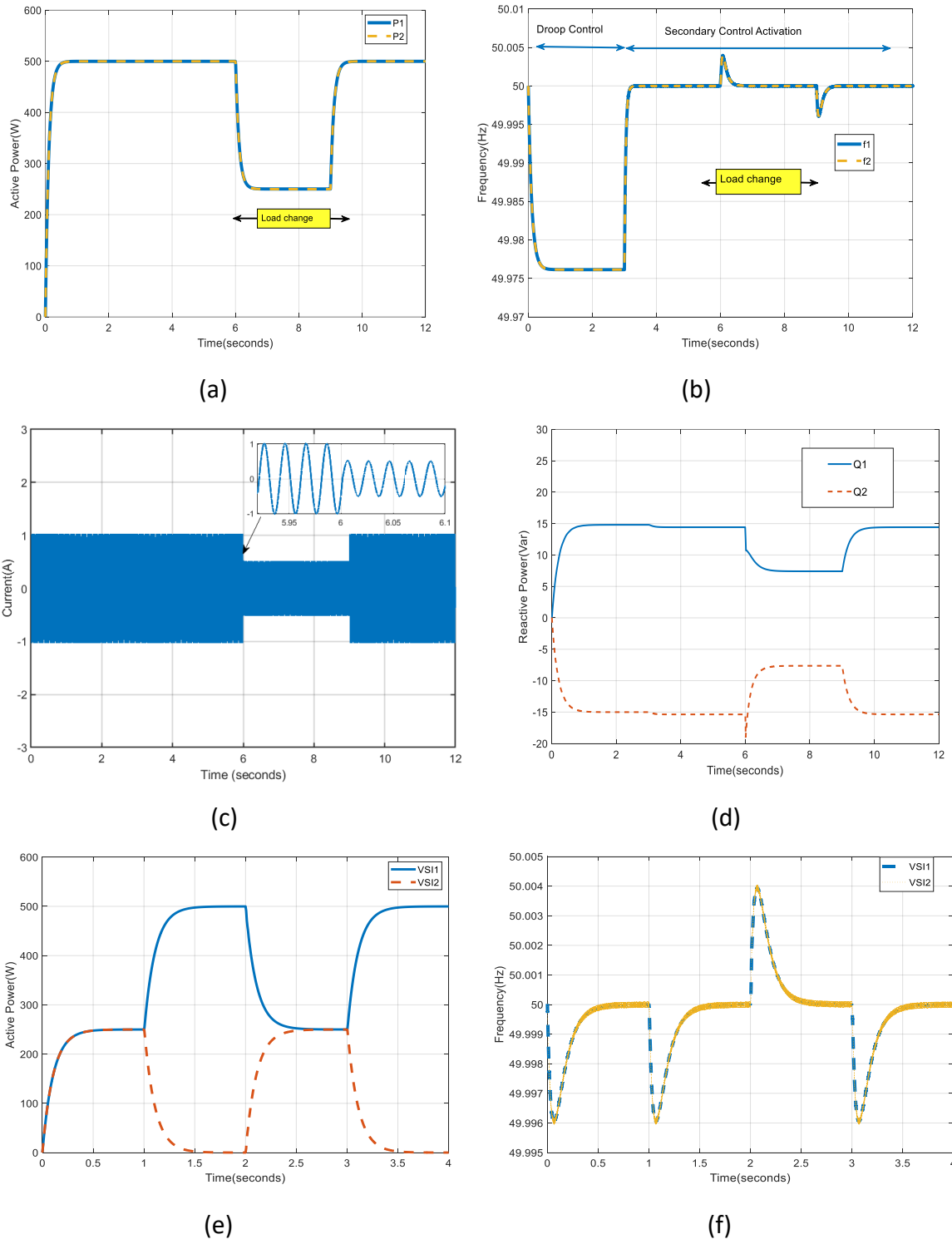


Figure 4-7: Performance of proposed controller under load disturbances with black start and plug and play test, (a) active power-sharing, (b) frequency restoration, (c) current, (d) reactive power (e) Black start and PNP - active power-sharing, and (f) Pnp frequency restoration

Study, Modelling and Control of a Multisource Microgrid

Chapter 4: Decentralized secondary control for frequency regulation based on fuzzy logic control in islanded microgrid

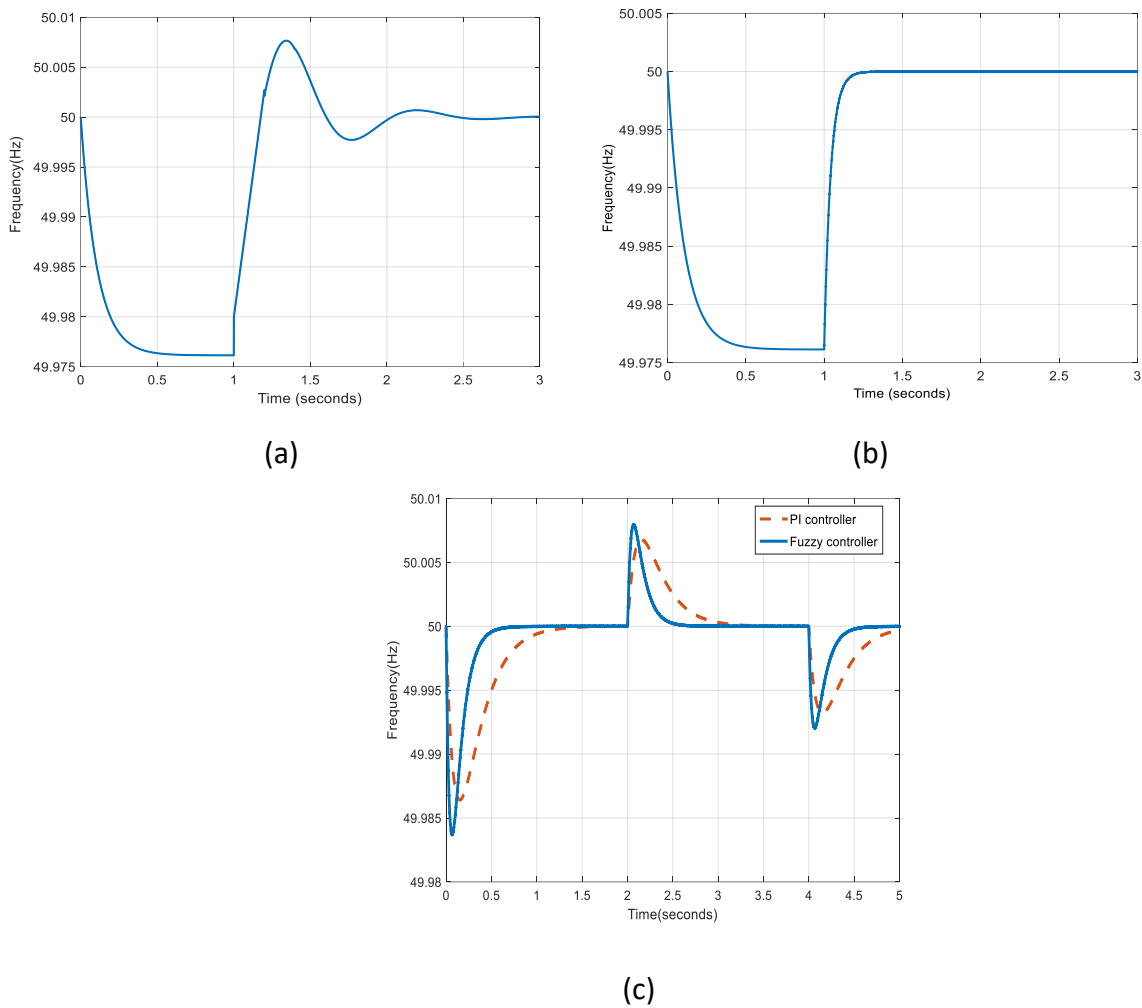


Figure 4-8: Performance of proposed controller, (a) frequency restoration under delay time 200ms - Centralized topology, (b) frequency restoration under delay time 200ms - decentralized topology and (c) comparison between fuzzy and PI controllers

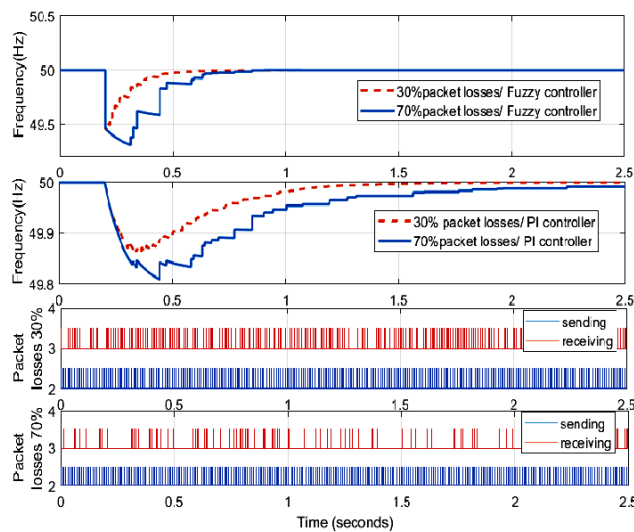


Figure 4-9: Performance of proposed secondary control considering data drop-out, when compared with PI controller

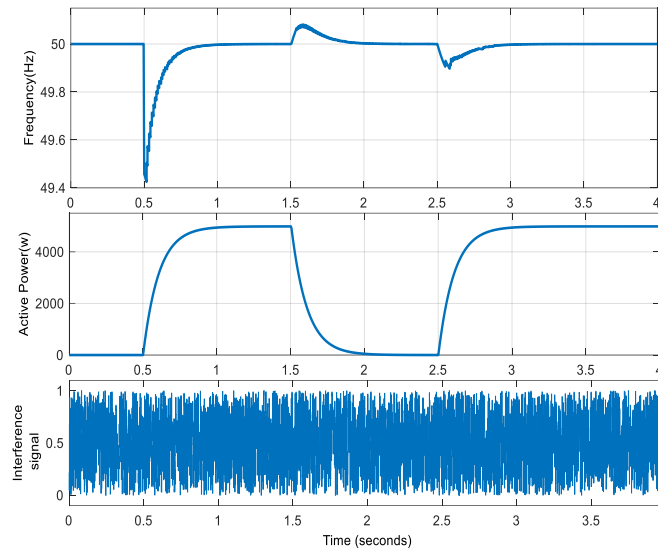


Figure 4-10: Performance of proposed controller under interferences

Table 4-4: Table 4. Performance evaluation of proposed scheme through time domain specifications.

Test scenario	Type of response	Type of Controller	Max. overshoot	Min. undershoot	Peak time (s)	Settling time (s)
1 Frequency restoration	frequency deviation Figure 7(b)	Fuzzy controller	5e-3	5e-3	0.066s	0,461s
2 Plug and play test	frequency deviation Figure 7(f)	Fuzzy controller	5e-3	5e-3	0.07s	0,537s
3 Frequency restoration under delay	frequency deviation Figure 8(a) and (b)	Fuzzy controller PI controller	0 1e-1	0 3e-3	0.2s 0.3s	0.2s 1.7s
4 Comparison test	frequency deviation Figure 8(c)	Fuzzy controller PI controller	7e-3 5e-3	1e-3 7e-4	0.66s 0.2s	0.48s 1.21s
5 Under packet losses 30% - 70%	frequency deviation Figure (9)	Fuzzy controller PI controller	0 0	0 0	0 0	0.6s – 0.65s 1.6s - >2.5s
6 Under interferences	frequency deviation Figure 10	Fuzzy controller	8e-2	5.6e-1	0.073s	0.5s

4.4 Conclusion

In this chapter, a decentralized secondary control for frequency regulation and active power-sharing in autonomous microgrids is introduced. The proposed communication-free SC was achieved using a fuzzy logic controller based on the local frequency error to generate an extra term to compensate the deviation and maintain accurate active power-sharing. The main contribution of this paper compared to the previous SC topologies was its decentralized control topology. Moreover, it offers a quick dynamic frequency recovery and it is much faster than conventional controllers with accurate active power tracking, its design and implementation are straightforward, no overshoots and oscillations in frequency are presented and no ripples in the steady-state response, it shows high flexibility and robustness during plug and play operation, further it is not impacted by the interferences. These performances are verified by simulation results and the comparison with the conventional PI regulator confirms that the proposed fuzzy controller is very effective in improving the transient stability of the overall system during load changes, data drop-out, and interferences especially in settling time where the improvement is estimated by 50%.

Chapter 5: Optimized virtual impedance design to improve reactive power sharing and microgrid stability

5.1 Introduction

Microgrid is key element for integrating renewable energy sources, however, its control tasks include many challenges, such as sensitivity to load changes and tripping events due to the existence of low inertial devices, moreover, each subsystem presents good stability in its nominal sets, but, the entire system stability could suffer due to serious interactions and coupling between subsystems, additionally, MG suffers from reactive power sharing issues due to the characteristics of the line impedance. The purpose of this study is to control and maintain the stability of parallel inverters forming an islanded MG while sharing the reactive power equally. This chapter proposes a novel approach to improving MG stability and reactive power sharing while maintaining other performance characteristics. Firstly, a novel small-signal model for autonomous MG including virtual impedances has been developed. Secondly, optimal virtual impedances are designed based on a new optimization algorithm using genetic algorithm. The eigenvalue analysis finds the stability ranges, and the optimization algorithm keeps the reactive power-sharing error at its lowest value throughout the objective function. The proposed approach is tested using MATLAB-Simulink software, and the results show the effectiveness of the proposed approach in enhancing the MG dynamic stability and minimizing the reactive power-sharing error.

The main contributions and novelties of this chapter can be listed as follows:

- First, an improved small-signal model for the island MGs with virtual impedances is proposed.
- The small-signal stability analysis is then carried out using the MG dynamic model.
- The optimal virtual impedances for converters in the MG are chosen using genetic algorithm (GA) that enhances the MG stability and eliminates reactive power mismatches without compromising MG performance.
- A novel objective function that makes it easier to accomplish the objectives simultaneously is proposed as part of the proposed optimization algorithm, which analyzes the MG stability at all feasible operating points.
- The investigations in [101], [7], and [102] are improved by this study.

- A systematic method to design virtual impedances to reduce reactive power imbalances between converters and boost the critical eigenvalues of the MG is suggested, and the stability of the MG's operation in the presence of virtual impedances is ensured.

This chapter is structured as follows. Small-signal analysis and MG modeling are introduced in Section 2. The virtual impedance design algorithm is described in Section 3. Section 4 contains the simulation results and discussions. Finally, the chapter is concluded in Section 5.

5.2 Microgrid modelling and small-signal stability analysis

A mathematical model of an islanded MG is developed in order to study and assess the added virtual impedance loop behaviour and its influence on system stability. This model has been created using state space representations of the latter's many components. Because the state space models are nonlinear, the small-signal model is formed by linearizing them around an operational point and combining them in a single reference frame. The MG seen in Figure 5-1 is split into three subsystems: inverters, lines, and loads. Each inverter is represented on its own reference frame, and its rotation frequency is determined by its local droop controller.

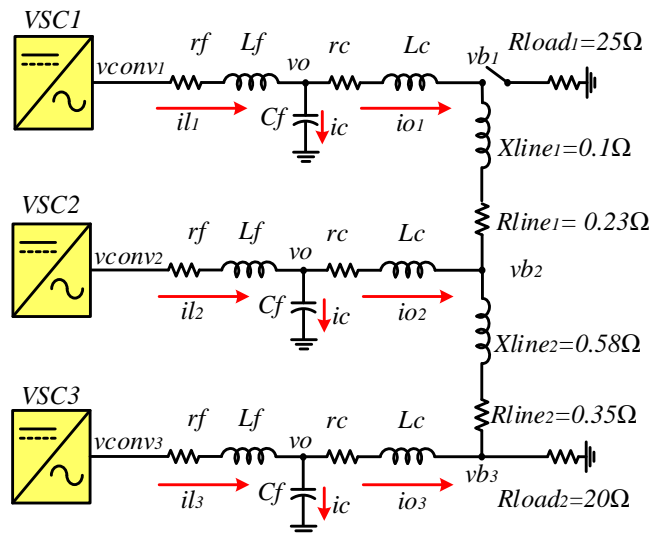


Figure 5-1: Configuration of tested MG

5.2.1 Power measurement-droop control and interface circuit

In islanding mode, operation DG units are interfaced to the MG using voltage source converters in a grid forming topology where the voltage and frequency set points are handled by the droop control as depicted in Figure 5-2. The active *P* and reactive *Q* powers can be obtained by calculating them using the dq components' voltage and current outputs and averaging them using a low-pass filter

(LPF) with reduced bandwidth. Therefore, the measured power P and Q are defined by the following equation:

$$\begin{cases} P = \frac{\omega_c}{s + \omega_c} \cdot p \Rightarrow \dot{P} = -P\omega_c + \frac{3}{2}(v_{od} \cdot i_{od} + v_{oq} \cdot i_{oq}) \\ Q = \frac{\omega_c}{s + \omega_c} \cdot q \Rightarrow \dot{Q} = -Q\omega_c + \frac{3}{2}(v_{oq} \cdot i_{od} - v_{od} \cdot i_{oq}) \end{cases} \quad (5.1)$$

Where ω_c is the cut-off frequency of the low-pass filter, v_{od} , v_{oq} , i_{od} , and i_{oq} are the sensed voltages and currents in the dq reference frame. Hence, the linearized model of power control can be expressed as follows:

$$\begin{cases} \Delta \dot{P} = -\omega_c \Delta P + \omega_c (I_{od} \Delta v_{od} + I_{oq} \Delta v_{oq} + V_{od} \Delta i_{od} + V_{oq} \Delta i_{oq}) \\ \Delta \dot{Q} = -\omega_c \Delta Q + \omega_c (I_{oq} \Delta v_{od} - I_{od} \Delta v_{oq} - V_{oq} \Delta i_{od} + V_{od} \Delta i_{oq}) \end{cases} \quad (5.2)$$

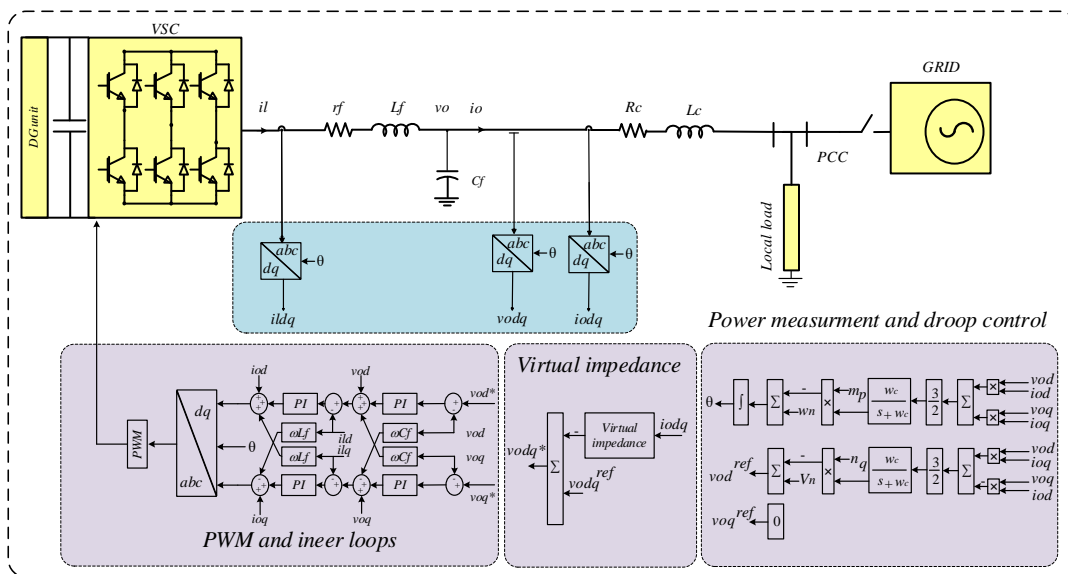


Figure 5-2: Proposed control scheme of a VSI in island mode

5.2.2 Virtual impedance equations

As written in equation (3), the virtual impedance is added in the droop control voltage loop, where R_v , X_v , and V_{vir} are, respectively, virtual resistance, virtual reactance, and virtual voltage drop. According to the control strategy, the q-axis voltage component is fixed at zero. In the next section, the optimization algorithm will be used to figure out the parameters of virtual resistance and virtual inductance.

$$\begin{cases} V_{vir} = (R_v \cdot i_{od} - X_v \cdot i_{oq}) \\ \Delta V_{vir} = (R_v \cdot \Delta i_{od} - X_v \cdot \Delta i_{oq}) \end{cases} \quad (5.3)$$

As previously stated, the voltage and frequency set points are determined by the voltage source converters throughout the droop control, as can be seen in the following equation:

$$\begin{cases} \omega^* = \omega_n - m_p \times (P - P_0) \\ \Delta \omega^* = -m_p \times \Delta P \\ V_{od}^* = V_{od_n} - n_q (Q - Q_0) - V_{vir} \\ \Delta V_{od}^* = -n_q \times \Delta Q - \Delta V_{vir} \end{cases} \quad (5.4)$$

Where V_{od_n} and ω_n denote the nominal voltage and frequency, and m_p , n_q denote the droop coefficients.

A common reference frame is required to build the small signal model. Hence the reference frame of one of the inverters is defined as the common D - Q reference frame. To translate the variables from an individual inverter d - q frame reference frame into the global D - Q frame, the angle difference δ for each inverter is defined as below:

$$\begin{cases} \delta = \int (\omega - \omega_{com}) \\ \Delta \dot{\delta} = \Delta \omega - \Delta \omega_{com} = -m_p \Delta P - \Delta \omega_{com} \end{cases} \quad (5.5)$$

Where ω_{com} is the angular frequency of the common frame. As depicted in Figure 5-3, the axis set (D - Q) is the common reference frame rotating at a frequency ω_{com} while axes (d - q)₁ and (d - q)₂ are the reference frames of the second and third inverters rotating at ω_1 and ω_2 , respectively.

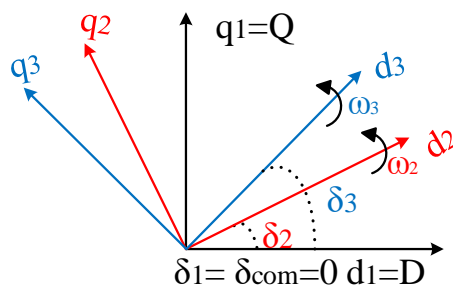


Figure 5-3: Reference frame transformation

5.2.3 Voltage controller loop

A typical proportional and integral (PI) regulator is used in the voltage control loop. The PI controller's input is the signal formed by comparing the sampled output voltage to the power controller's reference value, and a feed-forward gain is applied to correct for output current disturbances and provide the dq current reference components, as illustrated below:

$$\left\{ \begin{array}{l} \frac{d\phi_d}{dt} = v_{od}^* - v_{od} \\ \Delta\dot{\phi}_d = \Delta v_{od}^* - \Delta v_{od} \\ \frac{d\phi_q}{dt} = v_{oq}^* - v_{oq} \\ \Delta\dot{\phi}_q = \Delta v_{oq}^* - \Delta v_{oq} \\ i_{ld}^* = Fi_{od} - \omega_n C_f v_{oq} + K_{pv} (v_{od}^* - v_{od}) + K_{iv} \phi_d \\ \Delta i_{ld}^* = K_{iv} \Delta \phi_d + K_{pv} \Delta v_{od}^* - K_{pv} \Delta v_{od} - \omega_n C_f \Delta v_{oq} + F \Delta i_{od} \\ i_{lq}^* = Fi_{oq} + \omega_n C_f v_{od} + K_{pv} (v_{oq}^* - v_{oq}) + K_{iv} \phi_q \\ \Delta i_{lq}^* = K_{iv} \Delta \phi_q + K_{pv} \Delta v_{oq}^* + \omega_n C_f \Delta v_{od} - K_{pv} \Delta v_{oq} + F \Delta i_{oq} \end{array} \right. \quad (5.6)$$

Where K_{pv} , and K_{iv} are the voltage controller's proportional and integral gains, respectively; C_f is the LC filter's per-phase capacitance; and F is the feed-forward voltage controller gain.

5.2.4 Current controller loop

Similarly to the voltage controller, the current controller uses a PI regulator to eliminate the error between the sensed current and the reference one and then generates the PWM signal as shown in the equation below:

$$\left\{ \begin{array}{l} \frac{d\gamma_d}{dt} = i_{ld}^* - i_{ld} \\ \Delta\dot{\gamma}_d = \Delta i_{ld}^* - \Delta i_{ld} \\ \frac{d\gamma_q}{dt} = i_{lq}^* - i_{lq} \\ \Delta\dot{\gamma}_q = \Delta i_{lq}^* - \Delta i_{lq} \\ v_{id}^* = v_{od} - \omega_n L_f i_{lq} + K_{pc} (i_{ld}^* - i_{ld}) + K_{ic} \gamma_d \\ \Delta v_{id}^* = K_{ic} \Delta \gamma_d + K_{pc} \Delta i_{ld}^* - K_{pc} \Delta i_{ld} - \omega_n L_f \Delta i_{lq} \\ v_{iq}^* = v_{oq} + \omega_n L_f i_{ld} + K_{pc} (i_{lq}^* - i_{lq}) + K_{ic} \gamma_q \\ \Delta v_{iq}^* = K_{ic} \Delta \gamma_q + K_{pc} \Delta i_{lq}^* + \omega_n L_f \Delta i_{ld} - K_{pc} \Delta i_{lq} \end{array} \right. \quad (5.7)$$

Where K_{pc} , and K_{ic} denote the proportional and integral gains of current, respectively; i_{ld} , and i_{lq} denote the filter dq currents; and L_f is the per-phase inductance.

5.2.5 LCL filter model

To eliminate the harmonics created by the PWM switching inverter, an LCL filter is interfaced between the inverter and the point of coupling. The LCL filter dynamics are represented by the state equations below in (5.8), which assume that the inverter generates the desired inverter bridge voltage.

$$\left\{ \begin{array}{l} \frac{di_{ld}}{dt} = \frac{-r_f}{L_f} i_{ld} + \omega i_{lq} + \frac{1}{L_f} v_{id} - \frac{1}{L_f} v_{od} \\ \frac{di_{lq}}{dt} = \frac{-r_f}{L_f} i_{lq} - \omega i_{ld} + \frac{1}{L_f} v_{iq} - \frac{1}{L_f} v_{oq} \\ \frac{dv_{od}}{dt} = \omega v_{oq} + \frac{1}{C_f} i_{ld} - \frac{1}{C_f} i_{od} \\ \frac{dv_{oq}}{dt} = -\omega v_{od} + \frac{1}{C_f} i_{lq} - \frac{1}{C_f} i_{oq} \\ \frac{di_{od}}{dt} = \frac{-r_c}{L_c} i_{od} + \omega i_{oq} + \frac{1}{L_c} v_{od} - \frac{1}{L_c} v_{bd} \\ \frac{di_{oq}}{dt} = \frac{-r_c}{L_c} i_{oq} - \omega i_{od} + \frac{1}{L_c} v_{oq} - \frac{1}{L_c} v_{bq} \end{array} \right. \quad (5.8)$$

The state-space equations in (5.9) are obtained by linearizing (5.8) around the operational points:

$$\left\{ \begin{array}{l} \Delta \dot{i}_{ld} = -\frac{R_f}{L_f} \Delta i_{ld} + \omega_o \Delta i_{lq} - \frac{1}{L_f} \Delta v_{od} + \frac{1}{L_f} \Delta v_{id} + I_{lq} \Delta \omega \\ \Delta \dot{i}_{lq} = -\omega_o \Delta i_{ld} - \frac{R_f}{L_f} \Delta i_{lq} - \frac{1}{L_f} \Delta v_{oq} + \frac{1}{L_f} \Delta v_{iq} - I_{ld} \Delta \omega \\ \Delta \dot{v}_{od} = \frac{1}{C_f} \Delta i_{ld} + \omega_o \Delta v_{oq} - \frac{1}{C_f} \Delta i_{od} + V_{oq} \Delta \omega \\ \Delta \dot{v}_{oq} = \frac{1}{C_f} \Delta i_{lq} - \omega_o \Delta v_{od} - \frac{1}{C_f} \Delta i_{oq} - V_{od} \Delta \omega \\ \Delta \dot{i}_{od} = \frac{1}{L_c} \Delta v_{od} - \frac{R_c}{L_c} \Delta i_{od} + \omega_o \Delta i_{oq} - \frac{1}{L_c} \Delta v_{bd} + I_{oq} \Delta \omega \\ \Delta \dot{i}_{oq} = \frac{1}{L_c} \Delta v_{oq} - \omega_o \Delta i_{od} - \frac{R_c}{L_c} \Delta i_{oq} - \frac{1}{L_c} \Delta v_{bq} - I_{od} \Delta \omega \end{array} \right. \quad (5.9)$$

Where v_{bd} , v_{bq} are the dq axis nodes voltages; v_{id} , v_{iq} are the inverter voltages in the dq frame respectively; ω_o , I_{ld} , I_{lq} , V_{od} , V_{oq} , I_{od} , I_{oq} are steady-state values at the examined operating point.

5.2.6 Complete inverter model

To interface the output variables i_{odq} to the entire system model, they must be transferred to the common DQ frame using the transformation matrix as exhibited in (5.10) and (5.11):

$$\begin{bmatrix} i_{oDQ} \end{bmatrix} = [T] \begin{bmatrix} i_{odq} \end{bmatrix} = \begin{bmatrix} \cos(\delta) & -\sin(\delta) \\ \sin(\delta) & \cos(\delta) \end{bmatrix} \begin{bmatrix} i_{odq} \end{bmatrix} \quad (5.10)$$

The obtained linearized model of the output currents of the inverter is shown in (5.11):

$$\begin{bmatrix} \Delta i_{oDQ} \end{bmatrix} = \begin{bmatrix} \cos(\delta_o) & -\sin(\delta_o) \\ \sin(\delta_o) & \cos(\delta_o) \end{bmatrix} \begin{bmatrix} \Delta i_{odq} \end{bmatrix} + \begin{bmatrix} -I_{od} \sin(\delta_o) - I_{oq} \cos(\delta_o) \\ I_{od} \cos(\delta_o) - I_{oq} \sin(\delta_o) \end{bmatrix} \begin{bmatrix} \Delta \delta \end{bmatrix} \quad (5.11)$$

Similarly, the bus voltage is the input signal to the inverter model, which is stated in the DQ global reference frame. The bus voltage must be converted to the local inverter reference frame using the reverse transformation illustrated below:

$$\begin{bmatrix} v_{bdq} \end{bmatrix} = [T^{-1}] \begin{bmatrix} v_{bDQ} \end{bmatrix} = \begin{bmatrix} \cos(\delta) & \sin(\delta) \\ -\sin(\delta) & \cos(\delta) \end{bmatrix} \begin{bmatrix} v_{bDQ} \end{bmatrix} \quad (5.12)$$

$$B_{INVi} = \begin{bmatrix} 0 & \dots & 0 & -\frac{\cos \delta_o}{L_c} & -\frac{\sin \delta_o}{L_c} \\ 0 & \dots & 0 & \frac{\sin \delta_o}{L_c} & -\frac{\cos \delta_o}{L_c} \end{bmatrix}_{2 \times 5}^T ; B_{\omega com} = [-1 \ 0 \ \dots \ 0]_{1 \times 13}^T ;$$

$$C_{INV\omega i} = \begin{cases} [0 - m_p \ 0 \ \dots \ 0]_{1 \times 13} & i = 1 \\ [0 \ \dots \ 0]_{1 \times 13} & i \neq 1 \end{cases}$$

$$C_{INVCi} = \begin{bmatrix} -I_{od} \sin \delta_o - I_{oq} \cos \delta_o & 0 & \dots & 0 & \cos \delta_o & -\sin \delta_o \\ I_{od} \cos \delta_o - I_{oq} \sin \delta_o & 0 & \dots & 0 & \sin \delta_o & \cos \delta_o \end{bmatrix}_{2 \times 6}$$

5.2.7 Parallel inverters model

A small-signal model of the MG depicted in Fig.1, which is composed of three parallel inverters, can be obtained based on the model of individual inverters developed in (5.14) and (5.15), as below:

$$[\Delta \dot{x}_{INV}] = A_{INV} [\Delta x_{INV}] + B_{INV} [\Delta v_{bDQ}] \quad (5.17)$$

$$[\Delta i_{oDQ}] = C_{INVC} [\Delta x_{INV}] \quad (5.18)$$

Where

$$[\Delta x_{INV}] = [\Delta x_{inv1} \ \Delta x_{inv2} \ \Delta x_{inv3}]^T$$

$$[\Delta v_{bDQ}] = [\Delta v_{bDQ1} \ \Delta v_{bDQ2} \ \Delta v_{bDQ3}]^T$$

$$A_{INV} = \begin{bmatrix} A_{INV1} + B_{\omega com} C_{INV\omega 1} & & \\ & A_{INV2} + B_{\omega com} C_{INV\omega 2} & \\ & & A_{INV3} + B_{\omega com} C_{INV\omega 3} \end{bmatrix} ;$$

$$B_{INV} = \begin{bmatrix} B_{INV1} & & \\ & B_{INV2} & \\ & & B_{INV3} \end{bmatrix} ; C_{INVC} = \begin{bmatrix} C_{INVC1} & & \\ & C_{INVC2} & \\ & & C_{INVC3} \end{bmatrix}$$

5.2.8 Subsystems models (lines and loads)

For the MG presented in Figure 5-1, the small signal state-space model network can be obtained, as shown in equation (21), noticing that the model is in the common DQ reference frame:

$$[\Delta \dot{i}_{line DQ}] = A_{NET} [\Delta i_{lineDQ}] + B_{1NET} [\Delta v_{bDQ}] + B_{2NET} \Delta \omega \quad (5.19)$$

Where M_{INV} maps the DG connection points onto MG network nodes, M_{LOAD} maps load connection points onto nodes, and M_{NET} maps the connecting lines onto nodes. Fig. 1 consists of $s=3$ DG, $n=2$ lines, $p=2$ loads, and $m=3$ nodes.

$$R_N = \begin{bmatrix} r_N & & & \\ & \ddots & & \\ & & r_N & \\ & & & r_N \end{bmatrix}_{2m \times 2m}; \quad M_{LOAD} = \begin{bmatrix} -1 & & & & \\ 0 & -1 & & & \\ 0 & 0 & 0 & & \\ 0 & 0 & 0 & & \\ & & & -1 & 0 \\ & & & & -1 \end{bmatrix}_{2m \times 2p}$$

$$M_{INV} = \begin{bmatrix} 1 & & & & \\ & 1 & & & \\ & & 1 & & \\ & & & 1 & \\ & & & & 1 \end{bmatrix}_{2m \times 2s}; \quad M_{NET} = \begin{bmatrix} -1 & & & & \\ 0 & -1 & & & \\ 1 & 0 & -1 & & \\ & 1 & 0 & -1 & \\ & & 1 & 0 & \\ & & & 1 & \\ & & & & 1 \end{bmatrix}_{2m \times 2n}$$

Thus the $47 (2n + 2p + 13s)$ order small signal of the entire MG model can be obtained as follows:

$$\begin{bmatrix} \Delta \dot{x}_{INV} \\ \Delta \dot{i}_{line DQ} \\ \Delta \dot{i}_{loadDQ} \end{bmatrix} = A_{MG} \begin{bmatrix} \Delta x_{INV} \\ \Delta i_{line DQ} \\ \Delta i_{loadDQ} \end{bmatrix} \quad (5.22)$$

Where A_{MG} is presented following

$$A_{MG} = \begin{bmatrix} A_{INV} + B_{INV}R_N M_{INV} C_{INVc} & B_{INV}R_N M_{NET} & B_{INV}R_N M_{LOAD} \\ B_{1NET}R_N M_{INV} C_{INVc} + B_{2NET}C_{INV\omega} & A_{NET} + B_{1NET}R_N M_{NET} & B_{1NET}R_N M_{LOAD} \\ B_{1LOAD}R_N M_{INV} C_{INVc} + B_{2LOAD}C_{INV\omega} & B_{1LOAD}R_N M_{NET} & A_{LOAD} + B_{1LOAD}R_N M_{LOAD} \end{bmatrix}$$

5.3 Eigenvalue analysis and virtual impedance optimization

In order to investigate the effects of virtual impedance variation on the system stability and to determine the virtual impedance stability limits for further use as constraints in the optimization algorithm, an eigenvalue analysis is performed using the linearized system developed above. The steady-state operating point can be obtained using time-domain simulations in MATLAB-SIMULINK.

Figure 5-4(a) depicts the eigenvalue spectrum of the system, which is extracted from the system state matrix A_{MG} with R_v and L_v equal to zero. It can be observed that a large range of frequency components exists, and they can be grouped into three clusters. As analyzed in [144], the participation factors of the different states in the eigenvalues plot showed that the eigenvalues

located closer to the origin (cluster 1), which is considered the dominant system mode, that highly sensitive to the state variables of the power controller. Cluster 2 represents the medium frequency modes that are highly sensitive to the state variables of the inner loop controllers, and the output LC filter blocks. Cluster 3 is the high-frequency mode that are far from the origin. Analysis showed that they are sensitive to the state variables of the LC filter, the output inductor, the inner loops of the inverters, and the network line currents.

5.3.1 Effect of virtual impedance parameters on system eigenvalue spectrum

The best way to observe the effects of parameter variations on system eigenvalues is to vary them in a predefined interval of the parameters of interest and observe the migration of system eigenvalues. To investigate the effects of the virtual impedance parameters R_v and L_v , on system stability and due to the simple system configuration, this approach is adopted in the following. Fig.4(b) shows the migration of the eigenvalues as a function of the virtual resistance R_v in the interval of $[0, 10 \Omega]$ (the same value of R_v was used for all three inverters), the arrows show the direction of the migration for the eigenvalues, it can be observed that the increase of R_v causes a migration of low-frequency modes eigenvalues far from the origin which means more damping and more stability for the system, however, the medium frequency modes eigenvalues migrate toward the rightwards which make the system more sensitive to state variables of the inner loops controllers, and the output LC filter, thus a trade-off is needed to benefit from the low-frequency modes eigenvalues without a considerable impact on the medium frequency modes eigenvalues.

Similarly, Figure 5-4(c) shows the trajectory of the system eigenvalues during changing the virtual inductor L_v in the range $[0, 0.1H]$ (the same value of L_v was used for all three inverters), the arrows show the direction of the migration of the eigenvalues, it can be seen that the increase of L_v results in two steps migration for the low-frequency modes eigenvalues the first step is toward the leftwards which enhances the transient response, moreover, it makes the system less sensitive to the power control loops, however, the second step is toward the rightwards which eliminates the aforementioned advantages, the remaining clusters are migrated towards the leftwards.

5.3.2 Virtual impedance optimization

The stability limits of the virtual impedance parameters are determined from critical values using eigenvalue analysis, therefore the system stability will be guaranteed during the optimization operation, and improves computational efficiency. The limits of stability for the virtual impedance

parameters are $[0, 8 \Omega]$; and, $[0, 0.03 \text{ H}]$ for the virtual resistance and the virtual inductance, respectively. The main objective of the proposed optimization approach is typically minimizing the reactive power sharing error in steady-state and enhancing the transitory response of the system based on optimal virtual impedance design. Among the metaheuristic algorithms, Genetic Algorithm GA is a very famous population-based stochastic algorithm that is adopted in many research works such as renewable energies (including MGs design and control) to solve optimization problems. GA is an appropriate solution for this kind of application because it has the advantages of the inherent trait to deal with continuous/discrete problems, constraints are integrated into the genes, search is performed from multiple points as well as easy implementation.

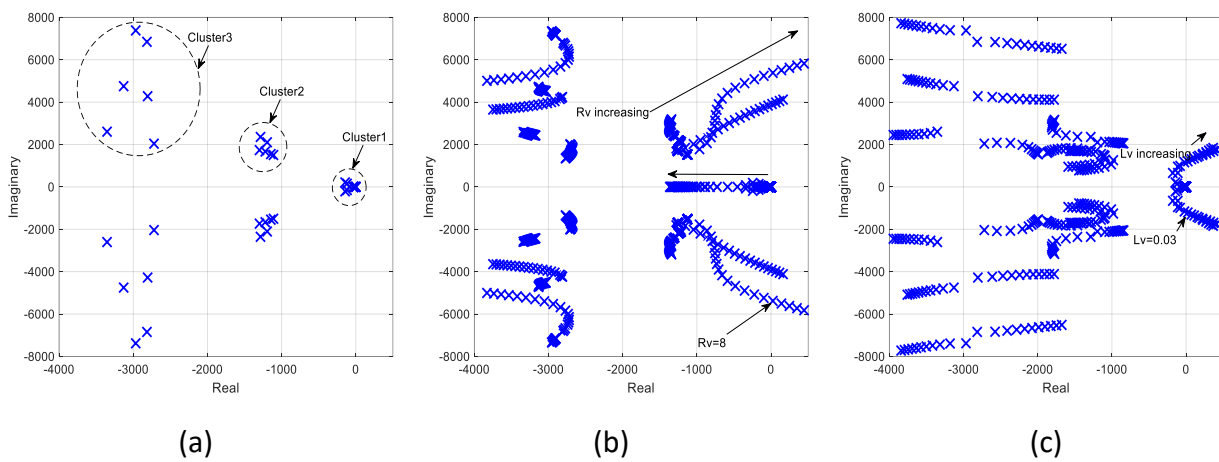


Figure 5-4: The eigenvalue spectrum of the system (a) without virtual impedance (b) effect of increasing the virtual resistance(R_v): $0 < R_v < 10\Omega$, (c) effect of increasing the virtual inductance (L_v): $0 < L_v < 0.1 \text{ H}$

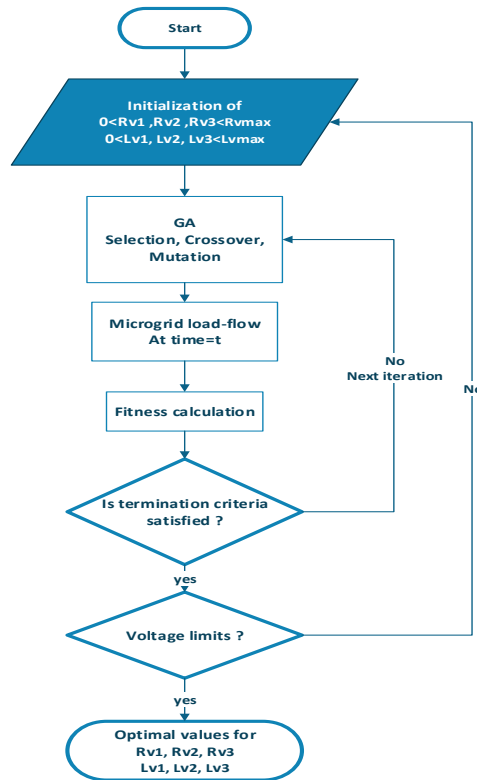


Figure 5-5: Flowchart algorithm for virtual impedance optimization

As a result, GA is adopted in this work to find the optimal virtual impedance values and hence improve reactive power sharing. Further details about GA algorithm can be found in [145].

The reason for adopting droop control is their high capability of sharing active power without using communications. However, it's not the case for reactive power, the mismatch in line impedance causes errors in reactive power sharing. Thus, the integral summation of the reactive power mismatches for all DG units multiplied by their reactive power droop coefficients is to be minimized. As a result, the objective function to be minimized must be relevant to the reactive power as follows:

$$O.F = \min \sum_{i=1}^{n_{DG}} \sum_{\substack{j=1 \\ j \neq i}}^{n_{DG}} |n_i Q_i - n_j Q_j| \quad (5.23)$$

Where Q_i and Q_j are measured reactive powers of DG_i and DG_j , respectively, similarly n_i and n_j are the voltage droop coefficients of DG_i and DG_j , and n is the number of DG units.

The optimization constraints are determined as mentioned in equation (5.24):

$$\left\{ \begin{array}{l} R_{v1}^{min} \leq R_{v1} \leq R_{v1}^{max} \\ R_{v2}^{min} \leq R_{v2} \leq R_{v2}^{max} \\ R_{v3}^{min} \leq R_{v3} \leq R_{v3}^{max} \\ L_{v1}^{min} \leq L_{v1} \leq L_{v1}^{max} \\ L_{v2}^{min} \leq L_{v2} \leq L_{v2}^{max} \\ L_{v3}^{min} \leq L_{v3} \leq L_{v3}^{max} \end{array} \right. \quad (5.24)$$

The main purpose is to minimize the fitness function (5.23) based on the constraints in (5.24).

The flowchart of the proposed optimal virtual impedance design is depicted in Figure 5-5 that can be resumed as follows:

- Initialization of the optimization variables which are $L_{v1}, L_{v2}, \dots, L_{vn}$, and $R_{v1}, R_{v2}, \dots, R_{vn}$ in the predefined range which is considered as the stability limits of the system.
- The GA population and the other parameters of the algorithm are assigned, and the GA algorithm is run, thus the selection, crossover, and mutation of the initial population occur.
- The time domain simulation under MATLAB Simulink at time= t according to the desired operating points.
- Calculation of the objective function
- If the convergence condition which is the number of iteration is satisfied the algorithm pass to check the voltage limits else another iteration will be started.
- The voltages in MG must remain in an acceptable range, if the voltage limits are not respected the algorithm returns to the first step to decrease the voltage drops because minimizing the reactive power exchanges implies voltage drops which need to be respected, another solution is to change the voltage set points within the respected boundaries.
- If the voltage limits are respected, the algorithm returns the optimal parameters for virtual inductances and resistances.

Noticing that the optimization algorithm is run off-line and the obtained virtual impedances are then used in converter controllers.

Using the GA algorithm for a population size of 20 and a number of iterations equal to 40. And after performing the algorithm depicted in Fig.5. The final optimal values for the virtual resistances and inductances are described in Table 5-1, which are used in the converters control loops.

Table 5-1: Optimized virtual impedances

R_{v1}	R_{v2}	R_{v3}	L_{v1}	L_{v2}	L_{v3}
0.037	0.016	0.064	0.02	0.018	0.017

Figure 5-6 shows the eigenvalues maps with the installed virtual impedance and without it, it is clear that the low-frequency modes eigenvalues with the optimal virtual impedance were shifted toward the leftwards part, which enhances the system stability and the dynamic response by offering more damping for the system.

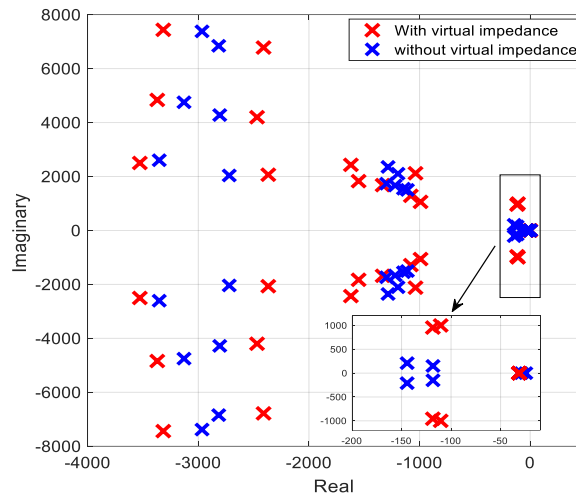


Figure 5-6: Eigenvalues trace comparison with and without virtual impedance

5.4 Validation of the proposed approach

A 3-BUS MG developed in [144] as mentioned in Fig.1 was implemented in MATLAB Simulink based on the obtained optimal control parameters in order to test its steady-state and transient performance in islanded operation mood. A constant voltage for the dc buses is considered in this simulation, the inverters parameters are demonstrated in Table 5-2. The main objective of the proposed optimal virtual impedances is to ensure a good dynamic response and enhance the reactive power sharing under different operating conditions, the transient performance was simulated by applying a step change in the load at bus1 number one from 0.5 to 1s which lead for large disturbances in active and reactive power sets.

5.4.1 Inverters output power and frequency

Fig.7 shows the injected active/reactive power and frequency under the proposed method compared with the control method in [7]. From Figure 5-7(d) it can be observed that in steady-state operation the active power sharing was equal for all the inverters under both methods, moreover, during the transient time in the black start or after the load disturbance at 0.5s a large overshoot followed by low-frequency oscillations are observed in[7].

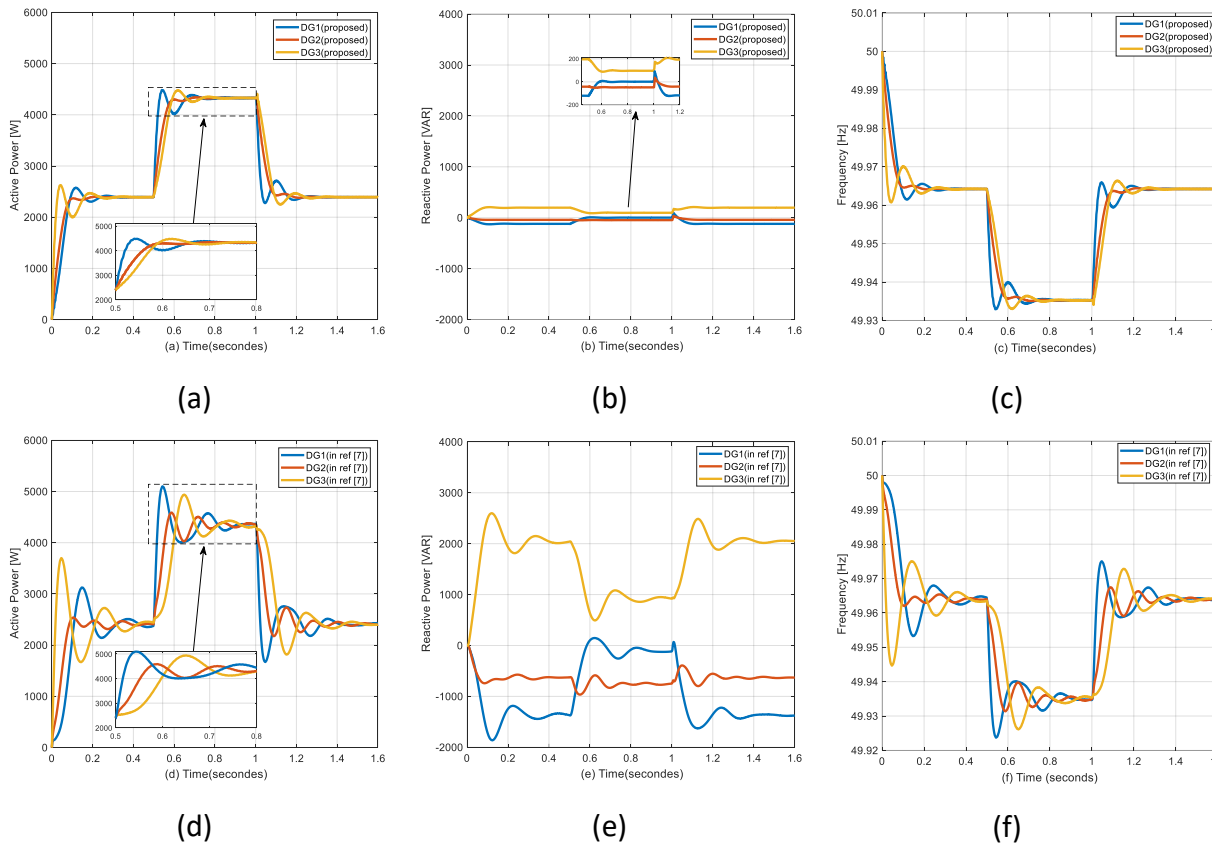


Figure 5-7: Comparison of control method in [7] with the proposed virtual impedance (a) active power; (b) reactive power; (c) frequency /using the proposed method, (d) active power; (e) reactive power; (f) frequency/ using method in [7]

In contrast, the proposed method in Figure 5-7(a) presents less overshoots and less oscillations with faster settling time than the former method. A comparison between the time domain characteristics of both methods was conducted in Table 5-3, the rise time (t_r), peak overshoot (M_p), and settling time (t_s) are elaborated at the instance 0.5 to 1s in order to highlight the dynamic improvement of the nd M_p are much better for the enhanced scheme. the proposed method during load disturbances, the rise time of the active power using the method in [7] is faster than the proposed scheme, this is directly related to the peak overshoot which is greater for all inverters using the conventional method, however, the t_s a

Figure.5-7(b,e) Illustrate the reactive output of the inverters, although there is no reactive loads connected to the system and due to the line impedances mismatch there is an exchange of the reactive power between inverters, for the method in [7] the amount of the reactive power exchange is huge especially before the introduction of the load disturbance as can be seen in Figure 5-7(e) (-1.5k Var, -0.5k Var, 2k Var) with the presence of big overshoots and low frequency oscillations, after the introduction of the load on the bus 1 this amount is reduced due to the power coupling and the location of the disturbance (-0.2k Var -0.7k Var 0.9k Var) but still a big amount which is one of the droop control imperfections, in comparison to the proposed method in Figure 5-7(b) the amount of the circulating reactive power is very small (-0.05k Var -0.13k Var 0.18k Var) without the presence of the low frequency oscillations and less overshoots, this amount can be neglected after the load disturbance introduction (-0.02k Var -0.08k Var 0.1k Var) which confirms the effectiveness of the proposed method for enhancing the reactive power sharing. From Table.5-3 the peak overshoot of DGs using the enhanced method are much lower than the conventional one, in addition, it is to be noted that higher overshoot implies a higher settling time for the conventional method.

5.4.2 Converters output current components

Figure 5-8 presents the dq-axis output currents components of the inverters, it can be observed that the dynamic response of the d-axis current component of each inverter mimics its active power response, similarly to the q-axis current component and the reactive. During the black start, the d-axis current components applying the method in [7] shows higher overshoot (DG1=9.5 A, DG2=7.8 A, DG3=16 A), however using the proposed method which exhibits lower overshoot except for the third inverter which is near to the load and hence it needs to respond quickly for the current demand (DG1=7.5 A, DG2=7.2 A, DG3=16 A), that is an important advantage of the proposed approach, noticing that the low frequency are more presented in the conventional method than the proposed one, the q-axis current component without applying the optimal virtual impedance shows different values (DG1=4 A, DG2=1 A, DG3=-5 A), in contrast, the presence of the optimal virtual impedance reduced them to an identical value (DG=DG2=DG3≈ 0A). The proposed optimal virtual impedances successfully illuminate the q-component current exchange between DGs, the time domain performance specification after the load connection are presented in Table.3, similarly, the settling time is faster using the optimal virtual impedance and the system is well-damped for both dq-axis components current.

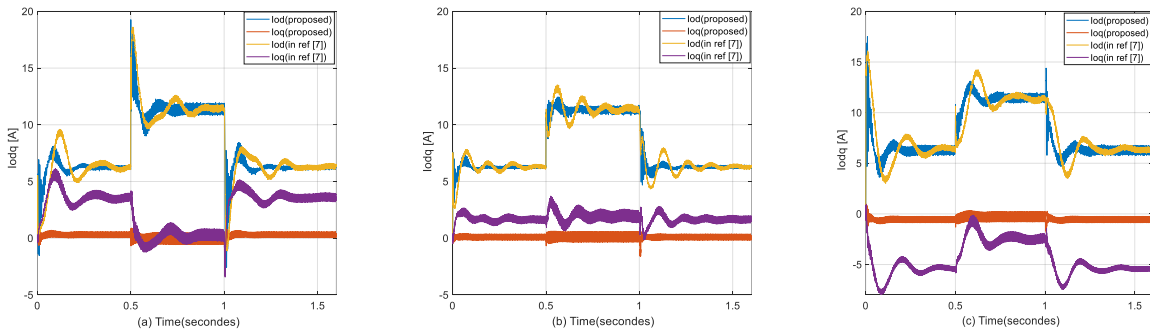


Figure 5-8: Comparison of output currents in control method in [7] with the proposed method (a) inverter1; (b) inverter 2; (c) inverter3

5.4.3 Converters voltage components

Figure 5-9 depicts the dq-axis output voltages of the three inverters, the q-axis voltage component (voq) for both methods is equal to zero in the steady-state regime because it is fixed to zero in the control diagram. The d-axis output voltage has the same values for the three inverters and using both methods which are around 380 V ($\pm 1v$), the load changes haven't a considerable effect on the voltage, this latter is kept in a permitted interval for both approaches and its drop is less than 3% which is in the acceptable range.

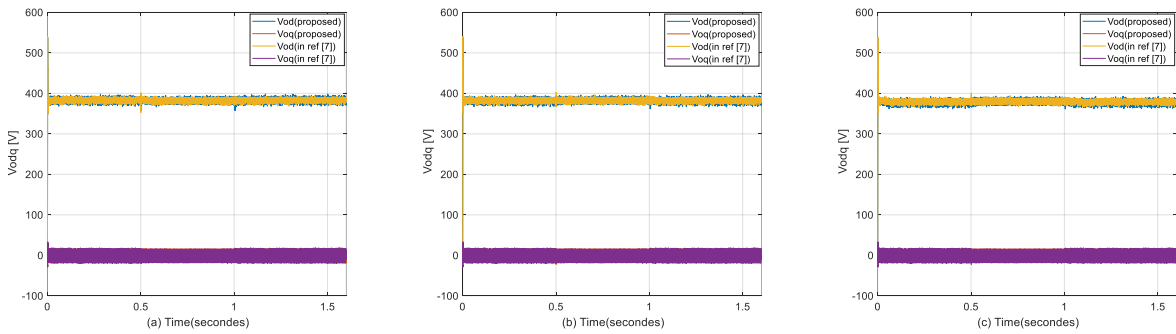


Figure 5-9: Comparison of voltage outputs in control method in [7] with the proposed method (a) inverter1; (b) inverter 2; (c) inverter3

5.4.4 Reactive power step

An additional test scenario is performed in order to confirm the reactive power sharing effectiveness, this test consists of a reactive load step on the bus number 1 (5k VAR) using the Simpower system load which is not a real case.

Figure 5-10 presents the reactive power sharing using the conventional droop control and the proposed virtual impedance, it is clear that the proposed method shares the reactive load equally between the inverters, however

using the conventional method the reactive load is supplied using the inverter one since it is the closest and the reactive power sharing is far different for the three inverters (DG1=4.1k Var, DG2=0.6k Var, DG3=0.3k Var) which ensure the high performance of reactive power sharing of the proposed optimal method, noticing that the voltage drop should be taken in consideration in the design procedure to maintain it in an acceptable range usually by changing the voltage sets.

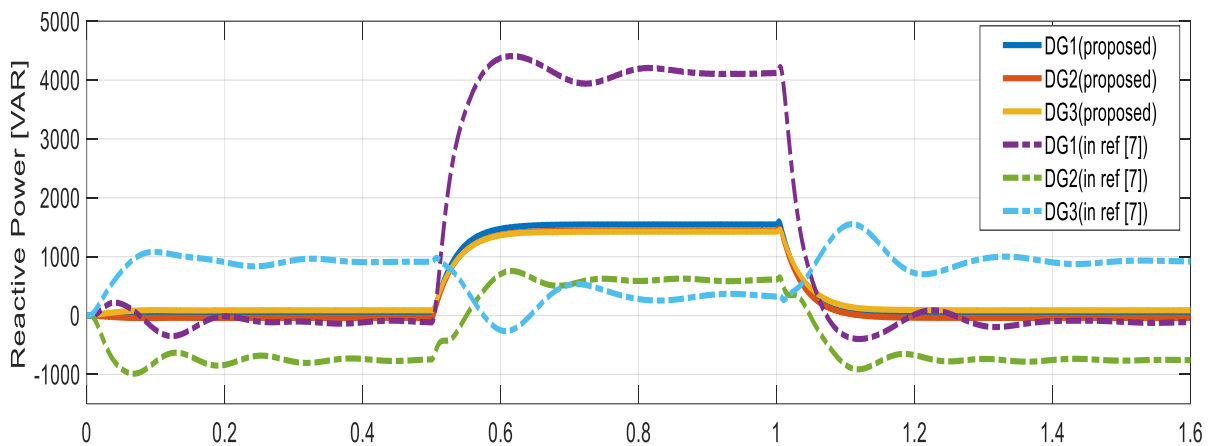


Figure 5-10: Comparison of reactive power sharing using the proposed method and the conventional method in [144]

5.5 Conclusions

This chapter presents an optimal approach for controlling parallel inverters in island MG. A small-signal model including virtual impedance is developed. Afterwards, the analysis of the eigenvalues is performed to determine the impact of virtual impedances parameters on the stability of the system. An identification of the limits of stability is carried out with an investigation of interactions between subsystems to ensure the stability of the system. An optimization algorithm is run offline taking into consideration the voltage drops in the flowchart process to keep the power mismatch at their minimum. The comparison of conventional approach with the proposed one shows significant improvement in terms of the dynamic response during load changes which confirms that the system is well-damped, moreover, less overshoots and less oscillations are presented, with faster settling time compared to the conventional method, time domain specification are measured to clarify the improvement of the optimal control. The proposed method shares the reactive load equally between

the inverters all of this without affecting other performances such as voltage which is maintained in its limits. At the end the proposed approach based on the small-signal model came with superior performances regarding the dynamic and steady-state response.

Table 5-2: Microgrid parameters

Inverter parameters (10 kVA rating)			
Parameter	Value	Parameter	Value
f_s	8 kHz	C_f	50 F
L_f	1.35 mH	r_f	0.1 Ω
L_c	0.35 mH	r_c	0.03 Ω
Droop control parameters			
m_p	9.4e-5 (= 0.3% droop)	n_q	1.3e-3 (= 2% droop)
W_n	314.16 rad/sec	V_n	381 V
W_c	31.41 rad/sec		
Voltage and current Controller parameters			
Voltage controller		Current controller	
K_{pv}	0.037	K_{iv}	393
K_{pc}	10.5	K_{ic}	16e3
bandwidth	400 Hz	bandwidth	1.6 kHz
F	0.75		
Lines and Loads parameters (see Fig.5-1)			

Table 5-3: Comparison of time domain specifications between the conventional method in [144] and the proposed control diagram

Sl. No	Parameters	Proposed [0,0.5s]			Conventional (ref [144]) [0,0.5s]		
		DG1	DG2	DG3	DG1	DG2	DG3
1	Active Power (P)	DG1	DG2	DG3	DG1	DG2	DG3
	tr (s)	0.079 s	0.069 s	0.022 s	0.102s	0.072 s	0.015 s
	Mp (%)	7.0%	2.0%	8.3%	30%	5.5%	54%
	ts (s)	0.15s	0.10 s	0.16 s	0.46 s	0.31s	0.49 s
2	Reactive Power (Q)	DG1	DG2	DG3	DG1	DG2	DG3
	tr (s)	0.06 s	0.06 s	0.07 s	0.06 s	0.07 s	0.07 s
	Mp (%)	0.5%	4.0%	3.5%	39%	17%	30%
	ts (s)	0.09 s	0.09 s	0.10 s	0.48s	0.40 s	0.50 s
3	i_{od}	DG1	DG2	DG3	DG1	DG2	DG3
	tr (s)	0.04 s	0.02 s	0.0007 s	0.07 s	0.03 s	0.0007 s
	Mp (%)	24%	11%	80%	50%	22 %	86%
	ts (s)	0.2 s	0.15 s	0.2 s	0.49 s	0.45 s	0.49 s
4	i_{oq}	DG1	DG2	DG3	DG1	DG2	DG3
	tr (s)	0.02s	0.006 s	0.01s	0.05s	0.014s	0.3 s
	Mp (%)	10%	13%	25%	60%	44%	43%
	ts (s)	0.1 s	0.4 s	0.13 s	0.48 s	0.4 s	0.47 s

General conclusion

In conclusion, this comprehensive study on Microgrid (MG) modeling and control represents a significant contribution to the understanding and advancement of MG systems.

The initial exploration provides a foundation by defining MG concepts and offering an in-depth analysis of various control techniques, including the well-explained droop control, virtual impedance approaches, and hierarchical control. This establishes a comprehensive overview of the current state-of-the-art in MG modeling and control.

The subsequent proposal of a systematic approach for designing hierarchical controlled three-phase MGs demonstrates a meticulous consideration of control structures, synchronization loops, and the dynamic response of the closed-loop system. The simulation results not only validate the proposed method's reliability but also underscore its effectiveness in enhancing MG system performance.

The introduction of a decentralized secondary control for frequency regulation and active power-sharing in autonomous microgrids signifies a paradigm shift. The innovative communication-free approach, employing a fuzzy logic controller, not only demonstrates superior performance in dynamic frequency recovery and transient stability but also showcases accurate active power-sharing without the complications of conventional controllers.

The optimization of parallel inverters in island MGs, detailed in the subsequent section, further reinforces the study's depth. The utilization of a small-signal model with virtual impedance and an offline optimization algorithm significantly enhances dynamic response, stability, and reactive load sharing. The proposed approach stands out, offering improvements over conventional methods in terms of reduced overshoots, fewer oscillations, and faster settling times.

Looking ahead, the outlined perspectives for future research, including the development of advanced synchronization techniques, optimal supervisory controllers, and experimental validation, highlight the commitment to continuous improvement in MG systems. These proposed directions aim not only to enhance the theoretical understanding but also to ensure practical implementation and the robustness of MG systems in real-world scenarios. In essence, this study contributes to the broader landscape of sustainable and resilient energy systems.

References

- [1] M. Prodanovic, « Power quality and control aspects of parallel connected inverters in distributed generation », 2004.
- [2] A. Cagnano, E. De Tuglie, et P. Mancarella, « Microgrids: Overview and guidelines for practical implementations and operation », *Appl. Energy*, vol. 258, p. 114039, 2020.
- [3] J. M. Guerrero, J. Matas, L. Garcia De Vicunagarcia De Vicuna, M. Castilla, et J. Miret, « Wireless-Control Strategy for Parallel Operation of Distributed-Generation Inverters », *IEEE Trans. Ind. Electron.*, vol. 53, n° 5, p. 1461-1470, oct. 2006, doi: 10.1109/TIE.2006.882015.
- [4] M. E. T. Souza et L. C. G. Freitas, « Grid-Connected and Seamless Transition Modes for Microgrids: An Overview of Control Methods, Operation Elements and General Requirements », *IEEE Access*, 2022.
- [5] J. Rocabert, A. Luna, F. Blaabjerg, et P. Rodriguez, « Control of power converters in AC microgrids », *IEEE Trans. Power Electron.*, vol. 27, n° 11, p. 4734-4749, 2012.
- [6] R. Rosso, X. Wang, M. Liserre, X. Lu, et S. Engelken, « Grid-forming converters: Control approaches, grid-synchronization, and future trends—A review », *IEEE Open J. Ind. Appl.*, vol. 2, p. 93-109, 2021.
- [7] N. Pogaku, M. Prodanovic, et T. C. Green, « Modeling, analysis and testing of autonomous operation of an inverter-based microgrid », *IEEE Trans. Power Electron.*, vol. 22, n° 2, p. 613-625, 2007.
- [8] N. Bottrell et T. C. Green, « Modeling microgrids with active loads », présenté à 2012 IEEE 13th Workshop on Control and Modeling for Power Electronics (COMPEL), 2012, p. 1-8.
- [9] Y. Han, H. Li, P. Shen, E. A. A. Coelho, et J. M. Guerrero, « Review of Active and Reactive Power Sharing Strategies in Hierarchical Controlled Microgrids », *IEEE Trans. POWER Electron.*, vol. 32, n° 3, p. 26, 2017.
- [10] A. Micallef, « Review of the current challenges and methods to mitigate power quality issues in single-phase microgrids », *IET Gener. Transm. Distrib.*, vol. 13, n° 11, p. 2044-2054, 2019.
- [11] D. Sharma, F. Sadeque, et B. Mirafzal, « Synchronization of inverters in grid forming mode », *IEEE Access*, vol. 10, p. 41341-41351, 2022.
- [12] A. M. Bouzid, J. M. Guerrero, A. Cheriti, M. Bouhamida, P. Sicard, et M. Benghanem, « A survey on control of electric power distributed generation systems for microgrid applications », *Renew. Sustain. Energy Rev.*, vol. 44, p. 751-766, 2015, doi: /10.1016/j.rser.2015.01.016.
- [13] T. K. Chau, S. S. Yu, T. Fernando, H. H.-C. Lu, et M. Small, « An investigation of the impact of PV penetration and BESS capacity on islanded microgrids—a small-signal based analytical approach », présenté à 2019 IEEE International Conference on Industrial Technology (ICIT), 2019, p. 1679-1684.
- [14] V. Paduani, M. Kaban, et P. Singh, « Small-signal stability of islanded-microgrids with DC side dynamics of inverters and saturation of current controllers », présenté à 2019 IEEE Power & Energy Society General Meeting (PESGM), 2019, p. 1-5.
- [15] J. M. Guerrero, L. G. De Vicuna, J. Matas, M. Castilla, et J. Miret, « Output impedance design of parallel-connected UPS inverters with wireless load-sharing control », *IEEE Trans. Ind. Electron.*, vol. 52, n° 4, p. 1126-1135, 2005.
- [16] U. B. Tayab, M. A. B. Roslan, L. J. Hwai, et M. Kashif, « A review of droop control techniques for microgrid », *Renew. Sustain. Energy Rev.*, vol. 76, p. 717-727, sept. 2017, doi: 10.1016/j.rser.2017.03.028.
- [17] J. M. Guerrero, J. C. Vasquez, J. Matas, M. Castilla, et L. G. de Vicuña, « Control strategy for flexible microgrid based on parallel line-interactive UPS systems », *IEEE Trans. Ind. Electron.*, vol. 56, n° 3, p. 726-736, 2008.
- [18] M. Gao, M. Chen, C. Jin, J. M. Guerrero, et Z. Qian, « Analysis, design, and experimental evaluation of power calculation in digital droop-controlled parallel microgrid inverters », *J. Zhejiang Univ. Sci. C*, vol. 14, p. 50-64, 2013.
- [19] J. He et Y. W. Li, « Analysis, design, and implementation of virtual impedance for power electronics interfaced distributed generation », *IEEE Trans. Ind. Appl.*, vol. 47, n° 6, p. 2525-2538, 2011.

- [20] J. He, Y. W. Li, J. M. Guerrero, F. Blaabjerg, et J. C. Vasquez, « An islanding microgrid power sharing approach using enhanced virtual impedance control scheme », *IEEE Trans. Power Electron.*, vol. 28, n° 11, p. 5272-5282, 2013.
- [21] J. Kim, J. M. Guerrero, P. Rodriguez, R. Teodorescu, et K. Nam, « Mode adaptive droop control with virtual output impedances for an inverter-based flexible AC microgrid », *IEEE Trans. Power Electron.*, vol. 26, n° 3, p. 689-701, 2010.
- [22] X. Wang, F. Blaabjerg, et Z. Chen, « An improved design of virtual output impedance loop for droop-controlled parallel three-phase voltage source inverters », présenté à 2012 IEEE Energy Conversion Congress and Exposition (ECCE), 2012, p. 2466-2473.
- [23] J. Zhang, J. Ning, L. Huang, H. Wang, et J. Shu, « Adaptive droop control for accurate power sharing in islanded microgrid using virtual impedance », présenté à IECON 2017-43rd Annual Conference of the IEEE Industrial Electronics Society, 2017, p. 2383-2388.
- [24] A. Micallef, M. Apap, C. Spiteri-Staines, et J. M. Guerrero, « Performance comparison for virtual impedance techniques used in droop controlled islanded microgrids », présenté à 2016 International Symposium on Power Electronics, Electrical Drives, Automation and Motion (SPEEDAM), 2016, p. 695-700.
- [25] Y. Daili, A. Harrag, et I. Bennia, « New droop control technique for reactive power sharing of parallel inverters in islanded microgrid », présenté à Artificial Intelligence and Renewables Towards an Energy Transition 4, 2021, p. 325-335.
- [26] J. C. Vasquez, J. M. Guerrero, A. Luna, P. Rodríguez, et R. Teodorescu, « Adaptive droop control applied to voltage-source inverters operating in grid-connected and islanded modes », *IEEE Trans. Ind. Electron.*, vol. 56, n° 10, p. 4088-4096, 2009.
- [27] W. Issa, S. Sharkh, T. Mallick, et M. Abusara, « Improved reactive power sharing for parallel-operated inverters in islanded microgrids », *J. Power Electron.*, vol. 16, n° 3, p. 1152-1162, 2016.
- [28] C.-T. Lee, C.-C. Chu, et P.-T. Cheng, « A new droop control method for the autonomous operation of distributed energy resource interface converters », *IEEE Trans. Power Electron.*, vol. 28, n° 4, p. 1980-1993, 2012.
- [29] J. Zhou et P.-T. Cheng, « A Modified $Q \cdot V$ Droop Control for Accurate Reactive Power Sharing in Distributed Generation Microgrid », *IEEE Trans. Ind. Appl.*, vol. 55, n° 4, p. 4100-4109, 2019.
- [30] H. Bevrani et S. Shokoohi, « An intelligent droop control for simultaneous voltage and frequency regulation in islanded microgrids », *IEEE Trans. Smart Grid*, vol. 4, n° 3, p. 1505-1513, 2013.
- [31] C. Dou, Z. Zhang, D. Yue, et H. Gao, « An improved droop control strategy based on changeable reference in low-voltage microgrids », *Energies*, vol. 10, n° 8, p. 1080, 2017.
- [32] U. Tamrakar, D. Shrestha, M. Maharjan, B. P. Bhattarai, T. M. Hansen, et R. Tonkoski, « Virtual inertia: Current trends and future directions », *Appl. Sci.*, vol. 7, n° 7, p. 654, 2017.
- [33] N. Soni, S. Doolla, et M. C. Chandorkar, « Improvement of transient response in microgrids using virtual inertia », *IEEE Trans. Power Deliv.*, vol. 28, n° 3, p. 1830-1838, 2013.
- [34] J. Liu, Y. Miura, et T. Ise, « Comparison of dynamic characteristics between virtual synchronous generator and droop control in inverter-based distributed generators », *IEEE Trans. Power Electron.*, vol. 31, n° 5, p. 3600-3611, 2015.
- [35] A. Fathi, Q. Shafiee, et H. Bevrani, « Robust frequency control of microgrids using an extended virtual synchronous generator », *IEEE Trans. Power Syst.*, vol. 33, n° 6, p. 6289-6297, 2018.
- [36] X. Hou, Y. Sun, X. Zhang, J. Lu, P. Wang, et J. M. Guerrero, « Improvement of frequency regulation in VSG-based AC microgrid via adaptive virtual inertia », *IEEE Trans. Power Electron.*, vol. 35, n° 2, p. 1589-1602, 2019.
- [37] J. M. Guerrero, J. C. Vasquez, J. Matas, L. G. De Vicuña, et M. Castilla, « Hierarchical control of droop-controlled AC and DC microgrids—A general approach toward standardization », *IEEE Trans. Ind. Electron.*, vol. 58, n° 1, p. 158-172, 2010.
- [38] J. C. Vasquez, J. M. Guerrero, M. Savaghebi, J. Eloy-Garcia, et R. Teodorescu, « Modeling, analysis, and design of stationary-reference-frame droop-controlled parallel three-phase voltage source inverters », *IEEE Trans. Ind. Electron.*, vol. 60, n° 4, p. 1271-1280, 2012.

- [39] J. M. Guerrero, J. Matas, L. G. D. V. De Vicuna, M. Castilla, et J. Miret, « Wireless-control strategy for parallel operation of distributed-generation inverters », *IEEE Trans. Ind. Electron.*, vol. 53, n° 5, p. 1461-1470, 2006.
- [40] I. Bennia, Y. Daili, et A. Harrag, « Hierarchical control of paralleled voltage source inverters in islanded single phase microgrids », présenté à Artificial Intelligence and Renewables Towards an Energy Transition 4, 2021, p. 302-313.
- [41] E. Planas, A. Gil-de-Muro, J. Andreu, I. Kortabarria, et I. M. de Alegría, « General aspects, hierarchical controls and droop methods in microgrids: A review », *Renew. Sustain. Energy Rev.*, vol. 17, p. 147-159, 2013.
- [42] D. Y. Yamashita, I. Vechiu, et J.-P. Gaubert, « A review of hierarchical control for building microgrids », *Renew. Sustain. Energy Rev.*, vol. 118, p. 109523, 2020.
- [43] Y. Khayat *et al.*, « On the secondary control architectures of AC microgrids: An overview », *IEEE Trans. Power Electron.*, vol. 35, n° 6, p. 6482-6500, 2019.
- [44] H. Bevrani, B. François, et T. Ise, *Microgrid dynamics and control*. John Wiley & Sons, 2017.
- [45] S. K. Sahoo, A. K. Sinha, et N. Kishore, « Control techniques in AC, DC, and hybrid AC–DC microgrid: a review », *IEEE J. Emerg. Sel. Top. Power Electron.*, vol. 6, n° 2, p. 738-759, 2017.
- [46] L. Meng, M. Savaghebi, F. Andrade, J. C. Vasquez, J. M. Guerrero, et M. Graells, « Microgrid central controller development and hierarchical control implementation in the intelligent microgrid lab of Aalborg University », présenté à 2015 IEEE Applied Power Electronics Conference and Exposition (APEC), 2015, p. 2585-2592.
- [47] M. Savaghebi, J. M. Guerrero, A. Jalilian, et J. C. Vasquez, « Secondary control for voltage unbalance compensation in an islanded microgrid », présenté à 2011 IEEE International Conference on Smart Grid Communications (SmartGridComm), 2011, p. 499-504.
- [48] T. Qian, Y. Liu, W. Zhang, W. Tang, et M. Shahidehpour, « Event-triggered updating method in centralized and distributed secondary controls for islanded microgrid restoration », *IEEE Trans. Smart Grid*, vol. 11, n° 2, p. 1387-1395, 2019.
- [49] T. Dragičević, R. Heydari, et F. Blaabjerg, « Super-high bandwidth secondary control of ac microgrids », présenté à 2018 IEEE Applied Power Electronics Conference and Exposition (APEC), 2018, p. 3036-3042.
- [50] A. Bendib, A. Chouder, K. Kara, A. Kherbachi, S. Barkat, et W. Issa, « New modeling approach of secondary control layer for autonomous single-phase microgrids », *J. Frankl. Inst.*, vol. 356, n° 13, p. 6842-6874, 2019.
- [51] S. Shokoohi, F. Sabori, et H. Bevrani, « Secondary voltage and frequency control in islanded microgrids: online ANN tuning approach », présenté à 2014 Smart Grid Conference (SGC), 2014, p. 1-6.
- [52] P. Babahajiani, Q. Shafiee, et H. Bevrani, « Intelligent demand response contribution in frequency control of multi-area power systems », *IEEE Trans. Smart Grid*, vol. 9, n° 2, p. 1282-1291, 2016.
- [53] S. Liu, X. Wang, et P. X. Liu, « Impact of communication delays on secondary frequency control in an islanded microgrid », *IEEE Trans. Ind. Electron.*, vol. 62, n° 4, p. 2021-2031, 2014.
- [54] B. Tavassoli, A. Fereidunian, et S. Mehdi, « Communication system effects on the secondary control performance in microgrids », *IET Renew. Power Gener.*, vol. 14, n° 12, p. 2047-2057, 2020.
- [55] C. Ahumada, R. Cárdenas, D. Saez, et J. M. Guerrero, « Secondary control strategies for frequency restoration in islanded microgrids with consideration of communication delays », *IEEE Trans. Smart Grid*, vol. 7, n° 3, p. 1430-1441, 2015.
- [56] X. Hou *et al.*, « Distributed hierarchical control of AC microgrid operating in grid-connected, islanded and their transition modes », *IEEE Access*, vol. 6, p. 77388-77401, 2018.
- [57] E. Espina, J. Llanos, C. Burgos-Mellado, R. Cardenas-Dobson, M. Martinez-Gomez, et D. Saez, « Distributed control strategies for microgrids: An overview », *IEEE Access*, vol. 8, p. 193412-193448, 2020.
- [58] Q. Shafiee, J. M. Guerrero, et J. C. Vasquez, « Distributed secondary control for islanded microgrids—A novel approach », *IEEE Trans. Power Electron.*, vol. 29, n° 2, p. 1018-1031, 2013.

- [59] S. Rivero, M. Tucci, J. C. Vasquez, J. M. Guerrero, et G. Ferrari-Trecate, « Stabilizing plug-and-play regulators and secondary coordinated control for AC islanded microgrids with bus-connected topology », *Appl. Energy*, vol. 210, p. 914-924, 2018.
- [60] J. W. Simpson-Porco, Q. Shafiee, F. Dörfler, J. C. Vasquez, J. M. Guerrero, et F. Bullo, « Secondary frequency and voltage control of islanded microgrids via distributed averaging », *IEEE Trans. Ind. Electron.*, vol. 62, n° 11, p. 7025-7038, 2015.
- [61] M. Shi, X. Chen, J. Zhou, Y. Chen, J. Wen, et H. He, « PI-consensus based distributed control of AC microgrids », *IEEE Trans. Power Syst.*, vol. 35, n° 3, p. 2268-2278, 2019.
- [62] G. Lou, W. Gu, J. Wang, W. Sheng, et L. Sun, « Optimal design for distributed secondary voltage control in islanded microgrids: Communication topology and controller », *IEEE Trans. Power Syst.*, vol. 34, n° 2, p. 968-981, 2018.
- [63] G. Lou, W. Gu, Y. Xu, M. Cheng, et W. Liu, « Distributed MPC-based secondary voltage control scheme for autonomous droop-controlled microgrids », *IEEE Trans. Sustain. Energy*, vol. 8, n° 2, p. 792-804, 2016.
- [64] L. Subramanian, V. Debusschere, H. B. Gooi, et N. Hadjsaid, « A distributed model predictive control framework for grid-friendly distributed energy resources », *IEEE Trans. Sustain. Energy*, vol. 12, n° 1, p. 727-738, 2020.
- [65] M. Chen, X. Xiao, et J. M. Guerrero, « Secondary restoration control of islanded microgrids with a decentralized event-triggered strategy », *IEEE Trans. Ind. Inform.*, vol. 14, n° 9, p. 3870-3880, 2017.
- [66] S. Weng, D. Yue, C. Dou, J. Shi, et C. Huang, « Distributed event-triggered cooperative control for frequency and voltage stability and power sharing in isolated inverter-based microgrid », *IEEE Trans. Cybern.*, vol. 49, n° 4, p. 1427-1439, 2018.
- [67] P. Ge, B. Chen, et F. Teng, « Event-triggered distributed MPC for voltage control of an islanded microgrid », *ArXiv Prepr. ArXiv200400394*, 2020.
- [68] S. Weng, Y. Xue, J. Luo, et Y. Li, « Distributed secondary control for islanded microgrids cluster based on hybrid-triggered mechanisms », *Processes*, vol. 8, n° 3, p. 370, 2020.
- [69] S. Xu *et al.*, « Distributed optimal frequency regulation for multiple distributed power generations with an event-triggered communication mechanism », *Processes*, vol. 8, n° 2, p. 169, 2020.
- [70] Y. Long, Y. Zhu, et W. Zhang, « A novel distributed event-triggered control for reactive power sharing based on hierarchical structure in islanded microgrid », *Meas. Control*, vol. 54, n° 5-6, p. 872-879, 2021.
- [71] X. Feng, A. Shekhar, F. Yang, R. E. Hebner, et P. Bauer, « Comparison of hierarchical control and distributed control for microgrid », *Electr. Power Compon. Syst.*, vol. 45, n° 10, p. 1043-1056, 2017.
- [72] J. M. Rey, P. Martí, M. Velasco, J. Miret, et M. Castilla, « Secondary switched control with no communications for islanded microgrids », *IEEE Trans. Ind. Electron.*, vol. 64, n° 11, p. 8534-8545, 2017.
- [73] J. M. Rey, C. X. Rosero, M. Velasco, P. Marti, J. Miret, et M. Castilla, « Local frequency restoration for droop-controlled parallel inverters in islanded microgrids », *IEEE Trans. Energy Convers.*, vol. 34, n° 3, p. 1232-1241, 2018.
- [74] Z. Zhang, C. Dou, D. Yue, B. Zhang, et W. Luo, « A decentralized control method for frequency restoration and accurate reactive power sharing in islanded microgrids », *J. Frankl. Inst.*, vol. 355, n° 17, p. 8874-8890, 2018.
- [75] M. Jayachandran et G. Ravi, « Decentralized model predictive hierarchical control strategy for islanded AC microgrids », *Electr. Power Syst. Res.*, vol. 170, p. 92-100, 2019.
- [76] Y. Khayat *et al.*, « Communication-less optimal frequency control of islanded microgrids », présenté à 2018 20th European Conference on Power Electronics and Applications (EPE'18 ECCE Europe), 2018, p. P-1.
- [77] R. Heydari, Y. Khayat, M. Naderi, A. Anvari-Moghaddam, T. Dragicevic, et F. Blaabjerg, « A decentralized adaptive control method for frequency regulation and power sharing in autonomous microgrids », présenté à 2019 IEEE 28th International Symposium on Industrial Electronics (ISIE), 2019, p. 2427-2432.
- [78] M. Shafiee-Rad, Q. Shafiee, et M.-R. J. Motlagh, « Decentralized scalable robust voltage control for islanded AC microgrids with general topology », présenté à 2020 11th Power Electronics, Drive Systems, and Technologies Conference (PEDSTC), 2020, p. 1-6.

- [79] K. Dehghanpour, Z. Wang, J. Wang, Y. Yuan, et F. Bu, « A survey on state estimation techniques and challenges in smart distribution systems », *IEEE Trans. Smart Grid*, vol. 10, n° 2, p. 2312-2322, 2018.
- [80] T. Wu, J. Liu, Z. Liu, S. Wang, et B. Liu, « Load power estimation based secondary control for microgrids », présenté à 2015 9th International Conference on Power Electronics and ECCE Asia (ICPE-ECCE Asia), 2015, p. 722-727.
- [81] G. Lou, W. Gu, L. Wang, B. Xu, M. Wu, et W. Sheng, « Decentralised secondary voltage and frequency control scheme for islanded microgrid based on adaptive state estimator », *IET Gener. Transm. Distrib.*, vol. 11, n° 15, p. 3683-3693, 2017.
- [82] W. Gu, G. Lou, W. Tan, et X. Yuan, « A nonlinear state estimator-based decentralized secondary voltage control scheme for autonomous microgrids », *IEEE Trans. Power Syst.*, vol. 32, n° 6, p. 4794-4804, 2017.
- [83] N. Mohammadi, K. Mohammadi, H. Bevrani, M. T. Beheshti, et H. Golpîra, « Decentralized Estimator-based Secondary Voltage and Reactive Power Control of an Islanded Microgrid », présenté à 2019 6th International Conference on Control, Instrumentation and Automation (ICCIA), 2019, p. 1-6.
- [84] Y. Khayat *et al.*, « Decentralized frequency control of AC microgrids: An estimation-based consensus approach », *IEEE J. Emerg. Sel. Top. Power Electron.*, vol. 9, n° 5, p. 5183-5191, 2020.
- [85] G. Zhang, C. Li, D. Qi, et H. Xin, « Distributed estimation and secondary control of autonomous microgrid », *IEEE Trans. Power Syst.*, vol. 32, n° 2, p. 989-998, 2016.
- [86] Y. Wang, Z. Chen, X. Wang, Y. Tian, Y. Tan, et C. Yang, « An estimator-based distributed voltage-predictive control strategy for AC islanded microgrids », *IEEE Trans. Power Electron.*, vol. 30, n° 7, p. 3934-3951, 2014.
- [87] M. Yazdani et A. Mehrizi-Sani, « Washout filter-based power sharing », *IEEE Trans. Smart Grid*, vol. 7, n° 2, p. 967-968, 2015.
- [88] Y. Han, H. Li, L. Xu, X. Zhao, et J. M. Guerrero, « Analysis of washout filter-based power sharing strategy—An equivalent secondary controller for islanded microgrid without LBC lines », *IEEE Trans. Smart Grid*, vol. 9, n° 5, p. 4061-4076, 2017.
- [89] J. Lu, M. Savaghebi, et J. M. Guerrero, « Second order washout filter based power sharing strategy for uninterruptible power supply », présenté à IECON 2017-43rd Annual Conference of the IEEE Industrial Electronics Society, 2017, p. 7854-7859.
- [90] C. A. Macana, E. Mojica-Nava, H. R. Pota, J. Guerrero, et J. C. Vasquez, « Accurate proportional power sharing with minimum communication requirements for inverter-based islanded microgrids », *Int. J. Electr. Power Energy Syst.*, vol. 121, p. 106036, 2020.
- [91] W. Issa, F. Al-Naemi, G. Konstantopoulos, S. Sharkh, et M. Abusara, « Stability analysis and control of a microgrid against circulating power between parallel inverters », *Energy Procedia*, vol. 157, p. 1061-1070, 2019.
- [92] X. Wang, Y. W. Li, F. Blaabjerg, et P. C. Loh, « Virtual-impedance-based control for voltage-source and current-source converters », *IEEE Trans. Power Electron.*, vol. 30, n° 12, p. 7019-7037, 2014.
- [93] C. Blanco, D. Reigosa, J. C. Vasquez, J. M. Guerrero, et F. Briz, « Virtual admittance loop for voltage harmonic compensation in microgrids », *IEEE Trans. Ind. Appl.*, vol. 52, n° 4, p. 3348-3356, 2016.
- [94] Y. Zhu, F. Zhuo, F. Wang, B. Liu, R. Gou, et Y. Zhao, « A virtual impedance optimization method for reactive power sharing in networked microgrid », *IEEE Trans. Power Electron.*, vol. 31, n° 4, p. 2890-2904, 2015.
- [95] X. Wu, C. Shen, et R. Iravani, « Feasible range and optimal value of the virtual impedance for droop-based control of microgrids », *IEEE Trans. Smart Grid*, vol. 8, n° 3, p. 1242-1251, 2016.
- [96] Z. Peng *et al.*, « Droop control strategy incorporating coupling compensation and virtual impedance for microgrid application », *IEEE Trans. Energy Convers.*, vol. 34, n° 1, p. 277-291, 2019.
- [97] B. Pournazarian, S. S. Seyedalipour, M. Lehtonen, S. Taheri, et E. Pouresmaeil, « Virtual impedances optimization to enhance microgrid small-signal stability and reactive power sharing », *IEEE Access*, vol. 8, p. 139691-139705, 2020.
- [98] Z. Jin et X. Wang, « A DQ-frame asymmetrical virtual impedance control for enhancing transient stability of grid-forming inverters », *IEEE Trans. Power Electron.*, vol. 37, n° 4, p. 4535-4544, 2021.

- [99] X. Li, Z. Li, L. Guo, J. Zhu, Y. Wang, et C. Wang, « Enhanced dynamic stability control for low-inertia hybrid AC/DC microgrid with distributed energy storage systems », *IEEE Access*, vol. 7, p. 91234-91242, 2019.
- [100] I. Bennis, A. Harrag, et Y. Dailia, « Small-signal modelling and stability analysis of island mode microgrid paralleled inverters », *J. Renew. Energ.*, vol. 24, n° 1, p. 105-120, 2021.
- [101] M. Rasheduzzaman, J. A. Mueller, et J. W. Kimball, « An accurate small-signal model of inverter-dominated islanded microgrids using dq reference frame », *IEEE J. Emerg. Sel. Top. Power Electron.*, vol. 2, n° 4, p. 1070-1080, 2014.
- [102] K. Yu, Q. Ai, S. Wang, J. Ni, et T. Lv, « Analysis and optimization of droop controller for microgrid system based on small-signal dynamic model », *IEEE Trans. Smart Grid*, vol. 7, n° 2, p. 695-705, 2015.
- [103] D. K. Dheer, N. Soni, et S. Doolla, « Improvement of small signal stability margin and transient response in inverter-dominated microgrids », *Sustain. Energy Grids Netw.*, vol. 5, p. 135-147, 2016.
- [104] D. K. Dheer, O. V. Kulkarni, S. Doolla, et A. K. Rathore, « Effect of reconfiguration and meshed networks on the small-signal stability margin of droop-based islanded microgrids », *IEEE Trans. Ind. Appl.*, vol. 54, n° 3, p. 2821-2833, 2018.
- [105] A. Aderibole, H. H. Zeineldin, M. S. El-Moursi, J. C.-H. Peng, et M. Al Hosani, « Domain of stability characterization for hybrid microgrids considering different power sharing conditions », *IEEE Trans. Energy Convers.*, vol. 33, n° 1, p. 312-323, 2017.
- [106] S. Leitner, M. Yazdani, A. Mehrizi-Sani, et A. Muetze, « Small-signal stability analysis of an inverter-based microgrid with internal model-based controllers », *IEEE Trans. Smart Grid*, vol. 9, n° 5, p. 5393-5402, 2017.
- [107] A. Khodadadi, P. H. Divshali, M. H. Nazari, et S. H. Hosseinian, « Small-signal stability improvement of an islanded microgrid with electronically-interfaced distributed energy resources in the presence of parametric uncertainties », *Electr. Power Syst. Res.*, vol. 160, p. 151-162, 2018.
- [108] D. K. Dheer, A. Vijay, O. V. Kulkarni, et S. Doolla, « Improvement of stability margin of droop-based islanded microgrids by cascading of lead compensators », *IEEE Trans. Ind. Appl.*, vol. 55, n° 3, p. 3241-3251, 2019.
- [109] Y. Yan, D. Shi, D. Bian, B. Huang, Z. Yi, et Z. Wang, « Small-signal stability analysis and performance evaluation of microgrids under distributed control », *IEEE Trans. Smart Grid*, vol. 10, n° 5, p. 4848-4858, 2018.
- [110] A. Garces, « Small-signal stability in island residential microgrids considering droop controls and multiple scenarios of generation », *Electr. Power Syst. Res.*, vol. 185, p. 106371, 2020.
- [111] M. Adelpour, M. Hamzeh, et K. Sheshyekani, « Comprehensive small-signal stability analysis of islanded synchronous generator-based microgrids », *Sustain. Energy Grids Netw.*, vol. 26, p. 100444, 2021.
- [112] S. Eberlein et K. Rudion, « Small-signal stability modelling, sensitivity analysis and optimization of droop controlled inverters in LV microgrids », *Int. J. Electr. Power Energy Syst.*, vol. 125, p. 106404, 2021.
- [113] Q. Geng et X. Zhou, « Small signal stability analysis of VSC based DC systems using graph theory », *Int. J. Electr. Power Energy Syst.*, vol. 137, p. 107830, 2022.
- [114] H. Abdelgabir, A. R. Boynuegri, A. Elrayyah, et Y. Sozer, « A complete small signal modelling and adaptive stability analysis of nonlinear droop-controlled microgrids », présenté à 2018 IEEE Applied Power Electronics Conference and Exposition (APEC), 2018, p. 3333-3339.
- [115] A. Llaría, O. Curea, J. Jiménez, et H. Camblong, « Survey on microgrids: unplanned islanding and related inverter control techniques », *Renew. Energy*, vol. 36, n° 8, p. 2052-2061, 2011.
- [116] I. Bennis, Y. Daili, et A. Harrag, « LCL Filter Design for Low Voltage-Source Inverter », présenté à International Conference on Artificial Intelligence in Renewable Energetic Systems, 2021, p. 332-341.
- [117] P. C. Loh et D. G. Holmes, « Analysis of multiloop control strategies for LC/CL/LCL-filtered voltage-source and current-source inverters », *IEEE Trans. Ind. Appl.*, vol. 41, n° 2, p. 644-654, 2005.
- [118] I. Bennis, A. Harrag, Y. Daili, A. Bouzid, et J. M. Guerrero, « Decentralized secondary control for frequency regulation based on fuzzy logic control in islanded microgrid », *Indones. J. Electr. Eng. Comput. Sci.*, vol. 29, n° 1, p. 85-100, 2023.

- [119] A. Haddadi, B. Boulet, A. Yazdani, et G. Joós, « A μ -based approach to small-signal stability analysis of an interconnected distributed energy resource unit and load », *IEEE Trans. Power Deliv.*, vol. 30, n° 4, p. 1715-1726, 2014.
- [120] A. M. Bouzid, M. S. Golsorkhi, P. Sicard, et A. Chériti, « H^∞ structured design of a cascaded voltage/current controller for electronically interfaced distributed energy resources », présenté à 2015 Tenth international conference on ecological vehicles and renewable energies (EVER), 2015, p. 1-6.
- [121] W. R. Issa, « Improved control strategies for droop-controlled inverter-based microgrid », 2015.
- [122] A. E. M. Bouzid, « Élaboration d'une méthode de contrôle pour améliorer la robustesse d'un micro réseau électrique », 2017.
- [123] L. Meng, E. R. Sanseverino, A. Luna, T. Dragicevic, J. C. Vasquez, et J. M. Guerrero, « Microgrid supervisory controllers and energy management systems: A literature review », *Renew. Sustain. Energy Rev.*, vol. 60, p. 1263-1273, 2016, doi: <https://doi.org/10.1016/j.rser.2016.03.003>.
- [124] Z. Rafique, H. M. Khalid, et S. Muyeen, « Communication systems in distributed generation: A bibliographical review and frameworks », *IEEE Access*, vol. 8, p. 207226-207239, 2020, doi: 10.1109/ACCESS.2020.3037196.
- [125] Q. Shafiee, J. M. Guerrero, et J. C. Vasquez, « Distributed secondary control for islanded microgrids—A novel approach », *IEEE Trans. Power Electron.*, vol. 29, n° 2, p. 1018-1031, 2013, doi: 10.1109/TPEL.2013.2259506.
- [126] B. Tavassoli, A. Fereidunian, et S. Mehdi, « Communication system effects on the secondary control performance in microgrids », *IET Renew. Power Gener.*, vol. 14, n° 12, p. 2047-2057, 2020, doi: 10.1049/iet-rpg.2019.1170.
- [127] S. Tan, J. M. Guerrero, P. Xie, R. Han, et J. C. Vasquez, « Brief survey on attack detection methods for cyber-physical systems », *IEEE Syst. J.*, vol. 14, n° 4, p. 5329-5339, 2020, doi: 10.1109/JSYST.2020.2991258.
- [128] Y. Khayat *et al.*, « Decentralized optimal frequency control in autonomous microgrids », *IEEE Trans. Power Syst.*, vol. 34, n° 3, p. 2345-2353, 2018, doi: 10.1109/TPWRS.2018.2889671.
- [129] R. Jackson, S. A. Zulkifli, N. M. B. Sham, et E. Pathan, « A Self-Frequency Restoration Control Based on Droop Strategy for Autonomous Microgrid », *Intl J. Renew. Energy Res.*, vol. 9, n° 2, p. 749-756, 2019.
- [130] I. Bennis, A. Harrag, et Y. Dailia, « Small-signal modelling and stability analysis of island mode microgrid paralleled inverters », *J. Renew. Energ.*, vol. 24, n° 1, p. 105-120, 2021, doi: <https://doi.org/10.54966/jreen.v24i1.975>.
- [131] P. S. Devi et R. V. Santhi, « Introducing LQR-fuzzy for a dynamic multi area LFC-DR model. », *Int. J. Electr. Comput. Eng. 2088-8708*, vol. 9, n° 2, 2019, doi: 10.11591/ijece.v9i2.pp861-874.
- [132] Y. Hocini, A. Allali, et H. M. Boulouiha, « Power fuzzy adaptive control for wind turbine. », *Int. J. Electr. Comput. Eng. 2088-8708*, vol. 10, n° 5, 2020, doi: 10.11591/ijece.v10i5.pp5262-5273.
- [133] I. Bennis, Y. Daili, et A. Harrag, « Hierarchical Control of Paralleled Voltage Source Inverters in Islanded Single Phase Microgrids », in *Artificial Intelligence and Renewables Towards an Energy Transition*, Cham, 2021, p. 302-313. doi: https://doi.org/10.1007/978-3-030-63846-7_30.
- [134] Y. Khayat *et al.*, « On the secondary control architectures of AC microgrids: An overview », *IEEE Trans. Power Electron.*, vol. 35, n° 6, p. 6482-6500, 2019, doi: 10.1109/TPEL.2019.2951694.
- [135] B. N. Alhasnawi, B. H. Jasim, B. E. Sedhom, E. Hossain, et J. M. Guerrero, « A new decentralized control strategy of microgrids in the internet of energy paradigm », *Energies*, vol. 14, n° 8, p. 2183, 2021, doi: <https://doi.org/10.3390/en14082183>.
- [136] B. N. Alhasnawi, B. H. Jasim, et B. E. Sedhom, « Distributed secondary consensus fault tolerant control method for voltage and frequency restoration and power sharing control in multi-agent microgrid », *Int. J. Electr. Power Energy Syst.*, vol. 133, p. 107251, 2021, doi: <https://doi.org/10.1016/j.ijepes.2021.107251>.
- [137] B. Ning, Q.-L. Han, et L. Ding, « Distributed Finite-Time Secondary Frequency and Voltage Control for Islanded Microgrids With Communication Delays and Switching Topologies », *IEEE Trans. Cybern.*, 2020, doi: 10.1109/TCYB.2020.3003690.

- [138] M. Yazdani et A. Mehrizi-Sani, « Washout filter-based power sharing », *IEEE Trans. Smart Grid*, vol. 7, n° 2, p. 967-968, 2015, doi: 10.1109/TSG.2015.2497964.
- [139] J. M. Rey, P. Martí, M. Velasco, J. Miret, et M. Castilla, « Secondary switched control with no communications for islanded microgrids », *IEEE Trans. Ind. Electron.*, vol. 64, n° 11, p. 8534-8545, 2017, doi: 10.1109/TIE.2017.2703669.
- [140] W. Gu, G. Lou, W. Tan, et X. Yuan, « A nonlinear state estimator-based decentralized secondary voltage control scheme for autonomous microgrids », *IEEE Trans. Power Syst.*, vol. 32, n° 6, p. 4794-4804, 2017, doi: 10.1109/TPWRS.2017.2676181.
- [141] G. Lou, W. Gu, L. Wang, B. Xu, M. Wu, et W. Sheng, « Decentralised secondary voltage and frequency control scheme for islanded microgrid based on adaptive state estimator », *IET Gener. Transm. Distrib.*, vol. 11, n° 15, p. 3683-3693, 2017, doi: <https://doi.org/10.1049/iet-gtd.2016.1910>.
- [142] A. El-Zonkoly, A. Khalil, et N. Ahmied, « Optimal tuning of lead-lag and fuzzy logic power system stabilizers using particle swarm optimization », *Expert Syst. Appl.*, vol. 36, n° 2, p. 2097-2106, 2009, doi: <https://doi.org/10.1016/j.eswa.2007.12.069>.
- [143] T. Mahto et V. Mukherjee, « A novel scaling factor based fuzzy logic controller for frequency control of an isolated hybrid power system », *Energy*, vol. 130, p. 339-350, 2017, doi: <https://doi.org/10.1016/j.energy.2017.04.155>.
- [144] N. Pogaku, M. Prodanovic, et T. C. Green, « Modeling, Analysis and Testing of Autonomous Operation of an Inverter-Based Microgrid », *IEEE Trans. Power Electron.*, vol. 22, n° 2, p. 613-625, mars 2007, doi: 10.1109/TPEL.2006.890003.
- [145] A. Harrag et S. Messalti, « Optimal GA-based PI control of SVC compensator improving voltage stability », *J. Renew. Energ.*, vol. 21, n° 2, p. 303-314, 2018.

Study, Modelling and Control of a Multisources Microgrid

Abstract

المخلص: تركز هاته الأطروحة على إجراء بحث أساسي فيما يتعلق بتقنيات التحكم في الشبكات الكهربائية المصغرة القائمة على الطاقات المتجددة والتي يلعب فيها العاكس الكهربائي دور حجر الأساس. بهدف تطوير تقنيات تحكم جديدة لتحسين الأداء والموثوقية. يتركز عمل هاته الأطروحة على النمذجة وتحليل الاستقرار وتصميم التحكم الهرمي للعاكسات المتوازية في شبكة كهربائية مصغرة. تشرح الأطروحة أوضاع التشغيل وتقنيات التحكم في الشبكات الكهربائية المصغرة من وضع التشغيل المعزول عن الشبكة الكهربائية الأساسية إلى وضع التشغيل المرتبط بها وحالة الانتقال بينهما. تقدم الأطروحة وتشرح مراحل تصميم التحكم الهرمي لمصادر الجهد المتوازية والتي تغذي الشبكة الكهربائية المصغرة، يتكون التحكم الهرمي من عدة مستويات مستوى تحكم داخلي أو صفري مهمته التحكم في التوتر والتيار الخاصين بالشبكة الكهربائية المصغرة، ومستوى أولي مهمته توفير القيم الإسمية للتوتر والتردد مع توزيع الأحمال بين العاكسات بصفة متساوية، ومستوى ثانوي مهمته استرجاع التوتر والتردد إلى قيمهم الإسمية بعد حدوث الاضطرابات في النظام. أيضا تقترح الأطروحة تحكماً ثانوياً لا مركزياً قائماً على المنطق الضبابي لاستعادة التردد وتقاسم الطاقة النشطة بالإضافة إلى تقنية تحكم محسنة تحافظ على الاستقرار وتوزع الطاقة التفاعلية بالتساوي بين العاكسات في الشبكة الكهربائية المصغرة.

كلمات مفتاحية: الشبكات المصغرة، التحكم الساقط، العاكسات المتوازية، التحكم الهرمي، التحكم الثانوي اللامركزي، المنطق الضبابي، الوضع المنعزل.

Résumé : La thèse se concentre sur le développement de nouvelles techniques de contrôle améliorées pour les micro-réseaux à base d'onduleurs afin d'améliorer leurs performances et leur fiabilité. La thèse décrit les modes de fonctionnement et les techniques de contrôle des micro-réseaux. Elle présente une conception de contrôle hiérarchique pour les onduleurs à source de tension en parallèle dans un micro-réseau avec des niveaux de contrôle interne, primaire et secondaire. La thèse propose également un contrôle secondaire décentralisé basé sur la logique floue pour la restauration de fréquence et le partage de puissance active. Aussi cette thèse propose une technique de contrôle améliorée qui maintient la stabilité et partage la puissance réactive de manière égale dans les micro-réseaux isolés.

Mots-clés : Micro réseau, Control statisme, Onduleurs parallèles, Control hiérarchique, Control secondaire décentralisé, Logique floue, Mode isolé.

Abstract: The main focus of this thesis is to conduct fundamental research regarding control techniques of inverter-based microgrids (MG). It aims to develop new and enhanced control techniques to improve performance and reliability. It emphasises on the modelling, stability analysis and hierarchical control design of parallel inverters in a MG. This thesis presents a general outline of MGs operation modes and control technics, starting by outlining the stand-alone and grid-connected modes besides the transition between them, additional power converters in AC MGs are classified, droop control, and virtual impedance are reviewed.; the hierarchical control layers are exhibited, especially the secondary control with their three classifications centralized, distributed, and decentralised. The diagram of the hierarchical control consists of inner, primary, and secondary control levels. The inner control commonly referred as zero level is used to regulate the VSI output voltage. The primary control is based on the droop control method and the virtual impedance loop to share the power accurately regardless of the line impedances. Secondary control is used to regulate the voltage and frequency to their rated values. Also this thesis proposes a fuzzy-based decentralized secondary control for frequency restoration and active power-sharing in an islanded MG. Further, this thesis proposes an improved control technique that maintains stability and shares reactive power equally in isolated MGs

Keywords: Microgrid, Droop control, Paralleled inverters, Hierarchical control, Decentralized secondary control Fuzzy logic, island mode.